THESIS FOR THE DEGREE OF DOCTOR OF PHILOSOPHY

Systematic Studies of Triplet Annihilating Species for Photochemical Upconversion

AXEL OLESUND

Department of Chemistry and Chemical Engineering
Chalmers University of Technology
Gothenburg, Sweden 2023

Systematic Studies of Triplet Annihilating Species for Photochemical Upconversion
AXEL OLESUND
ISBN: 978-91-7905-887-6
© AXEL OLESUND, 2023

Doktorsavhandlingar vid Chalmers Tekniska Högskola
Ny serie nr: 5353
ISSN: 0346-718X

Department of Chemistry and Chemical Engineering
Chalmers University of Technology
SE-412 96 Gothenburg
Sweden
Telephone +46 31 772 1000

Cover: Illustration of solar-driven photochemical upconversion, with some of the investigated annihilator species being presented in a sample.

Printed by Chalmers digitaltryck
Gothenburg, Sweden 2023

Systematic Studies of Triplet Annihilating Species for Photochemical Upconversion
Axel Olesund
Department of Chemistry and Chemical Engineering
Chalmers University of Technology

ABSTRACT

With climate change already setting new temperature records and causing more extreme weather events, transitioning to clean and renewable energy sources is more urgent than ever. Solar energy harvesting arguably holds the most promise with the abundance of terrestrial sunlight available. However, significant improvements to existing solar technologies would be beneficial as large parts of the solar spectrum currently can not be properly exploited in devices.

Triplet-triplet annihilation photochemical upconversion (TTA-UC) is a process in which the interplay between a light-absorbing sensitizer and an emissive annihilator compound renders the conversion of low-energy to high-energy light; a promising prospect for existing solar devices. Photovoltaic systems require incident photons that hold an energy above a certain threshold value called the band gap, and TTA-UC could be used to make use of photons with energies below the band gap of the photovoltaic cell. Additionally, many photochemical reactions require high-energy photons, commonly in the ultraviolet (UV) region, to proceed. TTA-UC provides a pathway towards driving such demanding reactions with visible light instead.

In this thesis, the properties of the annihilator species are investigated in a systematic fashion. TTA-UC is a process dependent on several energy transfer events which are diffusion-controlled in fluid media, but for device incorporation solid state solutions are often needed. Dimers based on diphenylanthracene (DPA) are investigated as potential candidates to take part in *intra*molecular (*i*)TTA-UC, in which the two annihilating triplets emanate from within the same molecule. It is shown that DPA dimers indeed enables *i*TTA-UC, and important insights regarding the underlying mechanism are highlighted.

Visible-to-UV TTA-UC has long suffered from much lower efficiencies than other spectral transformations. Pairing a set of annihilator molecules with nanocrystal (NC) sensitizers based on CdS yield important insights into the energetics regarding NC-sensitized TTA-UC, as well as improved conversion efficiencies when using 2,5-diphenyloxazole as the annihilator. Further improvements are achieved when switching to the organic sensitizer 4CzBN, which when paired with several UV-emitting annihilators yield efficient visible-to-UV TTA-UC. A record visible-to-UV TTA-UC quantum yield of 16.8% is reported for the best-performing system, which is an almost 2-fold improvement on the previous record.

Finally, it is shown that triplet excimer formation competes with TTA in annihilator species based on naphthalene, which will cause TTA-UC efficiencies to decrease. The excimer formation pathway can be modulated by switching the type of substituent used, with more bulky substituents promoting TTA. The collective insights gathered herein provide a road map for future annihilator design, moving us closer to the ultimate goal of harnessing TTA-UC for solar energy conversion.

Keywords: solar energy conversion, photochemical upconversion, triplet-triplet annihilation

To Lisa and Ida

NOMENCLATURE

1,2-DPA$_2$	1,2-bis(10-phenylanthracen-9-yl)benzene
1,3-DPA$_2$	1,3-bis(10-phenylanthracen-9-yl)benzene
1,4-DPA$_2$	1,4-bis(10-phenylanthracen-9-yl)benzene
1-NCA	1-naphthoic acid
3-PCA	Phenanthrene-3-carboxylic acid
4-BCA	Biphenyl-4-carboxylic acid
4CzBN	2,3,5,6-tetra(9H-carbazol-9-yl)benzonitrile
9,9'-PA$_2$	10,10'-diphenyl-9,9'-bianthracene
CdS	Cadmium sulfide
CO_2	Carbon dioxide
cw	Continuous-wave
$^1D^*$	Singlet excimer
$^3D^*$	Triplet excimer
ΔE_{S-T}	Singlet-triplet energy gap
DET	Dexter energy transfer
DPA	9,10-diphenylanthracene
DS	Double sensitization
E_{ph}	Photon energy
eV	Electron volt
f	Spin-statistical factor
FRET	Förster resonance energy transfer
HOMO	Highest occupied molecular orbital
IC	Internal conversion
IR	Infrared
ISC	Intersystem crossing
iTTA-UC	Intramolecular photochemical upconversion
I_{ex}	Excitation intensity
I_{th}	Excitation threshold intensity
k_i	Rate constant for process i
LUMO	Lowest unoccupied molecular orbital
$^1M^*$	Singlet excited monomer
$^3M^*$	Triplet excited monomer
MO	Molecular orbital
MR-TADF	Multiple resonance thermally activated delayed fluorescence
Naph	Naphthalene
NCs	Nanocrystals
ns-TA	Nanosecond transient absorption
O_2	Molecular oxygen
Φ_i	Quantum yield for process i
PPD	2,5-diphenyl-1,3,4-oxadiazole
PPO	2,5-diphenyloxazole
PtOEP	Platinum octaethylporphyrin
PV	Photovoltaics
PWS	Photocatalytic water-splitting
rISC	Reverse intersystem crossing
S_1	First singlet excited state
τ	Lifetime
T_1	First triplet excited state

TADF	Thermally activated delayed fluorescence
TCSPC	Time correlated single photon counting
TET	Triplet energy transfer
TiO_2	Titanium dioxide
TP	*p*-terphenyl
TETA	Triplet energy transfer between annihilators
TTA	Triplet-triplet annihilation
TTA-UC	Triplet-triplet annihilation photochemical upconversion
UC	Upconversion
UV	Ultraviolet
Vis-to-UV	Visible to ultraviolet
VR	Vibrational relaxation

THESIS

This thesis is based on the work performed in the following papers, and will be referred to according to the Roman numerals below in the text:

Paper I **Diphenylanthracene Dimers for Triplet-Triplet Annihilation Photon Upconversion: Mechanistic Insights for Intramolecular Pathways and the Importance of Molecular Geometry**. Axel Olesund, Victor Gray, Jerker Mårtensson, and Bo Albinsson. *J. Am. Chem. Soc.* **2021**, *143(15)*, 5745–5754.

Paper II **Efficient Visible-to-UV Photon Upconversion Systems based on CdS Nanocrystals Modified with Triplet Energy Mediators**. Lili Hou, Axel Olesund, Shameel Thurakkal, Xiaoyan Zhang, and Bo Albinsson. *Adv. Funct. Mater.* **2021**, *31(47)*, 2106198.

Paper III **Approaching the Spin-Statistical Limit in Visible-to-Ultraviolet Photon Upconversion**. Axel Olesund, Jessica Johnsson, Fredrik Edhborg, Shima Ghasemi, Kasper Moth-Poulsen, and Bo Albinsson. *J. Am. Chem. Soc.* **2022**, *144(8)*, 3706-3716.

Paper IV **Bulky Substituents Promote Triplet-Triplet Annihilation Over Triplet Excimer Formation in Naphthalene Derivatives**. Axel Olesund, Shima Ghasemi, Kasper Moth-Poulsen, and Bo Albinsson. *J. Am. Chem. Soc.* **2023**, *145(40)*, 22168-22175.

CONTRIBUTION REPORT

Paper I Performed all photophysical characterization, analyzed all of the data and carried out all simulations. Wrote the paper.

Paper II Performed some photophysical characterization. Analyzed some of the data and wrote the paper together with the other authors.

Paper III Conceived the project. Performed most of the photophysical characterization, analyzed all of the data and took part in the development of new methodology. Wrote the paper.

Paper IV Conceived the project. Performed all photophysical characterization and analyzed all of the data. Wrote the paper.

Synthesis and NMR measurements were carried out by Shima Ghasemi and Dr. Victor Gray. DFT calculations were performed by Prof. Bo Albinsson. The new methodology in Paper III was conceived by Dr. Fredrik Edhborg.

The author has published the following papers not included in this thesis.

Paper A **Untapping Solar Energy Resources**. Bo Albinsson and Axel Olesund. *Nat. Photonics* **2020**, *14(9)*, 528-530.

Paper B **Best Practice in Determining Key Photophysical Parameters in Triplet–Triplet Annihilation Photon Upconversion.**. Fredrik Edhborg, Axel Olesund, and Bo Albinsson. *Photochem. Photobiol. Sci.* **2022**, *21(7)*, 1143-1158.

Paper C **Triplet States of Cyanostar and its Anion Complexes**. Fredrik Edhborg, Axel Olesund, Vikrant Tripathy, Yang Wang, Tumpa Sadhukhan, Andrew Olsson, Niels Bisballe, Krishnan Raghavachari, Bo Laursen, Bo Albinsson, and Amar Flood. *J. Phys. Chem. A* **2023**, *127(28)*, 5841-5850.

CONTENTS

1

Solar Energy Conversion

It should come as no surprise that our society urgently needs to move away from the combustion of fossil fuels. The use of renewable energy sources, with wind and solar energy leading the way,[1] has, luckily, expanded significantly in recent years. Solar energy is particularly promising given its abundance on Earth. More than 10^8 GW of solar power reaches Earth's surface,[2] which translates to about 5000 times more energy than the world energy consumption.[3] Utilization of this energy is a challenging task which will be heavily reliant on further technological progress.

1.1 Unconventional Ways of Breaking the Detailed-Balance Limit in Photovoltaics

Solar energy can be harvested in a number of different ways, of which photovoltaics (PV) represents the most mature technology. A PV cell makes use of the photovoltaic effect and typically consists of a semiconducting material, such as silicon.[4] If the incident sunlight has enough energy it can be absorbed by the PV cell, causing the excitation of an electron, which can then be used for electricity generation. The band gap of the light-absorbing material dictates the energy that incident photons must have to be absorbed by the PV cell. For silicon the band gap lies at 1.12 eV, which translates to infrared (IR) light with a wavelength of around 1100 nm. This means that photons of longer wavelengths (*i.e.*, lower energy) can not be absorbed by a silicon PV cell and are, thus, wasted. Other efficiency losses are caused by, *e.g.*, electron-hole recombination and thermalization. Taken together, the upper efficiency limit of a single-junction silicon PV cell (often called the detailed-balance limit)[5,6] lies just above 30%, meaning that more than two thirds of incident solar energy is wasted. In practice, the efficiencies of commercial silicon-based PV typically lie closer to 20%,[7] further highlighting the potential for improvement in this area. On the lab scale, there are other PV cells with much higher efficiencies, often as a result of combining a number of different materials in the same cell.[8] Efforts aiming at improvements of specific PV systems are of obvious importance, but other less conventional ways of improving efficiencies have gained some attention from the scientific community in recent years. Instead of focusing on making changes to the device itself, these processes instead manipulate the constitution of incoming light. These light conversion techniques can be divided into two segments: downconversion and upconversion.

1.1.1 Downconversion

In downconversion, a photon of high energy is split into two photons of lower energy (Figure 1.1a), and the most studied downconversion technique is called singlet fission.[9] This process could help alleviate the issues regarding thermalization losses in PV cells. When a photon of much higher energy than that of the band gap is absorbed, the excess energy is released as heat, and the absorbed photon produces the same current as any other photon absorbed. If the photon energy is more than twice higher than the band gap, singlet fission could be used to create two photons (or electron-hole pairs) with enough energy to still be used in the PV cell. This requirement on the photon energy is true for photons with a wavelength of 550 nm or shorter for a silicon-based PV cell. In theory, this could boost the efficiency of such devices to above 40%,[10,11] even though more realistic values lie a bit lower.[12] While the details of downconversion and singlet fission are outside the scope of this thesis, it presents an intriguing pathway towards more efficient PV devices.

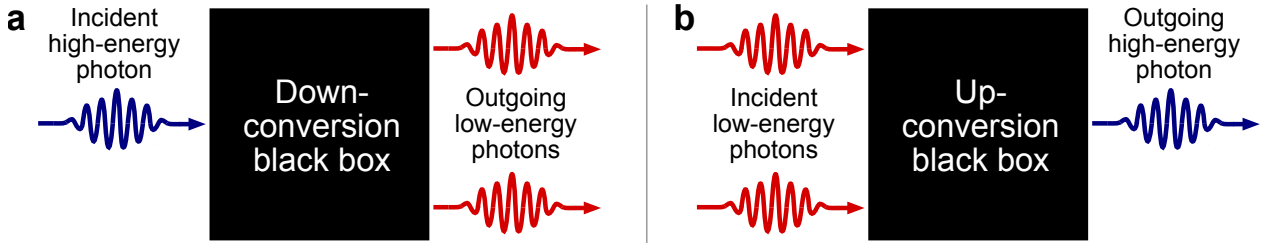

FIGURE 1.1: Simplified schematics of light manipulation processes. (a) In downconversion a high-energy photon is split into two low-energy photons. (b) In upconversion two incident low-energy photons are transformed into one high-energy photon.

1.1.2 Upconversion

On the opposite side we have upconversion, where the energy of two low-energy photons are combined to form a photon of higher energy (Figure 1.1b). There are several different possible upconversion mechanisms to consider. Second-harmonic generation, or frequency doubling,[13] and two-photon absorption[14] are non-linear processes in which the energy from two photons are combined. These processes are useful for several applications within lasing and microscopy, but function only with coherent and rather intense irradiation. This means that their usefulness for solar energy applications is restricted. The same problem is prevalent when doing upconversion using lanthanide ions owing to the weak and narrow absorption bands of lanthanides,[15,16] even though research efforts on combining modified lanthanide-based upconversion systems with PV devices are underway.[17]

Luckily, upconversion may also function using non-coherent, low-intensity light sources, such as sunlight. The process that works under such conditions is called triplet-triplet annihilation upconversion (TTA-UC), or photochemical upconversion.[18,19] This is the process of interest in this thesis, and one that due to its compatibility with low-intensity, non-coherent excitation has gained significant research interest in the last 20 years. While downconversion would be useful for the management of high-energy photons, TTA-UC could instead improve PV efficiencies

by combining the energy of two photons with energies below that of the band gap (Figure 1.2).[20–24] The upconverted photon could then be absorbed by the PV cell. Theory predicts possible efficiencies of silicon-based PV of almost 50%,[25,26] which is perhaps not surprising given that terrestrial sunlight has plenty of photons in the IR part of the spectrum[27] (Figure 1.2, gray spectrum). Whereas there is yet only one example of TTA-UC from below the band gap of silicon,[23,28] several research groups have sought to improve PV efficiencies by the inclusion of TTA-UC systems.[29]

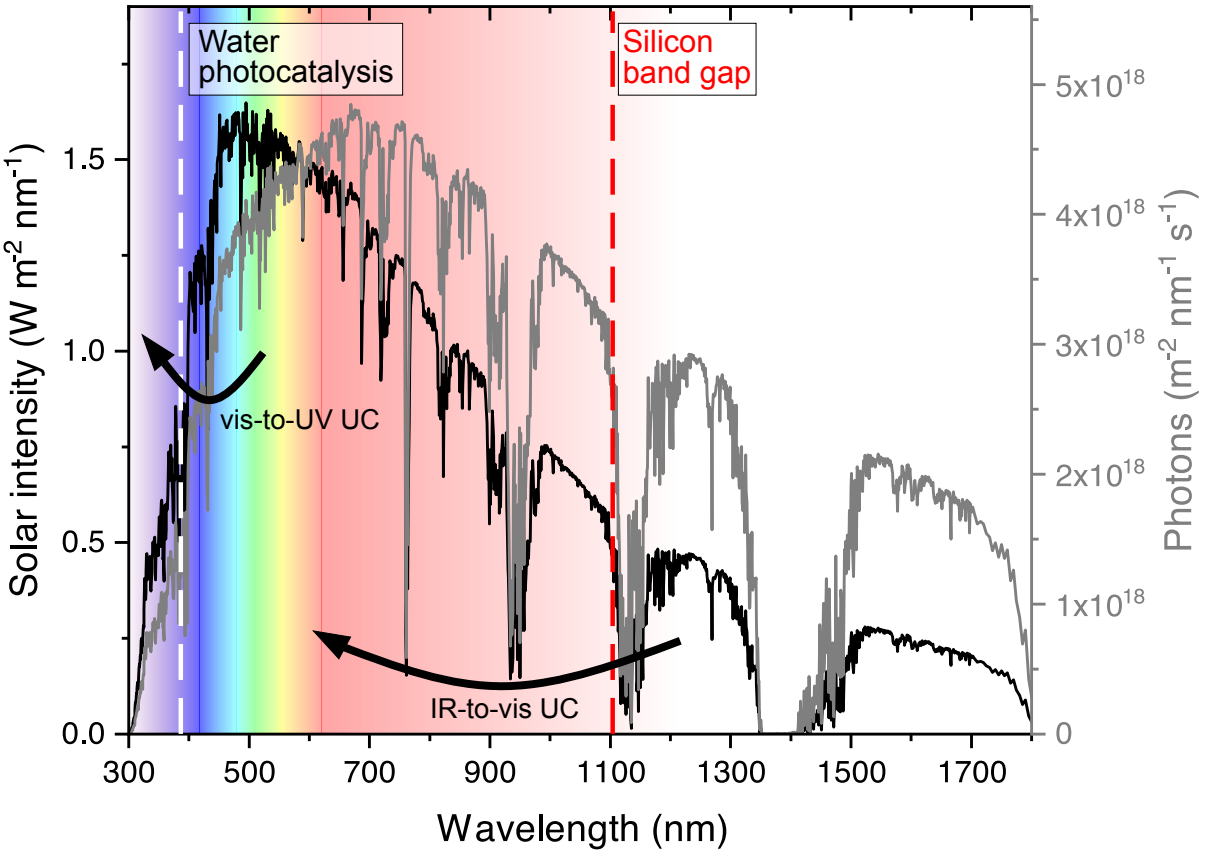

FIGURE 1.2: Terrestrial solar irradiance in units based on energy (black) or number of photons (gray). Dashed lines mark the thresholds for hydrogen production via water photocatalysis (white), and the band gap of silicon solar cells (red), respectively. Spectral data acquired from reference 27.

1.2 Solar Fuels

Photosynthesis is a natural process that plants use to store solar energy in chemical bonds for later use,[30] and is a process that scientists have tried to understand and emulate for decades. Such efforts are often referred to as artificial photosynthesis.[31,32] In the natural process, water and carbon dioxide (CO_2) are transformed into energy-rich hydrocarbons via a complex reaction mechanism involving several electron transfer steps. However, trying to produce solar fuels in a fashion that fully imitates photosynthesis is perhaps not the right way to go, since eventual combustion of such fuels would lead to further CO_2 emission.

There are other ways of storing solar energy in chemical bonds, with hydrogen gas (H_2)

arguably holding the strongest appeal for large-scale application.[33] The appeal of H_2 is manifold: it is abundant, has an energy density about three times higher than typical liquid fossil fuels, and is envisioned to be useful in a wide range of applications.[34] In addition to this, H_2 can be produced during photocatalytic water-splitting (PWS), with water being the only byproduct during combustion, and can also be used in subsequent production of, *e.g.*, ammonia. However, current H_2 production is heavily reliant on fossil fuels,[32] and the development of efficient PWS systems is necessitated.

PWS is a process involving two separate electron transfer steps. It is thermodynamically uphill, and therefore requires external stimuli, *e.g.*, light, to proceed.[35] Since water itself has very limited absorption in the visible range, a light-absorbing catalyst is typically needed. Although PWS functions under visible light irradiation, UV-absorbing catalysts have generally been more successful as most visible light-absorbing catalysts suffer from low stability.[36] In particular, titanium dioxide (TiO_2), which due to a large band gap of 3.2 eV only absorbs in the UV, has been widely employed as a PWS catalyst owing to its suitable energetics, high photochemical stability, and low price.[37–39]

Even though TiO_2 is arguably the most well-studied catalyst for PWS, more recent efforts make use of completely different materials with highly promising results.[40,41] It would, however, be beneficial for the further development of PWS systems if the spectral range of light absorption could be expanded to include the entire visible spectrum, while maintaining the favourable properties of UV-absorbing catalysts. Some attempts at combining TTA-UC with PWS have been undertaken with varying success,[42–48] although most of these use visible light-producing TTA-UC systems.

1.3 Outline and Scope of Thesis

Herein, this thesis contains systematic investigations of the triplet annihilator species, which is one of two interacting species during the TTA-UC process. This thesis aims at improving the understanding of their properties, as well as improving their performance in different TTA-UC systems. In Chapter 1, different light-manipulating techniques and their use for solar energy conversion have been briefly introduced. In Chapter 2, a review of recent advances in the research field of TTA-UC is presented, which is followed by a theoretical section covering the fundamentals of light-matter interactions, as well as important concepts in TTA-UC. Chapter 3 contains the experimental methods used for this thesis, including some details focusing on the kinetics of TTA-UC. The results from Paper I are then presented in Chapter 4, which focuses on annihilator dimers and their performance in *intra*molecular TTA-UC. In particular, important mechanistic insights are collected which will be key for the further development of solid state TTA-UC systems. Chapter 5 covers Paper II-IV, which all focus on improving the performance and understanding of visible-to-ultraviolet (vis-to-UV) TTA-UC systems. This was primarily done by careful examinations of different annihilator compounds and what factors affect their performance in TTA-UC.

2

Photochemical Upconversion

In this chapter, an overview of research within the TTA-UC field is presented to give context to the undertakings of this thesis. A section on the theoretical groundwork in physical chemistry needed for the full understanding of TTA-UC (and other relevant photophysical processes) then follows. This includes a presentation of the materials needed in TTA-UC and their properties, and an explanation of some of the most important parameters that are used when evaluating TTA-UC performance.

2.1 Recent Progress in TTA-UC

The TTA mechanism has been known ever since the 1960's, when Parker and Hatchard first observed delayed fluorescence from solutions of phenanthrene and anthracene.[49] For a long time TTA was perhaps seen as more of a curiosity with no practical relevance, but this was soon to change. About 20 years ago, researchers realized that TTA holds promise as a spectral conversion technique, with potential applications in solar energy conversion.[50–52] A surge of interest then followed, and efficient systems for conversion between different visible wavelengths (primarily green-to-blue) were quite rapidly developed,[42,53] with the first system approaching the theoretical conversion maximum being reported in 2015.[54]

2.1.1 Liquid and Solid State TTA-UC

To achieve TTA-UC two different species are needed, which are called sensitizer and annihilator, respectively. These will be introduced in more detail in Section 2.4, but for now it suffices to state that the TTA-UC process depends on energy transfer between these species, and that they must be in close spatial proximity. Thus, the best-performing systems are typically found in diffusion-controlled environments, *i.e.*, in liquid solvents.[55] The fluid surroundings allow for collisions between the species which promote the energy transfer events.

The archetypal sensitizer-annihilator pair is perhaps that of platinum- or palladium octaethylporphyrins (PtOEP or PdOEP) and 9,10-diphenylanthracene (DPA), which can perform efficient green-to-blue TTA-UC in solution.[56–62] However, implementing TTA-UC systems with PV will require solid state solutions.[63] With the early success of particularly DPA as the annihilator species, several studies on (quasi) solid state TTA-UC followed, albeit with low reported TTA-UC efficiencies.[64,65] Many examples of solid state systems have since then been reported,[63] ranging between polymeric systems,[66–71] gels,[72–76] films,[20,22,77–80] and more. Attempts at combining solid state TTA-UC with solar energy conversion devices have also been undertaken,[81–86] but these systems must be improved to have practical relevance.

The decent efficiency of several of the solid state systems are due to the soft nature of the chosen media, which allows for some molecular diffusion to still take place. Alternatively, the TTA-UC process could proceed in an *intra*molecular fashion, with the TTA step specifically taking place within a single annihilator molecule. Such systems could overcome the need for molecular diffusion, and would instead rely on exciton migration within a multichromophoric annihilator. A few reports on such systems exist,[67,69,76,87,88] but a better mechanistic understanding of the underlying processes is needed to make such systems viable for solid state applications.

2.1.2 Visible-to-Ultraviolet TTA-UC

Using TTA-UC to drive photochemical transformations have been the subject of numerous studies, but these have primarily been performed using spectral conversion within the visible or (near-)infrared region.[89–93] While a few studies have harnessed TTA-UC to drive demanding reactions with blue[46,94–98] or green[99,100] light, the development of such systems have been hampered by low or moderate vis-to-UV TTA-UC efficiencies.

Pioneering work was done by the Castellano group in 2009, reporting the first vis-to-UV TTA-UC system employing 2,5-diphenyloxazole (PPO) as the annihilator and biacetyl as the sensitizer.[101] The TTA-UC quantum yield (Φ_{UC}, which due to the 2-to-1 nature of TTA has a theoretical maximum of 50%) was below 1%, and subsequent efforts only saw minor efficiency improvements. A breakthrough was achieved in the early 2020's, when the first reports on vis-to-UV TTA-UC with Φ_{UC} above 10% was reported, utilizing a new annihilator chromophore based on naphthalene.[102,103]

Since then interest have increased even more, with numerous studies on new sensitizer and annihilator compounds. While PPO has gained the most attention as a UV annihilator,[65,104–109] a few others have also been reported, including terphenyl compounds,[98,107,110] pyrenes,[100,107,111] naphthalene and oxazole derivatives,[95,98,99,112–114] and compounds based on biphenyl[115–117] and benzene.[96] The vis-to-UV TTA-UC systems have also employed a plethora of different sensitizers, including metal complexes,[95,98,100,102,108,111,113,116] organic compounds,[94,99,101,103,107,110,114] and inorganic nanocrystals.[104,105,109,117] Despite these efforts, the field struggles with finding sensitizer/annihilator pairs that can match the performance of the best blue light-generating TTA-UC systems, which yield Φ_{UC} of around 40%.[54,118] Efficiency improvements will be needed to further enable the incorporation of vis-to-UV TTA-UC in photochemical transformations schemes in general, and in PWS systems in particular.

2.2 Fundamentals of Light-Matter Interactions

Light consists of propagating perpendicular electric and magnetic fields that move through space. These fields are oscillating in a wavelike fashion, with the distance between two maxima being defined as the wavelength (λ) of the light. As was shown in Figure 1.2, terrestrial sunlight mainly consists of visible light (400 nm $< \lambda <$ 750 nm), but also an appreciable amount of (near)-IR light (750 nm $< \lambda <$ ~20 μm), as well as small amounts of UV light (100 nm $< \lambda <$ 400 nm).

With the advent of quantum mechanics came important realizations regarding the fundamental properties of light and matter. Several scientists in the early 1900's laid the foundation to what is known as the wave-particle duality, stating that all particles also possess wavelike properties. This is particularly true for light: it has wavelike properties such as a wavelength, but can also be seen as particles holding well-defined quanta of energy. Light particles are called photons, and their energy (E_{ph}) relates to the wavelength of the electromagnetic field via Planck's constant ($h = 6.626 \times 10^{-34}$ J s) and the speed of light ($c = 2.998 \times 10^{8}$ m s^{-1}) using Equation 2.1.

$$E_{ph} = \frac{hc}{\lambda} \tag{2.1}$$

From this follows that UV light is of higher energy than visible light, which in turn has higher energy than IR light.

2.2.1 Electronic States

Everything around us consists of atoms. These consist of a nucleus of neutrally charged neutrons and positively charged protons, with negatively charged electrons orbiting the nucleus. These particles, just like photons, possess both wave- and particle-like qualities and must be described using quantum mechanics. Atoms are best described using mathematical functions called wave functions, which when describing the behavior of electrons in atoms and molecules are often referred to as orbitals. These hold information about the probability of finding an electron at a certain point in space around the nuclei. Wave functions also contain information about the energies of a quantum system, which are located at discrete, well-defined levels, in contrast to macroscopic objects. The orbital energies can be extracted from the wave functions using the Schrödinger Equation.[119] Molecules are made up of atoms, and as such are also subject to quantum mechanical treatment. Their wave functions are called molecular orbitals (MOs) and are created through linear combinations of atomic orbitals. From hereon, we will mainly focus on the properties of molecules.

The quantum states of electrons are important when describing molecules. Electrons in atoms are defined by four different quantum numbers, each describing either the energy, angular momentum, orientation, or spin. To understand the electronic states which are of importance for this thesis, we will focus on the electron spin property. Electrons are fermions, which are particles that are defined by possessing a spin of either +1/2 (spin up) or -1/2 (spin down). The Pauli exclusion principle states that two fermions in a system (*e.g.*, a molecule) can not have the same set of quantum numbers.[120] This means that a MO can hold a maximum of two electrons, and these electrons must have opposite spin. The two electrons are then said to be paired, and the total spin $S = 0$ for the molecule. A molecule with $S = 0$ is said to be in a singlet state. The name stems from the spin multiplicity of a state, which is defined as $2S + 1$. The ground state of molecules are typically singlet states, but also excited states can be singlets (Figure 2.1a).

When defining the state of a molecule it is typically only the electrons in high-energy MOs that must be considered (paired electrons in lower-lying MOs do not contribute to the total spin). The highest occupied MO is called HOMO, and the lowest unoccupied MO is called

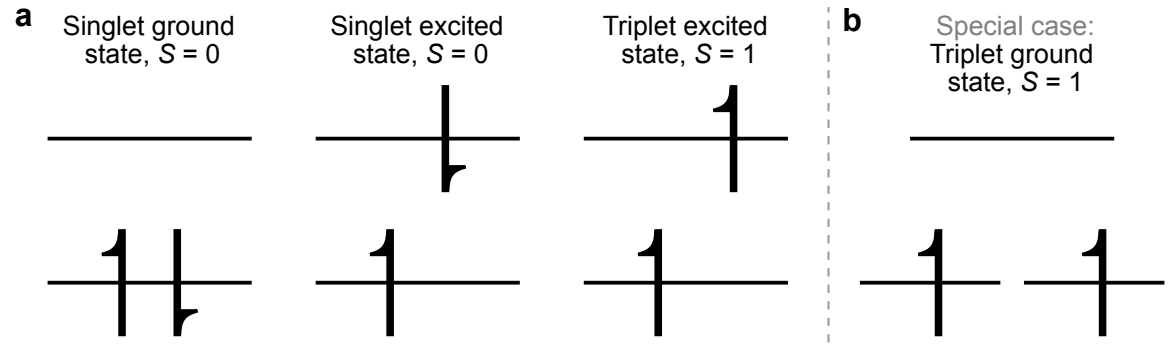

FIGURE 2.1: (a) Electronic structure of singlet and triplet states, with electrons shown as up- or down arrows. Singlet states have a total spin $S = 0$, whereas triplet states have $S = 1$. (b) If the highest occupied MO is degenerate the ground state will be a triplet in some molecules, in accordance with Hund's rule.

LUMO. MOs can be degenerate, *i.e.*, have the same energy, and in some molecules there are degenerate HOMOs. If there are only two HOMO electrons available, Hund's rule stipulates that the total energy will be lower if these electrons have equal spin and occupy different MOs (Figure 2.1b).[121] This leads to a total spin $S = 1$, a spin multiplicity $2S + 1 = 3$, and are, thus, referred to as triplet states. Triplet excited states are common, since these can exist even when there are no degenerate MOs available. In fact, the processes of interest in this thesis heavily depend on the involvement of triplet excited states, as will be detailed further. While almost all molecules have singlet ground states, molecular oxygen (O_2) is one important exception from this rule, having a triplet ground state.[122]

2.2.2 Radiative and Non-Radiative Transitions

TTA-UC is a process that heavily depends on materials that are capable of interacting with light in different ways. When working with optical transitions we only need to consider the electrons occupying frontier MOs (*i.e.*, HOMO and LUMO) as all lower-lying electrons are much more tightly bound to the nuclei, making them inaccessible. The electrons in a molecule can interact with the electromagnetic field of light, which can give rise to several different optical transitions. Light absorption is a common phenomenon that only occurs if Bohr's frequency condition is fulfilled (Equation 2.2). The energy of the absorbed photon must match that of the energy difference between the initial (E_n) and final (E_{n+1}) states.

$$E_{ph} = E_{n+1} - E_n = \Delta E \tag{2.2}$$

With few exceptions, light absorption will move the molecule from its singlet ground state to a singlet excited state. A number of different processes may then take place, as summarized in Figure 2.2. Intramolecular photophysical processes can be categorized into radiative transitions, *i.e.*, events which involve light absorption or emission, and non-radiative transitions. The two main emission events are called fluorescence and phosphorescence. During fluorescence the molecule is deactivated from an excited state to a state with the same spin multiplicity (typically singlet $\rightarrow$ singlet), whereas phosphorescence involves deactivation between states of different

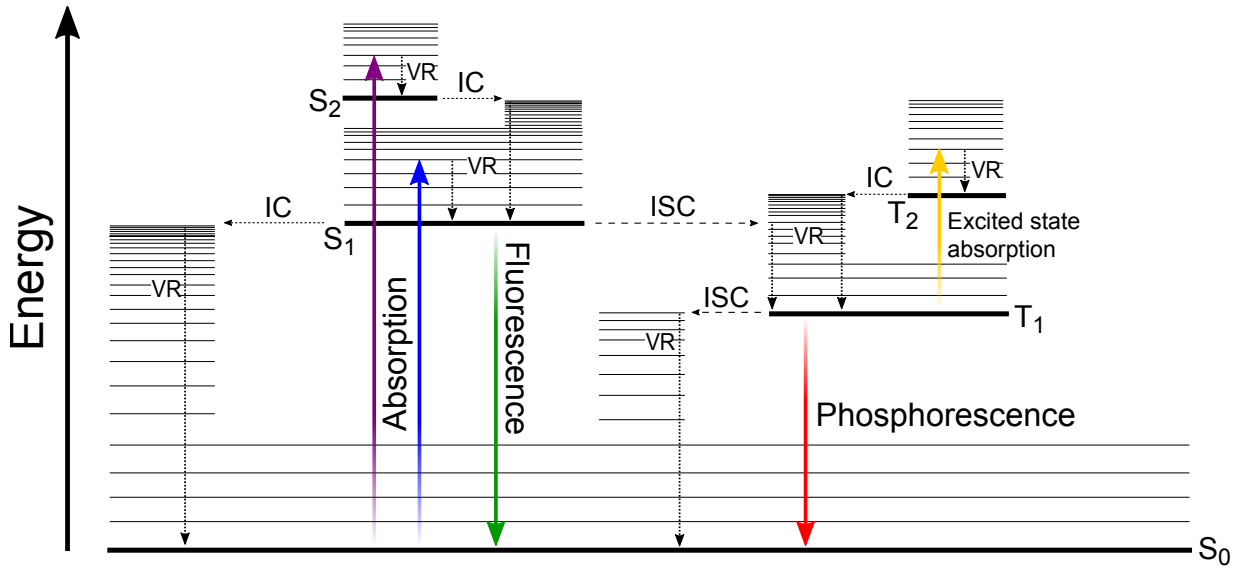

FIGURE 2.2: Jablonski diagram depicting intramolecular photophysical processes. Singlet and triplet states are denoted S and T, respectively, with subscripts indicating ground state (0) or excited states (1, 2). Vibrational levels are indicated by thin horizontal lines. VR = vibrational relaxation, IC = internal conversion, ISC = intersystem crossing.

spin multiplicity (typically triplet → singlet). Moving between singlet and triplet states must involve a spin flip of one electron (as can be understood from Figure 2.1), which is a formally forbidden process. This means that phosphorescence is much slower than optically allowed transitions such as fluorescence.[123]

The non-radiative transitions depicted in Figure 2.2 are similarly affected. Internal conversion (IC) is typically much faster than intersystem crossing (ISC), since the latter is a spin-forbidden transition. Due to the close spacing in energy, IC between excited states is particularly fast. The spacing between S_0 and S_1 is typically much larger, which results in that fluorescence becomes competitive with non-radiative decay. Therefore, according to Kasha's rule,[124] fluorescence takes place from the first singlet excited state (S_1), although rare exceptions with S_2 emission are known.[125] Fluorescence typically has rates of 10^8 - 10^9 s^{-1}, resulting in singlet lifetimes (τ) on the order of nanoseconds. Triplet state lifetimes are longer, typically on the micro- or millisecond timescale (sometimes even seconds), owing to phosphorescence and ISC rates on the order of 10^0 - 10^6 s^{-1}. However, ISC between excited states is often much faster, especially in compounds containing heavy elements, which is a result of enhanced spin-orbit coupling.[126] Excited states can also absorb light, leading to the population of even higher-lying states.

2.2.3 Thermally Activated Delayed Fluorescence

Hund's rule stipulates that triplets will always have a lower energy than the corresponding singlet state. The singlet-triplet energy difference, ΔE_{S-T}, is quite large in most molecules, but by clever molecular design in which the exchange energy is minimized owing to spatial

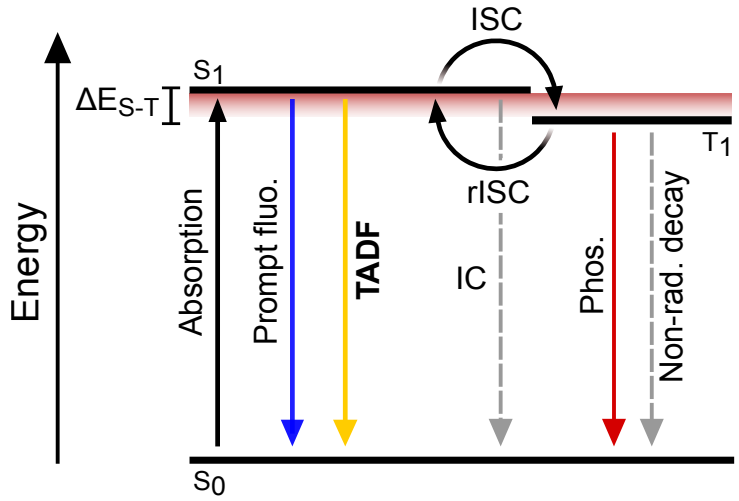

FIGURE 2.3: Jablonski diagram depicting the different processes involved in thermally activated delayed fluorescence (TADF).

separation of HOMO and LUMO, ΔE_{S-T} can be minimized.[127] A small ΔE_{S-T} enables reverse intersystem crossing (rISC), in which the molecule moves from the first triplet excited state (T_1) to S_1 (Figure 2.3). rISC is a thermally activated process with a rate constant (k_{rISC}) that is highly sensitive to both ΔE_{S-T} and temperature (Equation 2.3):

$$k_{rISC} \propto exp\left(-\frac{\Delta E_{S-T}}{k_B T}\right) \tag{2.3}$$

Here, k_B is the Boltzmann constant. rISC will, thus, be faster in molecules with a small ΔE_{S-T}. The fluorescence kinetics in TADF-active molecules will be biexponential with a short component owing to prompt fluorescence, and a long-lived component which is due to TADF.

2.2.4 Quantum Yields and Lifetimes

The performance of different systems, to a large extent, depends on how efficiently certain photophysical processes progress. The efficiency of a specific process is measured using quantum yields, which is a dimensionless parameter. The quantum yield of a process i is denoted Φ_i, and is defined by Equation 2.4.

$$\Phi_i = \frac{\text{number of events}}{\text{number of photons absorbed}} \tag{2.4}$$

This definition will in turn give rise to different expressions for Φ_i, which are often based on the rate constants of relevant processes. To exemplify this, the fluorescence quantum yield (Φ_f) of a compound is given by Equation 2.5a, in which k_f is the rate of fluorescence, and k_{nr} is the rate of all non-radiative processes from S_1. In some instances, it can be more convenient to talk about the *efficiency* of a certain process. The rISC efficiency (η_{rISC}) of TADF-active compounds relates to the rates of all processes emanating from T_1 (Equation 2.5b), but does not specifically take into account the absorption and ISC events needed to populate T_1 in the first place.

$$\Phi_f = \frac{k_f}{k_f + k_{nr}} \tag{2.5a}$$

$$\eta_{rISC} = \frac{k_{rISC}}{k_{rISC} + k_{nr} + k_{ph}} \tag{2.5b}$$

Here, k_{ph} is the rate of phosphorescence. Maximizing the quantum yields/efficiencies of the processes of interest is vital for optimizing the performance of a system.

Closely related to quantum yields are lifetimes (τ), which is a measure of the average time a specific state persists. As long as all deactivation processes are (pseudo) first order, the lifetime of a state is given as the reciprocal of the different deactivation rate constants (Equation 2.6).

$$\tau = \frac{1}{\Sigma_j k_j} \tag{2.6}$$

2.3 Intermolecular Interactions

Although intramolecular interactions are vital to the properties of molecules, most natural processes, such as photosynthesis, are highly dependent on complex interplay between different species, *i.e.*, *inter*molecular interactions.[128]

2.3.1 Excimer Formation

The electronic structure of a molecule will change when moving to an excited state, which can lead to electronic interactions that are not possible in the ground state. As the concentration of a fluid, flat-aromatic molecular solution increases, the fluorescence spectra often change, with a broad, structure-less emission feature at longer wavelengths appearing. This emission emanates from excited dimers, or excimer, states of the molecule. The first and most famous example of excimer fluorescence is that of pyrene, which starts forming excimers already below millimolar concentrations.[129–131] Singlet excimers are formed when a singlet excited monomer ($^1M^*$) interacts electrostatically with a ground state moiety (^1M) in an attractive fashion. As the excimer decays back to the ground state, it again dissociates into separate molecules (Equation 2.7a). While singlet excimers ($^1D^*$) are more common, triplet excited states ($^3M^*$) may also partake in excimer formation, resulting in triplet excimers ($^3D^*$, Equation 2.7b).[131,132] Excimer fluorescence ($h\nu_1$) or phosphorescence ($h\nu_2$) may or may not be emitted from the excimer before dissociating.

$$^1M^* \ + \ ^1M \ \rightarrow \ ^1D^* \ \rightarrow \ ^1M \ + \ ^1M \ (+ \ h\nu_1) \tag{2.7a}$$

$$^3M^* \ + \ ^1M \ \rightarrow \ ^3D^* \ \rightarrow \ ^1M \ + \ ^1M \ (+ \ h\nu_2) \tag{2.7b}$$

Excimers form not only according to the intermolecular description above, but may also form in an intramolecular fashion. Excimer formation is then independent on concentration, but instead sensitive to temperature and choice of solvent. This is because the interacting moieties must

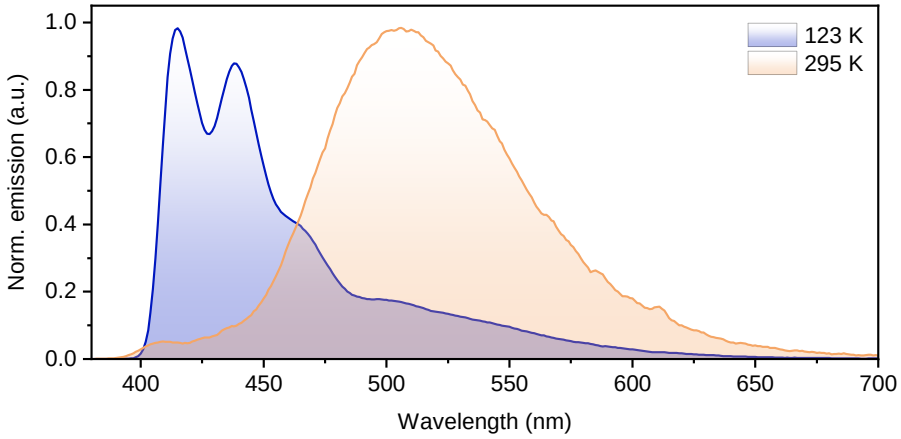

FIGURE 2.4: Example of monomeric and excimeric emission from a dimer molecule. At high temperature (orange), the formation of an intramolecular excimer proceeds efficiently, leading to long-wavelength emission. At low temperature (blue), excimer formation is prevented by the surrounding solvent which has formed a glass, and the individual monomers instead primarily emits.

align in the correct way for the excimer to form.[133–135] One such example is given in Figure 2.4 for the dimer molecule 1,2-DPA$_2$ (see Paper I for more details). At room temperature, the dimer easily obtains the favorable excimer conformation, leading to long-wavelength, unstructured excimer emission. At cryogenic temperatures, the structural reorganization is prevented as the surrounding solvent creates a glassy matrix, leading to primarily short-wavelength, vibronically structured emission from the independent monomers.

2.3.2 Excitation Energy Transfer

Other bimolecular interactions of great interest are those concerning excitation energy transfer. Excitation energy can be transferred from an excited donor molecule to a ground state acceptor molecule by two different mechanisms. Förster resonance energy transfer (FRET) is a Coulombic interaction that depends on the dipole-dipole interaction between donor and acceptor,[136] but is not of particular interest in this thesis. The second mechanism is called Dexter Energy Transfer (DET), which is an exchange interaction.[137] The exchange interaction is a purely quantum phenomenon, but can be thought of as the virtual exchange of electrons between donor and acceptor (Figure 2.5).

DET is a radiation-less process which depends on the spatial overlap between donor and acceptor frontier orbitals, meaning that DET can only proceed efficiently if the interacting species are in close proximity (typically <1 nm). Since the electron density exponentially decreases when moving further away from the atomic nuclei, the rate of DET (k_{DET}) is exponentially dependent on the donor-to-acceptor distance (R_{DA}, Equation 2.8).[138]

$$k_{DET} = J\, exp(-2R_{DA}/L) \tag{2.8}$$

Here, L is the effective orbital radius, and J is the spectral overlap as defined in Equation 2.9.

$$J = \int_0^\infty f_D(\sigma)\varepsilon_A(\sigma)d\sigma \tag{2.9}$$

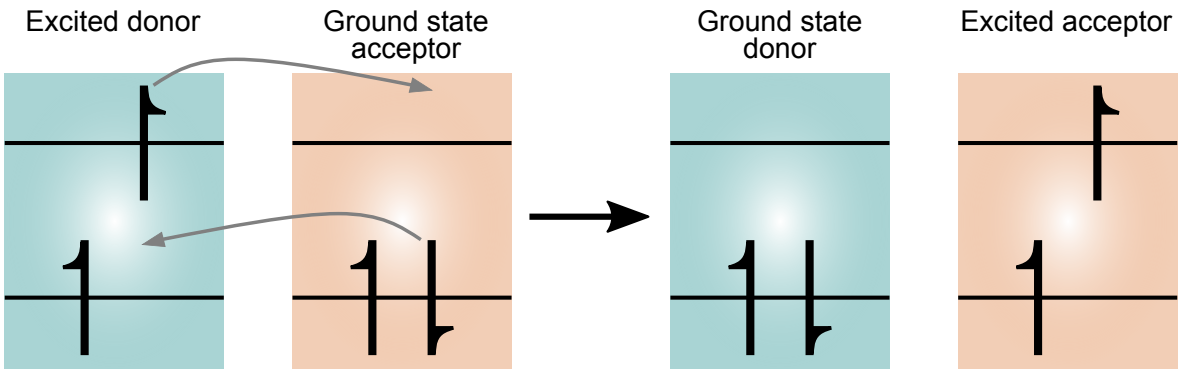

FIGURE 2.5: Dexter energy transfer can be seen as the virtual exchange of electrons between an excited donor and a ground state acceptor. Exemplified here is the transfer of a triplet excitation, with the virtual electron exchange indicated by gray arrows.

Here, f_D is the area-normalized donor emission spectrum, ε_A the area-normalized acceptor absorption spectrum, and σ the wavenumber in cm^{-1}. DET is, thus, promoted for interacting species with substantial spectral overlaps, but is insensitive to, *i.e.*, Φ_f of the donor (which is not the case for FRET).[139] The DET distance dependence means that high efficiencies are most easily achieved in fluid environments, in which collisions between donors and acceptors are responsible for energy transfer. DET is the only mechanism that works for triplet energy transfer (TET), and is therefore vitally important for TTA-UC. As was detailed in Section 2.1.1, achieving high TTA-UC efficiencies in solid state materials is hard, mainly due to difficulties in achieving sufficient donor-acceptor interactions in the absence of diffusional motion.[63]

2.3.3 Triplet-Triplet Annihilation

At the center of photochemical upconversion lies a process called triplet-triplet annihilation (TTA). This is a special type of DET in which two triplet excitations interact in a spin-allowed fashion to form one singlet excited state and one singlet ground-state molecule. This process can proceed with high efficiency if the total energy of the two interacting triplets is higher than the resulting excited singlet state, *i.e.*, if $2 \times E(T_1) > E(S_1)$. The diagram in Figure 2.6 shows the full TTA-UC process from start to finish. As can be seen, its success not only depends on efficient TTA between the species referred to as the annihilators, but also depends on efficient Dexter-type TET from a donor molecule usually referred to as the sensitizer.

2.4 Materials for TTA-UC

The properties of sensitizers and annihilators are key to achieve efficient TTA-UC. The sensitizer is responsible for light absorption, triplet generation, and triplet sensitization of the annihilator via TET (Figure 2.6). To promote TET, all other deactivation, such as non-radiative decay and phosphorescence, from the sensitizer triplet should be as slow as possible. Additionally, it is vital to remove as much oxygen as possible from the sample, since oxygen is an efficient triplet quencher (which will be detrimental to downstream TTA as well).[122] Thus, a long triplet excited

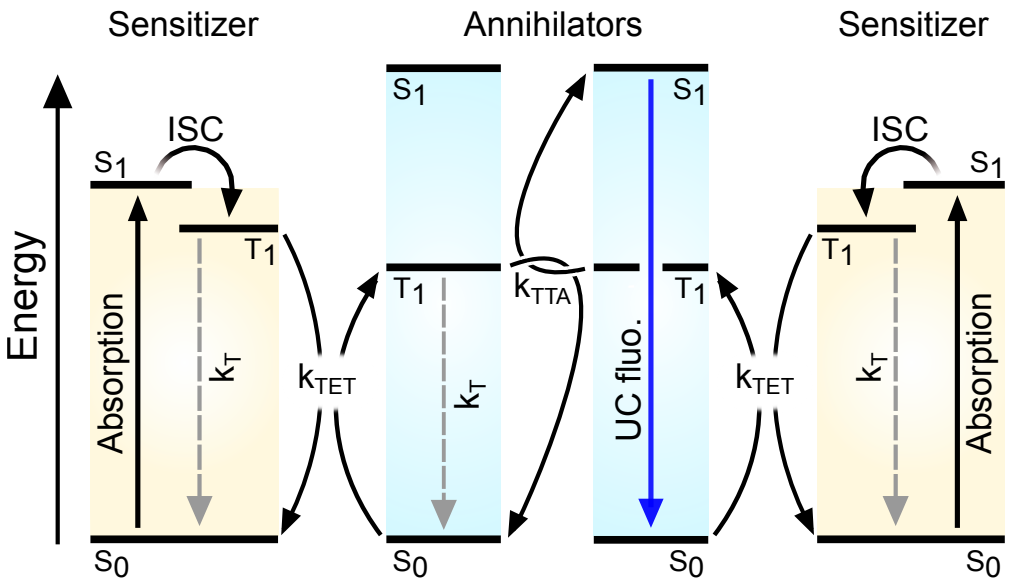

FIGURE 2.6: Jablonski diagram showing how triplet-triplet annihilation photochemical upconversion (TTA-UC) progresses. Rate constants for the most important processes are included as follows: k_T = spontaneous triplet decay, k_{TET} = triplet energy transfer, k_{TTA} = triplet-triplet annihilation.

state lifetime (τ_T) is an important property of a good sensitizer. In addition to this, ΔE_{S-T} should be as small as possible to minimize energy losses. Finally, reabsorption of outgoing light should be avoided as much as possible. The sensitizer absorption should, therefore, optimally not overlap with that of the upconverted fluorescence spectrum in order to maximize the output light intensity.

2.4.1 Triplet Sensitizers

There are several different classes of compounds that fulfil the above-mentioned criteria to a large extent, of which the most widely used are metal complexes and semiconducting nanocrystals (NCs).[19,140] The inclusion of heavy metal elements promotes ISC by means of enhanced spin-orbit coupling,[126] thus facilitating triplet generation in metal complexes (which often include platinum, palladium, iridium etc.) as well as in semiconducting NCs (which often include cadmium or lead).[104,141–146]

A variety of metal complexes have been used for TTA-UC,[52,93,111,116,147–149] with metal porphyrins arguably finding the most widespread use.[55,64,65,81] Porphyrins possess optical properties that are especially suitable in the context of TTA-UC. Their molecular structure gives rise to two distinct, strongly light-absorbing bands which are separated in energy,[150,151] presenting a suitable optical window where upconverted light is subject to little to no reabsorption from the porphyrin. Virtually unity Φ_{ISC}, moderate ΔE_{S-T}, and τ_T often on the order of 100's of μs make metal porphyrins attractive sensitizer options.[60,69,152]

Semiconducting NCs (often referred to as quantum dots) are a class of materials made up from small groupings of atoms in crystal arrangements. The nanoscale of these materials gives them interesting properties that distinguish them both from molecules and from their bulk counterpart. The band gap of NCs can be controlled by the size of the NCs, with a

larger diameter giving a smaller band gap.[153] The optical properties of NCs may, thus, be synthetically controlled with precise control over the band gap. Timely enough, the Nobel Prize in Chemistry was recently awarded to pioneers in the field of semiconducting NCs: Louis Brus, Alexey Ekimov, and Moungi Bawendi.[154]

Together with a negligible ΔE_{S-T}, strong light absorption, and efficient triplet generation,[155] NCs hold several of the properties one would look for in a sensitizer. Significant drawbacks are, however, found in their substantial high-energy absorption, which in the context of TTA-UC will lead to significant reabsorption of upconverted light. Additionally, their excited state lifetimes are often orders of magnitude shorter than for molecular sensitizers. Stemming from the first observation of TET from NCs to surface-bound molecules,[141] τ_T of such sensitizers are typically elongated using organic mediator molecules which bind to the NC surface via anchoring groups.[141,156,157] There are also recent examples of triplet sensitizing NCs free of toxic cadmium or lead, including InP,[158] $CuInS_2$,[159] and $CuInSe_2$.[160]

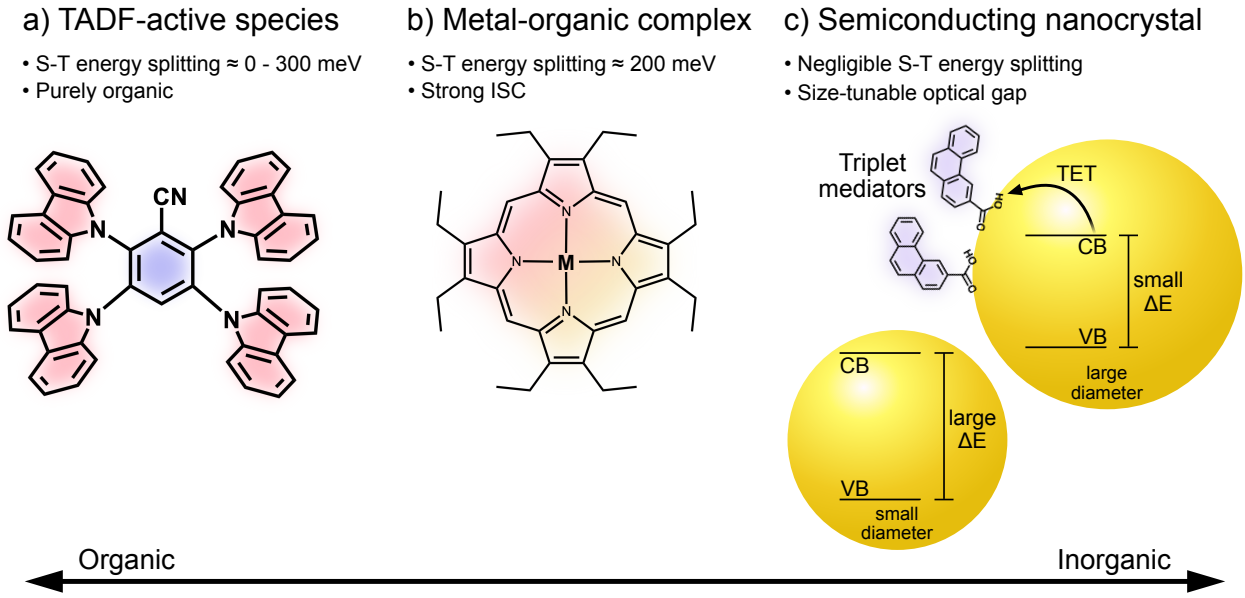

FIGURE 2.7: Three different classes of triplet sensitizers, spanning from purely organic to inorganic. (a) TADF-active species, (b) metal-organic complexes, and (c) semiconducting NCs.

Due to the scarcity and cost of rare earth metals such as platinum and iridium, the search for purely organic sensitizers has seen a surge in recent years. While organic triplet sensitizers such as benzophenone and biacetyl are well-known, these display very poor light absorption with molar absorptivities as low as ∼10-100 M^{-1} cm^{-1} at relevant wavelengths, deeming them unsuitable as triplet sensitizers.[161,162] The last decade has seen an explosion in research on TADF-active materials, which due to their ability to efficiently convert triplets into singlets via rISC are attractive as emitter materials in organic light-emitting diodes.[163–165] TADF-active molecules also possess efficient ISC, small to moderate ΔE_{S-T}, τ_T in the μs regime,[166] and decent light absorption. A TADF-active molecule was first used as a sensitizer for TTA-UC in 2015,[167] but several examples have since then followed with promising results.[110,115] A special class of TADF-active materials, showing multiple resonance (MR)-TADF, has also recently

been used as sensitizers for TTA-UC, and are especially interesting due to stronger and more narrow absorption than conventional TADF compounds.[99,114] A summary of the three classes of sensitizers presented above is found in Figure 2.7.

2.4.2 Triplet Annihilators

The properties of the annihilator species, which can undergo TTA between two T_1 states to form S_1 and S_0 states (Figure 2.6), are crucial to the performance of TTA-UC systems. The interplay between sensitizer and annihilator requires that this donor-acceptor pair is chosen appropriately in terms of excited state energetics. Specifically, for TET to be thermodynamically favored it is beneficial if T_1 of the annihilator lie energetically slightly below T_1 of the sensitizer,[168,169] even though endothermic TET can be accessible.[170,171] τ_T should, as for the sensitizer, be as long as possible (preferably in the ms regime) to provide ample time for annihilator triplets to collide and interact. Even though the S_1 state could be exploited directly, most studies so far rely on fluorescence as the final step. For such systems to perform with highest possible efficiency, the annihilator must have a high Φ_f. Finally, the internal energy alignment of the excited states is important. As mentioned earlier, for TTA to proceed the energy requirement $2 \times E(T_1) > E(S_1)$ should be fulfilled (although endothermic TTA has been reported in, *e.g.*, rubrene).[78,172] Annihilator materials are typically based on polycyclic aromatic hydrocarbons, with 2,5-diphenyloxazole (PPO, emits UV light),[65,94,101,104] 9,10-diphenylanthracene (DPA, emits blue light),[42,51,57,58,64,173] and rubrene (emits yellow light)[78,172,174,175] representing annihilators that have been widely used for different spectral regimes.

2.5 Key Performance Metrics in TTA-UC Systems

Having introduced the different species needed for TTA-UC, it is time to look at the system as a whole. There are several different metrics used when evaluating the performance of TTA-UC systems, and these are in most cases related to each other in some way.

2.5.1 The TTA-UC Quantum Yield

The overall efficiency of a TTA-UC system is measured with the upconversion quantum yield (Φ_{UC}). It is usually defined as the ratio between the number of emitted upconverted (high-energy) photons and absorbed low-energy photons. Since the production of one upconverted photon requires the absorption of two low-energy photons (Figure 2.6), the theoretical maximum of Φ_{UC} is 50%. Some authors choose to normalize this value so that the reported values are out of a 100% theoretical maximum, and are then usually referred to as the upconversion efficiency (denoted with either Φ'_{UC} or η_{UC}).[176] In this thesis, the 50% theoretical maximum definition of Φ_{UC} will be used throughout.

Φ_{UC} can be thought of as the product of the quantum yield of each process leading up to the final emission of the upconverted photon (Equation 2.10). If the quantum yield of ISC, TET, TTA, or fluorescence is low, then Φ_{UC} will also be low. However, in oxygen-free and optimized systems these quantum yields have the ability to approach unity.

$$\Phi_{UC} = \Phi_{ISC}\Phi_{TET}\Phi_{TTA}\Phi_f \tag{2.10}$$

Φ_{TET} is defined by Equation 2.11, in which k_{TET} is the rate of TET from sensitizer to annihilator, k_T is the rate of first-order spontaneous triplet decay of the sensitizer, and $[\mathrm{A}]_0$ is the annihilator ground state concentration.

$$\Phi_{TET} = \frac{k_{TET}[^1A]_0}{k_{TET}[^1A]_0 + k_T} \tag{2.11}$$

Since k_T is the reciprocal of τ_T, a long sensitizer τ_T will lead to a higher Φ_{TET}. As TET is diffusionally controlled (in liquid environments), the maximum k_{TET} in common non-polar solvents lie around the diffusion limit 10^{10} M^{-1} s^{-1}.[123] Most experimentally measured k_{TET} for exothermic TET lie at or slightly above 10^9 M^{-1} s^{-1}, and are commonly measured using Stern-Volmer kinetics (Equation 2.12). The dynamic quenching of the sensitizer will lead to a decrease in τ_T (or in emission intensity if the sensitizer is emissive), which depends on the amount of quenching agent (*i.e.*, annihilator) that is present. A linear relationship between τ_T and $[^1\mathrm{A}]_0$ should then be obtained, in accordance with the Stern-Volmer equation below.[123]

$$\frac{\tau_0}{\tau} = \frac{I_0}{I} = 1 + k_{TET}\tau_0[^1A]_0 \tag{2.12}$$

Using a sensitizer with $\tau_0 \approx 100$ μs, such as PtOEP,[152] then necessitates a $[^1\mathrm{A}]_0 \approx 1$ mM to achieve Φ_{TET} above 99% for typical TTA-UC systems.

A high $[^1\mathrm{A}]_0$ is not only helpful to promote TET. The result of efficient TET is a high concentration of triplet excited annihilators, $[^3\mathrm{A}^*]$, on which TTA depends quadratically. The kinetics of TTA-UC and the experimental determination of Φ_{TTA} are covered in Section 3.3, but for now it is sufficient to conclude that efficient TET results in high $[^3\mathrm{A}^*]$, which in turn leads to higher Φ_{TTA}.

Φ_{UC} is commonly determined using relative actinometry. The integrated emission intensity (I) of the UC sample is then compared to that of a reference sample, which consists of a fluorophore with a known Φ_f. Taking into account also the absorption at the excitation wavelength (A) and the refractive index (η) of the solvents used for each sample, Φ_{UC} is determined using Equation 2.13.

$$\Phi_{UC} = \Phi_{f,r}\left(\frac{1-10^{-A_r}}{1-10^{-A_{UC}}}\right)\left(\frac{I_{UC}}{I_r}\right)\left(\frac{\eta_r}{\eta_{UC}}\right)^2 \tag{2.13}$$

Here, UC and r subscripts denote UC and reference sample, respectively. Depending on the ultimate purpose of the TTA-UC system, different definitions of Φ_{UC} are of interest. When investigating the intrinsic properties of annihilators it is often useful to measure the generated Φ_{UC}, denoted $\Phi_{UC,g}$.[176] This is a measure of the number of UC photons being emitted from the sample in absence of any reabsorption. As visualized in Figure 2.8, UC samples often have very strong absorption at higher energies. This leads to reabsorption of some of the upconverted photons, causing the observed UC spectrum to diverge from the fluorescence spectrum of an optically dilute sample of the annihilator. At longer wavelengths the sample absorption is typically lower, and the observed emission matches that of pure fluorescence well. Making

a proper fitting to the observed UC spectrum then gives the spectrum one would observe if reabsorption was not a factor (dashed line in Figure 2.8), and its integrated emission intensity can be used in Equation 2.13 to obtain $\Phi_{UC,g}$. Using this definition of Φ_{UC} is crucial when evaluating some system properties, *e.g.*, the spin-statistical factor, a metric which is otherwise underestimated.

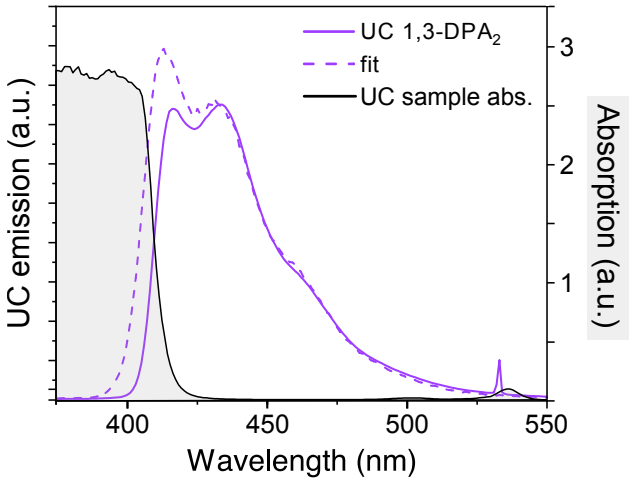

FIGURE 2.8: The measured UC emission from a sample with 6.6 μM PtOEP (sensitizer) and 1 mM 1,3-DPA$_2$ (annihilator, solid purple) does not perfectly match the fluorescence of an optically dilute sample of 1,3-DPA$_2$ (dashed) at shorter wavelengths due to reabsorption of UC emission by the sample itself.

2.5.2 Spin-Statistics of TTA

Although the theoretical maximum of Φ_{UC} is 50%, there are few systems that reach above 20%. The reason for this relates to the spin-statistics which dictate the products of TTA. In the absence of a magnetic field, there are three triplet eigenstates degenerate in energy (Equation 2.14). In the $|s,m\rangle$ notation below, s (which is 1 for all triplets) is the total spin of the state, and m is the spin projection onto the system's z axis.

$$|1,1\rangle = \uparrow\uparrow \tag{2.14a}$$

$$|1,0\rangle = \frac{1}{\sqrt{2}}(\uparrow\downarrow + \downarrow\uparrow) \tag{2.14b}$$

$$|1,-1\rangle = \downarrow\downarrow \tag{2.14c}$$

When two strongly-exchange coupled triplets interact, the spin-statistics dictate that there are nine possible outcomes: five quintet states, three triplet states, and one singlet state. Quintet states require the simultaneous excitation of two electrons and often lie much higher in energy than twice the energy of the interacting triplets. Thus, quintet states are unattainable and may be disregarded in the analysis. The formed triplet, which is typically in the second excited state (T_2), is for most annihilator molecules energetically accessible, which is also the case for the formed S_1 states. The T_2 states will then decay non-radiatively back to T_1. This means

that from the TTA interactions between four triplet pairs (eight T_1 states in total), one singlet excited state is formed and three triplet excited states are regenerated (Equation 2.15).

$$T_1 + T_1 \rightarrow \begin{cases} S_1 + S_0 \\ T_2 + S_0 \rightarrow T_1 + S_0 \text{ (multiplicity of 3)} \end{cases} \tag{2.15}$$

Hence, five T_1 states are destroyed during four TTA events. Out of these five T_1 states, two are used to form the sought-after S_1. This means that the spin-statistical factor (f) for S_1 generation during TTA is 2/5 for most annihilator molecules, which translates to a maximum Φ_{UC} of 20%. It is common that f is also included as a pre-factor in Equation 2.10. Circumventing the limit that f imposes on upconversion efficiencies has been the subject of some research within the field, and includes examples in which T_2 is energetically inaccessible[54,118] as well as cases in which the T_2 state can be converted to S_1 via high-level reverse intersystem crossing.[177–179]

2.5.3 Excitation Threshold Intensity

Apart from having a high efficiency of the overall TTA-UC process, it is also important to consider under what conditions the highest possible efficiency can be reached. It was previously noted that achieving a high $[^3A^*]$ is vital to reach high TTA efficiencies. $[^3A^*]$ is a product of TET from $[^3S^*]$, which in turn is dependent on the intensity of incident excitation light (I_{ex}). At low I_{ex}, $[^3A^*]$ will be low and the annihilator triplets will primarily decay through first-order processes. At high I_{ex}, $[^3A^*]$ will be high, thus making TTA the dominating decay mechanism. The transition between these regimes is defined in terms of the excitation threshold intensity (I_{th}, Figure 2.9a), which is the excitation intensity at which half of the triplet annihilator population decays through TTA. In the high-intensity regime ($I_{ex} > I_{th}$), the intensity of upconverted light will be linearly dependent on I_{ex}, which means that Φ_{UC} reaches a saturation value (Figure 2.9b). In the low-intensity regime ($I_{ex} < I_{th}$), the output light intensity is instead quadratically dependent on I_{ex}, and Φ_{UC} will increase with I_{ex}.

Under steady-state conditions and under the assumption that TET from sensitizer to annihilator is efficient, I_{th} is defined by Equation 2.16.

$$I_{th} = \frac{k_T^2}{2k_{TTA}\alpha[^1S]_0} \tag{2.16}$$

Here, k_T and k_{TTA} are the rate constants for first- and second-order annihilator triplet decay, respectively, α is the absorption cross-section of the sensitizer (cm^2), and $[^1S]_0$ is the sensitizer ground state concentration. I_{th} is, thus, a system parameter which is influenced by the properties of both the sensitizer and the annihilator. For solar applications, a low I_{th} is sought after. Optimally, I_{th} should lie at or below the intensity of incident sunlight integrated over the absorption of the sensitizer, as this would maximize the system efficiency also using sunlight. For some applications, a high I_{th} is instead wanted. This is the case for applications in which the quadratic dependency on I_{ex} is important for their functionality, such as when TTA-UC is used for 3D printing.[180] It should be noted that the traditional method of determining I_{th}, as visualized in Figure 2.9a, for a long time was thought to give I_{th} exactly at the crossing point between the quadratic and linear regimes. However, this was recently put under scrutiny,[181]

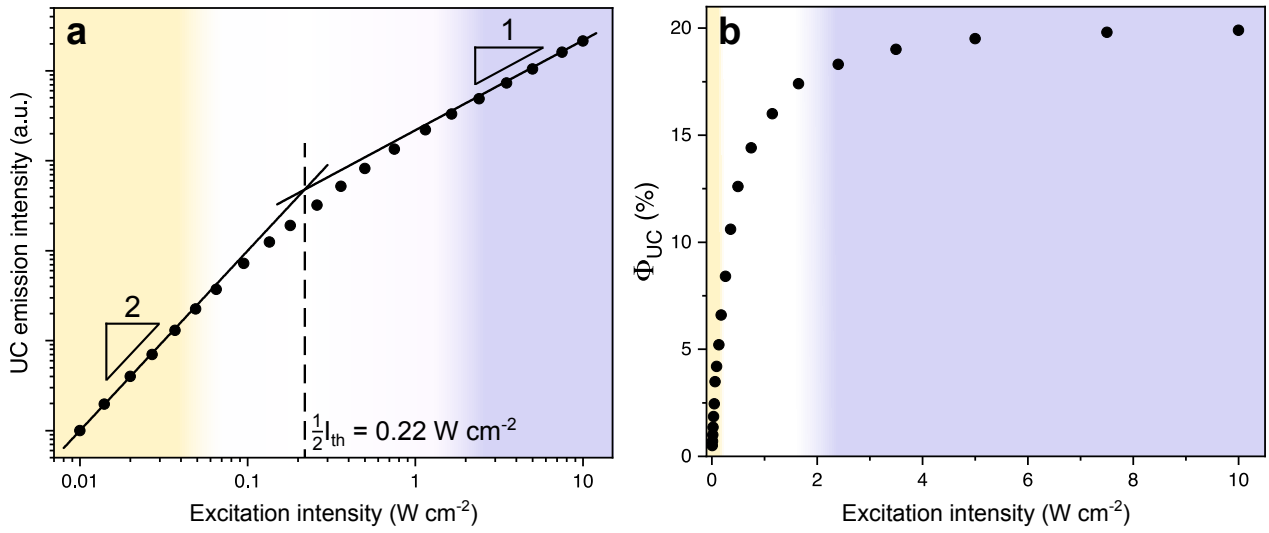

FIGURE 2.9: Excitation intensity (I_{ex}) dependence on (a) TTA-UC emission intensity, and (b) Φ_{UC}. In the low-intensity regime (yellow) the emission intensity quadratically depends on I_{ex}, giving a linear slope of ∼2 on a log-log plot. At high I_{ex} TTA dominates, yielding a linear dependence on I_{ex} (slope ∼1) and a saturated value for Φ_{UC}.

and it has been shown that the crossing point in reality corresponds to the value of $\frac{1}{2}I_{th}$. This shortcoming shall be overcome with the new methodology presented in Section 3.3, in which I_{th} can be extracted also from samples that do not fully converge towards purely quadratic and linear dependencies on I_{ex}.

3

Spectroscopy Methods

Vital to performing research is having a toolbox of methods suited for the specific purpose. Spectroscopic techniques lie at the heart of research in photophysics and photochemistry, and in this chapter a brief introduction to the methods used in this thesis are presented.

3.1 Steady-State Measurements

3.1.1 Absorption and Emission of a Liquid Sample

Most photophysical processes are initiated by an absorption event in which the molecule is excited to a higher-lying state. The absorbance of a sample can be calculated using Equation 3.1, which is called the Lambert-Beer law.[182]

$$log_{10}\left(\frac{I_0(\lambda)}{I(\lambda)}\right) = A(\lambda) = \varepsilon(\lambda)cl \tag{3.1}$$

Here, I_0 and I are the light intensities before and after the sample, respectively, $A(\lambda)$ is the absorbance, ε is the molar absorption coefficient (M^{-1} cm^{-1}), c is the sample concentration (M), and l is the path length (cm). The setup for measuring absorption is presented in Figure 3.1a. The detectors measure the transmitted light intensity $I(\lambda)$ for one wavelength at a time, which is selected by the monochromator in front of the sample. The difference in ε at different wavelengths then results in the emergence of an absorption spectrum as the monochromator sweeps over a predefined wavelength interval. Absorption measurements yield information about the presence of different species in a sample, the concentration of those species, as well as information about the presence of different transitions and excitations for a given species.

The emission from a sample can be measured in a similar fashion (Figure 3.1b). A suitable excitation wavelength is chosen using a monochromator and is kept constant throughout the measurement. The emitted light is then measured perpendicularly to the excitation path to avoid any influence from the excitation source. A second monochromator is placed after the sample, sweeping over a predefined wavelength range in order to collect an emission spectrum.

Steady-state emission can be used to determine excited state properties, *e.g.*, fluorescence quantum yields (Φ_f), which is determined by comparing the integrated emission intensity to that of a reference compound with a known Φ_f. It can also be used to investigate the efficiency of energy transfer by measuring how the emission intensity varies as a quencher is added to the sample. Steady-state emission is also important when investigating TTA-UC. To ensure that high TTA-UC efficiencies are reached, a continuous-wave (cw), monochromatic laser is used as

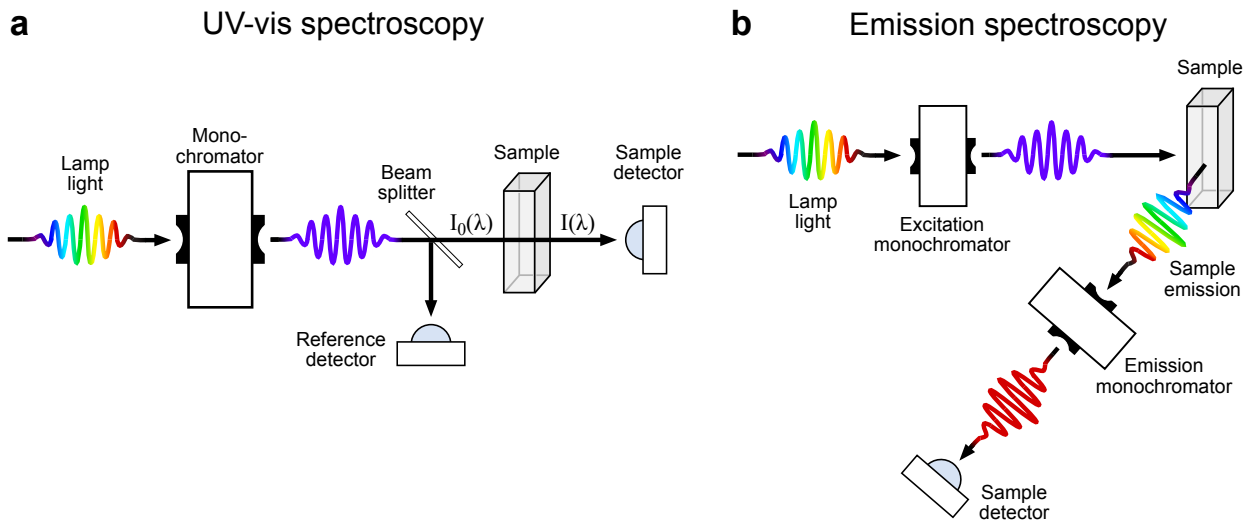

FIGURE 3.1: Experimental setups used for measuring (a) absorption, and (b) emission from a liquid sample.

the excitation source instead of a lamp, thus making the excitation monochromator superfluous in such measurements. The excitation power can be modified by varying the pumping current to the laser, or by placing a neutral density filter between the laser and the sample.

3.2 Time-Resolved Measurements

As evidenced by this thesis, knowing the lifetimes of different states is in many cases pivotal. Time-resolved techniques are then needed, which all rely on using a pulsed excitation source instead of a continuous one.

3.2.1 Determining Lifetimes from Emission

Two different setups are used when measuring time-resolved emission. Lifetimes on the nanosecond timescale (*e.g.*, prompt fluorescence) are measured using time correlated single photon counting (TCSPC). A setup similar to that of Figure 3.1b is used, with the important difference that the laser light is pulsed, typically with a high (MHz) repetition rate. Following each pulse, photons are emitted from the sample. The TCSPC setup is constructed such that only the first photon to reach the detector is observed, and the time it takes for the photon to reach the detector following excitation is measured using specialized electronics. The measurement results are stored in a histogram, which can be analyzed to obtain the lifetime(s) of the emitting species. Prompt fluorescence typically decays mono-exponentially, and the measured intensity is then fitted to Equation 3.2:

$$I(t) = A\ exp(-\frac{t}{\tau_f}) \tag{3.2}$$

where t is time and τ_f is the fluorescence lifetime. If two or more species emit light of the same wavelength, the above expression must be modified to include more exponential terms.

When measuring slower kinetics on the micro- or millisecond timescale, such as phosphorescence or TTA-UC emission, the TCSPC setup is typically not used since the need for slow repetition rates would lead to very time-consuming measurements. Additionally, on these timescales, electronics are fast enough to measure multiple photons per excitation while maintaining a satisfactory time-resolution. In contrast to the TCSPC setup, a Nd:YAG laser equipped with an optical parametric oscillator (OPO) is used to create the pumped excitation light. The use of an OPO allows for facile tuning of the excitation wavelength, ranging from well below 400 nm into the infrared region (>800 nm). It is also possible to use cw diode lasers coupled to a pulse-generating device for excitation, as detailed in Section 3.3. Phosphorescence decay typically follows the mono-exponential behavior of Equation 3.2, whereas TTA-UC emission follows more complex kinetics (see Section 3.3).

3.2.2 Non-Emissive Species and How to Find Them

Transient species are not always detectable by emission, and one must then reside to transient absorption techniques. In nanosecond transient absorption (nsTA),[183] a setup such as that of Figure 3.2a is used. A high-intensity (typically 1 mJ/pulse) short (10 ns) monochromatic pulse, referred to as the pump, excites the sample, leading to excitation of a fraction of the molecules from the ground state to excited states (Figure 3.2b). After a defined time delay Δt, the sample is subject to the probe, which is often a broadband lamp, such as a quartz-halogen lamp. The detector then measures the intensity of transmitted probe light. The measurement is then repeated without any initial pump excitation. Combining these two measurements gives the differential absorption, ΔA, which is calculated according to Equation 3.3. I_+/I_- are the transmitted probe light intensities with and without pump excitation, respectively.

$$\Delta A = log_{10}\left(\frac{I_-}{I_+}\right) \tag{3.3}$$

In contrast to steady-state absorption, ΔA can take both positive and negative values. By using a time-gated CCD camera, spectra such as those in Figure 3.2c are obtained. A positive value (region I and III) is indicative of absorption from an excited state. A negative value (region II) may arise from either the depletion of the ground state (and is then referred to as the ground state bleach) or from emission from the sample.

The differential spectra are typically collected at different Δt, allowing for probing of the transient development of different species. In Figure 3.2c, region I and II follow the same kinetics, which could indicate that these peaks originate from the same transient species. At small Δt (black spectra), large $|\Delta A|$ values are observed in these regions, which then decay toward zero as Δt increases (blue spectra). In contrast, the peak in region III rises with increasing Δt, indicating that this represents a different excited state species which is populated at a slower rate.

The probe can also be chosen to be of a single wavelength. Single-wavelength kinetic traces, such as those shown in Figure 3.2d for region I, II, and III, are then obtained. Such measurements are useful when extracting the lifetimes of the excited state species, rather than only identifying them by analysis of the peak positions.

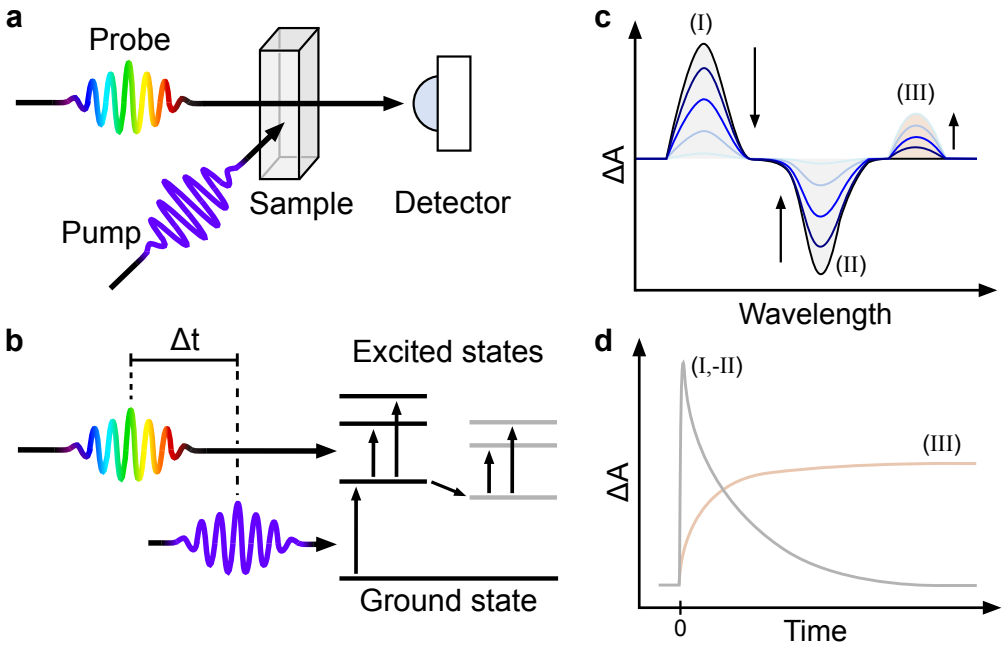

FIGURE 3.2: (a) Schematic of nsTA experimental setup. (b) Schematic of how a nsTA measurement works. The pump excites a fraction of the ground state molecules to an excited state. The probe arrives at a time delay Δt after the pump, probing the transient species present in the sample at time Δt. (c) Both positive and negative ΔA values can be seen. The peaks in region I and II decay to zero as Δt increases, whereas the peak in region III increases with time. (d) The kinetic evolution of the transient species can be analyzed by probing at specific wavelengths. Here, the peaks in region I and II show the same kinetic decay, indicating that these peaks originate from the same species. The peak in region III belongs to a different species, potentially formed from the species probed in region I and II.

3.3 Characterizing TTA-UC Systems with Time-Resolved Emission

To fully characterize a TTA-UC system, a combination of steady-state and time-resolved measurements are needed. TTA-UC emission can be used for determining the TTA-UC quantum yield, Φ_{UC}, the excitation threshold intensity, I_{th}, and the annihilator triplet lifetime, τ_T. The rate constant of triplet-triplet annihilation, k_{TTA}, and the TTA quantum yield, Φ_{TTA}, have typically been extracted from separate TA measurements. While TA measurements are in many cases possible, these are trickier to perform than emission measurements, mainly due to high sensitivity to the pump/probe overlap and, sometimes, complex analysis of the data due to competing absorption and emission events.[58,184]

To facilitate the characterization, a new method has been developed in our group (as reported in Paper B).[169] With this method, I_{th}, τ_T, k_{TTA}, and Φ_{TTA} can be extracted from the same set of time-resolved emission measurements, removing the need for TA measurements entirely, thus making TTA-UC characterization simpler, more efficient, and more accessible.

3.3.1 Theoretical Framework

The fate of annihilator molecules in their T_1 state dictates the kinetics of TTA-UC. Typically, the triplets decay through two different channels in solution. The intrinsic non-radiative decay is a first-order (*i.e.*, mono-exponential) process in which a triplet returns to the ground state. In contrast, the TTA process, in which two triplets interact to form one singlet excited state and one ground state, is a second-order process. The time-evolution of the triplet excited annihilator concentration is then given by Equation 3.4.

$$\frac{d[^3A^*]}{dt} = k_{gen} - k_T[^3A^*] - 2k_{TTA}[^3A^*]^2 \tag{3.4}$$

k_{gen} is the rate of triplet annihilator generation, $k_T[^3A^*]$ is the rate of depopulation through first-order spontaneous decay processes, and $2k_{TTA}[^3A^*]^2$ the rate of depopulation through second-order TTA. The factor 2 in front of k_{TTA} is here explicitly written out to indicate that two triplet annihilators are consumed in each TTA event.

The analytical solution to the decaying terms of Equation 3.4 is well-known,[185] and yields the expression in Equation 3.5 for the decay of triplet annihilators.

$$[^3A^*(t)] = [^3A^*]_0 \frac{1-\beta}{\exp(t/\tau_T) - \beta} \tag{3.5}$$

Here, $[^3A^*(t)]$ is the annihilator triplet concentration, $[^3A^*]_0$ the initial annihilator triplet concentration, τ_T $(= 1/k_T)$ is the intrinsic triplet excited state lifetime, and β is a dimensionless parameter indicating the fraction of initial annihilator triplets that decay through the TTA channel. Since the TTA-UC emission intensity is proportional to $[^3A^*(t)]^2$, it will decay according to Equation 3.6.

$$I_{UC}(t) \propto [^3A^*(t)]^2 = \left([^3A^*]_0 \frac{1-\beta}{\exp(t/\tau_T) - \beta}\right)^2 \tag{3.6}$$

The expression in Equation 3.6 has been used extensively to analyze TTA-UC systems previously, yielding information about the important parameters τ_T and β.

Taking a closer look at the definition of β, one sees that it includes both $[^3A^*]_0$ and k_{TTA} (Equation 3.7). Thus, if $[^3A^*]_0$ was known, k_{TTA} could be extracted from the global fit of TTA-UC decay.

$$\beta = \frac{2k_{TTA}[^3A^*]_0}{k_T + 2k_{TTA}[^3A^*]_0} \tag{3.7}$$

Time-resolved TTA-UC emission measurements are typically performed using a short, high-intensity laser pulse for excitation. When doing so, estimating $[^3A^*]_0$ is very tricky. Conversely, a good estimate of $[^3A^*]_0$ is obtainable if cw excitation is used instead.

3.3.2 Experimental Setup and Data Analysis

In the new method described herein, a diode laser is coupled to a pulse generator to generate a square-shaped excitation pulse of tunable width (Figure 3.3a). The TTA-UC sample is excited for an extended period of time set by the pulse width (typically a few ms), during which the

observed TTA-UC emission will increase as more and more triplet annihilators are formed and subsequently annihilated. After some time, when the rate of triplet generation matches that of triplet depopulation, the emission intensity will reach a steady-state value (Figure 3.3b). At this point, the laser is turned off and the emission signal decays according to Equation 3.6.

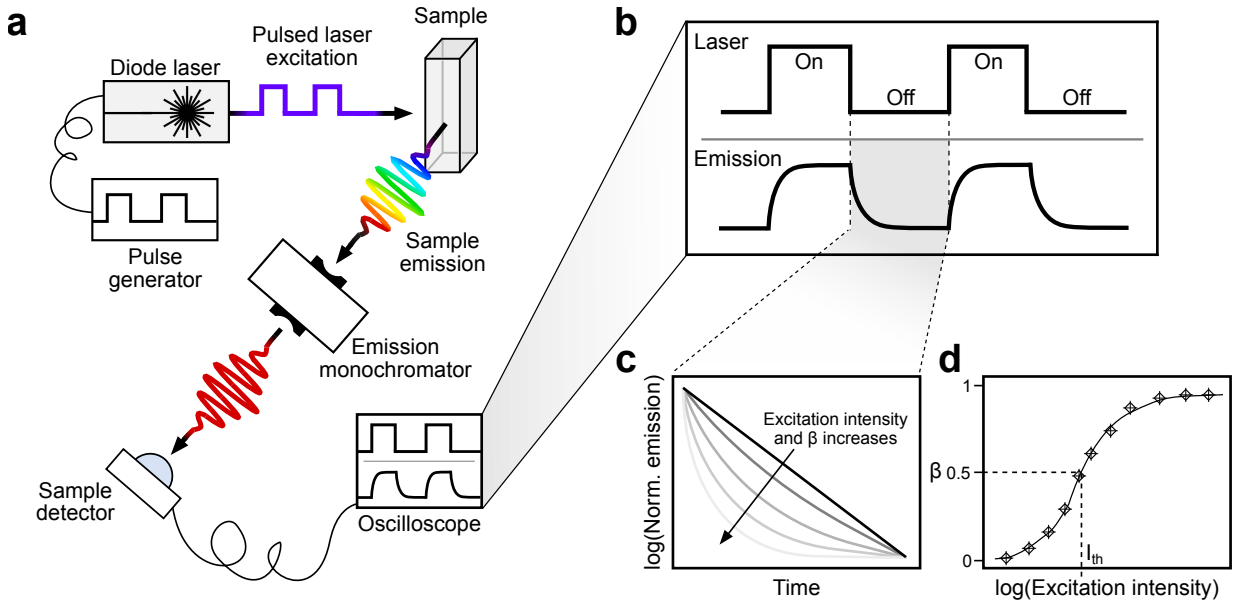

FIGURE 3.3: (a) Experimental setup. (b) The excitation pulse width is tuned such that the measured emission intensity signal is saturated before the laser is turned off. During the laser-off stage, the emission decay is measured as in a normal time-resolved measurement using short-pulsed excitation. (c) I_{UC} will decay faster at higher I_{ex}, yielding higher values of β. Globally fitting τ_T to several measurements collected at different I_{ex} increases accuracy. (d) I_{th} of the system under investigation is found at the I_{ex} yielding $\beta = 0.5$.

Using a cw diode laser in pulsed mode enables having the sample in a well-defined state at the beginning of the emission decay. Since the sample with respect to $[^3A^*]$ is in steady state, and as this steady-state concentration will equal that of $[^3A^*]_0$, Equation 3.4 can be rewritten as Equation 3.8.

$$\frac{d[^3A^*]}{dt} = 0 = k_{ex}\Phi_{ISC}\Phi_{TET} - k_T[^3A^*]_0 - 2k_{TTA}[^3A^*]_0^2 \tag{3.8}$$

The first term corresponds to k_{gen} in Equation 3.4, and includes the quantum yields of inter-system crossing (ISC) and triplet energy transfer (TET), both of which can be obtained from separate experiments. k_{ex} is in turn calculated from Equation 3.9, yielding values from 10^{-5} - 10^{-1} M s^{-1} under typical excitation conditions.

$$k_{ex} = \frac{I_{ex}\lambda(1 - 10^{-A})}{hcN_AV_{ex}} \tag{3.9}$$

Here, I_{ex} is the excitation intensity (W), λ is the excitation wavelength (m), A is the sample absorbance at λ, h is Planck's constant (Js), c is the speed of light (m s^{-1}), N_A is Avogadro's number (mol^{-1}), and V_{ex} is the excitation volume (dm^3). Equation 3.7 and 3.8 make up a

solvable equation system with two unknowns, k_{TTA} and $[^3A^*]_0$. These can now be obtained from time-resolved emission measurements, which are fitted to Equation 3.6 with k_{TTA} and $[^3A^*]_0$ as fitting parameters.

For increased accuracy, one can measure how I_{UC} evolves in time at several different excitation intensities (Figure 3.3c). Altering the excitation intensity will alter $[^3A^*]_0$ and, thus, also β. The set of decays can then be fitted globally using τ_T as a fixed parameter, while β is fitted independently to each decay. This method then yields a reliable value of τ_T while the β values give Φ_{TTA} for each measurement, in accordance with Equation 3.10.

$$\Phi_{TTA} = \frac{1}{2}\beta = \frac{k_{TTA}[^3A^*]_0}{k_T + 2k_{TTA}[^3A^*]_0} \tag{3.10}$$

An additional benefit of measuring a set of decays at different excitation intensities is that I_{th} falls out as a byproduct of the fitting procedure. I_{th} is defined as the steady-state excitation intensity at which half of the excited annihilator triplets decay by TTA. In other words, I_{th} can be found as the excitation intensity which results in $\beta = 0.5$ (Figure 3.3d). From a practical viewpoint, the method presented herein requires far fewer measurements for extracting I_{th} than is needed in the traditional method, which is used in, *e.g.*, Paper I. It can also be useful in situations where intensity measurements are difficult, such as when working with light-scattering samples.

4

Intramolecular Photochemical Upconversion

This chapter focuses on the main findings from Paper I.[184] In this paper, a set of dimer molecules were synthesized and investigated as potential annihilators. The dimeric nature of these molecules, with two identical chromophores covalently linked, allows them to hold two excitons simultaneously. It was envisioned that this would enable TTA to proceed in an intramolecular fashion. We sought to elucidate the mechanism that is responsible for intramolecular TTA-UC (*i*TTA-UC), as there are different mechanistic models for *i*TTA-UC that exist in the literature.

4.1 Models of Intramolecular TTA-UC

Two main models for *i*TTA-UC have been proposed previously, with the main difference lying in how the second of the two triplet excitons is transferred to the annihilator. The first model will be referred to as the *triplet energy transfer between annihilators* (TETA) model.[61,186] Following regular TET from sensitizer to annihilator to populate T_1 of the first of two annihilator moieties (here denoted ^{1}A-^{3}**A***), the second annihilator moiety accepts a triplet exciton from another ^{1}A-^{3}**A*** annihilator via TET (here explicitly denoted TET_2). In the TETA model, TET_2 depends on the relative orientation between the annihilator moieties during their collision, and two other (non)-interactions may also take place (Equation 4.1a).[61]

The second model is called the *double sensitization* (DS) model. TET_2 is here assumed to proceed in a similar fashion to regular TET, with a T_1 sensitizer being responsible for populating both moieties of the annihilator dimer (Equation 4.1b).[67,69,187,188] In both models, *i*TTA may then proceed in ^{3}**A***-^{3}**A*** dimers, forming a ^{1}**A***-^{1}A dimer capable of emitting UC light.

$$\textbf{TETA model:} \begin{cases} {}^1\text{A-}{}^3\mathbf{A^*} + {}^1\text{A-}{}^3\mathbf{A^*} \xrightarrow[50\%]{\text{TET}_2} {}^3\mathbf{A^*}\text{-}{}^3\mathbf{A^*} + {}^1\text{A-}{}^1\text{A} \\ {}^1\text{A-}{}^3\mathbf{A^*} + {}^3\mathbf{A^*}\text{-}{}^1\text{A} \xrightarrow[25\%]{\textit{inter}\text{-TTA}} {}^1\mathbf{A^*}\text{-}{}^1\text{A} + {}^1\text{A-}{}^1\text{A} \\ {}^3\mathbf{A^*}\text{-}{}^1\text{A} + {}^1\text{A-}{}^3\mathbf{A^*} \xrightarrow[25\%]{\text{no interaction}} {}^3\mathbf{A^*}\text{-}{}^1\text{A} + {}^1\text{A-}{}^3\mathbf{A^*} \end{cases} \tag{4.1a}$$

$$\textbf{DS model:} \quad {}^3\text{S}^* + {}^1\text{A-}{}^3\mathbf{A^*} \xrightarrow[100\%]{\text{TET}_2} {}^3\mathbf{A^*}\text{-}{}^3\mathbf{A^*} + {}^1\text{S} \tag{4.1b}$$

The two models are summarized in Figure 4.1, in which the conventional intermolecular pathway (which is present alongside *i*TTA-UC) is also included. The overall TTA-UC performance of

the dimers were evaluated alongside the mechanistic study on *i*TTA-UC, and the results are summarized in the following section.

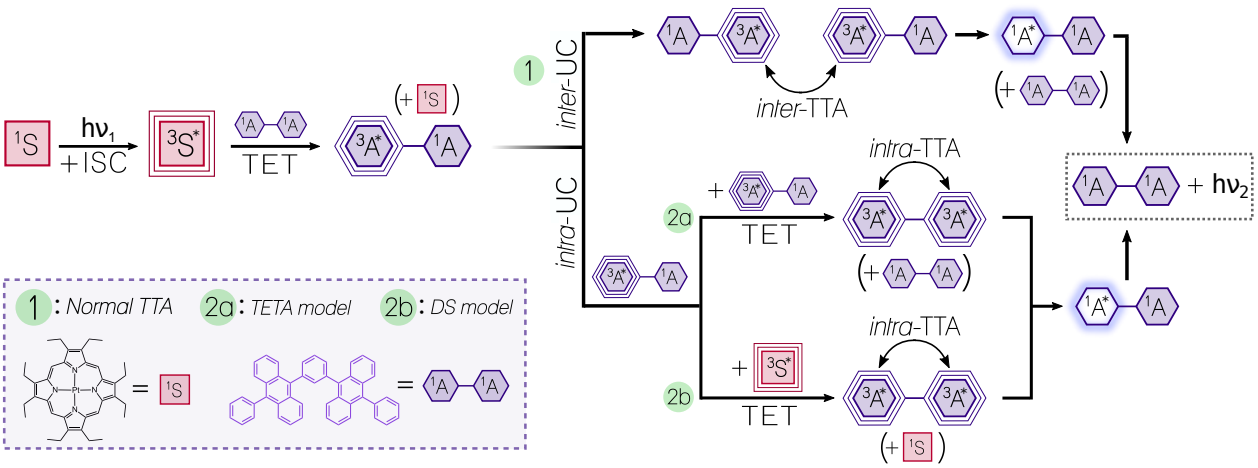

FIGURE 4.1: Schematic of suggested pathways for TTA-UC with dimeric annihilator compounds (here represented by 1,3-DPA$_2$). Designations: S = sensitizer, A = annihilator moiety (spin multiplicity denoted by left superscript), * = excited state. Upon light absorption (hν_1) and rapid ISC, the sensitizer populates the triplet excited state of one annihilator moiety through TET. The TTA event forms a singlet excited state, and one high-energy photon (hν_2, hν_2 > hν_1) is emitted. (1) Conventional intermolecular TTA between two triplet excited dimers. (2a) TET between annihilators (TETA) model: The triplet excited dimer becomes doubly excited following TET from another triplet excited annihilator. (2b) Double sensitization (DS) model: The ground state moiety of the singly triplet excited dimer is populated with another triplet following TET from a sensitizer molecule. Reprinted with permission from ref. 184. Copyright 2021 American Chemical Society.

4.2 Evaluating TTA-UC Performance of Dimeric Annihilators

Four symmetric dimers based on DPA were synthesized, and their molecular structures are presented alongside their steady-state absorption and fluorescence spectra in Figure 4.2. 1,2-bis(10-phenylanthracen-9-yl)benzene (1,2-DPA$_2$), 1,3-bis(10-phenylanthracen-9-yl)benzene (1,3-DPA$_2$), and 1,4-bis(10-phenylanthracen-9-yl)benzene (1,4-DPA$_2$) all have a central phenyl ring connecting the two annihilator moieties. This feature is lacking in the fourth dimer, 10,10'-diphenyl-9,9'-bianthracene (9,9'-PA$_2$), in which the moieties are instead directly covalently linked. Only small differences between the absorption spectra of the dimers can be seen, indicating that the dimeric nature does not significantly perturb the electronic structure of the ground state.

The fluorescence characteristics are again similar, with 1,2-DPA$_2$ being the obvious exception with a red-shifted and broader fluorescence spectrum. Using temperature-dependent measurements, it was concluded that the red-shifted fluorescence is caused by the formation of an intramolecular singlet excimer. Upon absorption, one chromophore moiety populates S_1, which is followed by excimer formation between the S_0 and S_1 moieties. This is made possible due to the close spatial proximity between the moieties and the structural flexibility of the molecule. When lowering the temperature the excimer formation process is mitigated, and vibronically resolved, short-wavelength fluorescence is seen from the individual monomers (Figure

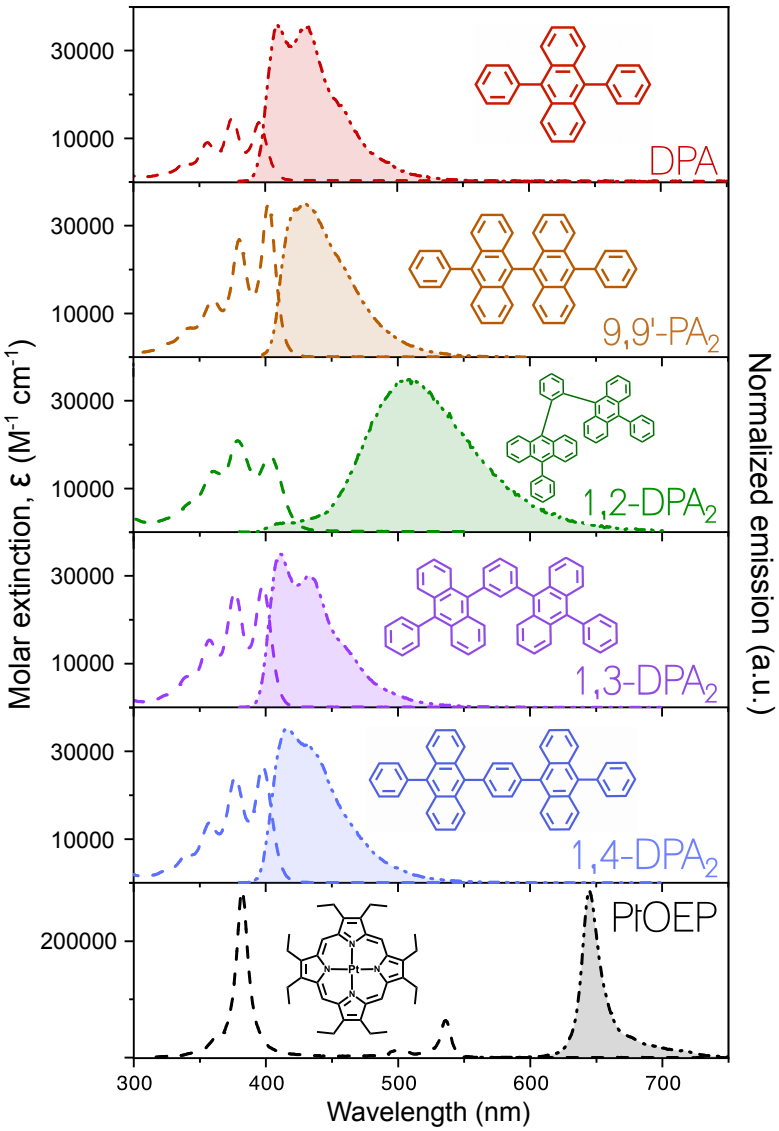

FIGURE 4.2: Absorption (dashed) and normalized emission (dash-dot) spectra of the investigated annihilators and the sensitizer PtOEP in deaerated toluene. Reprinted with permission from ref. 184. Copyright 2021 American Chemical Society.

4.3). The excited state behavior of 1,2-DPA_2 is suboptimal for TTA-UC, since the red-shifted fluorescence reduces the obtainable anti-Stokes shift.[189]

As for the parent monomer DPA, Φ_f is above 95% for all investigated annihilators, making them excellent candidates for TTA-UC. When paired with the sensitizer PtOEP (Figure 4.2), strong UC emission was observed from all samples upon 532 nm excitation. The system with DPA performs the best both in terms of $\Phi_{UC,g}$ and I_{th} (Figure 4.4), with 1,3-DPA_2 being outstanding in this regard among the dimers, despite all systems showing efficient TET and sufficient thermodynamic driving force in the TTA event (Table 4.1). The excellent performance of DPA and 1,3-DPA_2 could instead be ascribed to them having significantly longer τ_T, which was concluded to be the annihilator parameter with the most impact on TTA-UC performance.

The superior performance of 1,3-DPA_2 was interpreted in terms of differences in the geometric motifs of the dimers. It is well-known that linkage in the meta-position decreases the

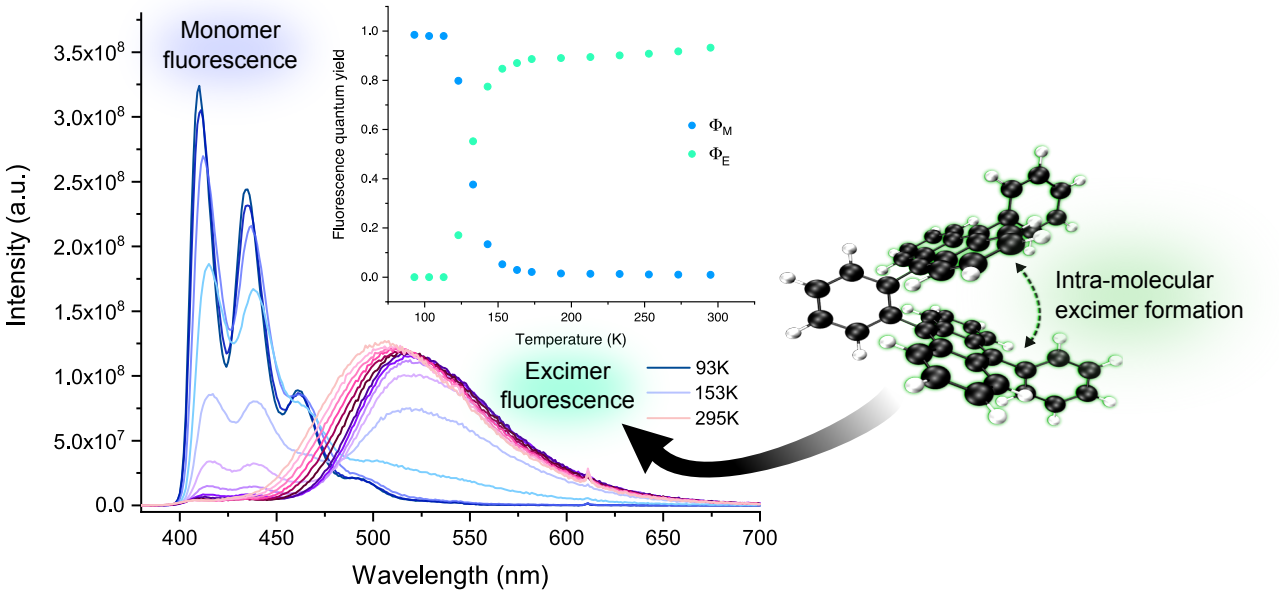

FIGURE 4.3: Steady-state fluorescence of 1,2-DPA$_2$ in deaerated 2-methyltetrahydrofuran at different temperatures. The broad feature at longer wavelengths is fluorescence from an intramolecular excimer state which is readily formed at room temperature. Inset: Fluorescence quantum yield of the excimer state (Φ_E) and the monomer state (Φ_M) at different temperatures. Reprinted with permission from ref. 184. Copyright 2021 American Chemical Society.

electronic coupling between moieties.[190–192] This decrease in electronic coupling suggests that 1,3-DPA$_2$ should better retain the properties of monomeric DPA, which then also explains why DPA and 1,3-DPA$_2$ have similar values of τ_T (Table 4.1). Similar results have been reported for other families of dimers based on DPA, but those results were interpreted in terms of more efficient *i*TTA-UC according to the TETA model for the meta-linked dimer.[61]

TABLE 4.1: Important TTA-UC parameters determined for DPA and the dimers.

	$\Phi^a_{UC,g}$	I_{th} (mW cm^{-2})	k_{TET} (M^{-1} s^{-1})	k_{TTA} (M^{-1} s^{-1})	τ_T (ms)	2 × E(T$_1$) - E(S$_1$) (eV)
DPA	0.240	15	1.78	3.01	5.5	0.29
9,9'-PA$_2$	0.150	605	0.99	3.73	0.56	0.36
1,2-DPA$_2$	0.140	142	0.95	2.89	0.80	0.34
1,3-DPA$_2$	0.212	44	1.04	2.81	4.7	0.32
1,4-DPA$_2$	0.149	1343	0.96	4.00	0.29	0.32

[a]Out of a 50% theoretical maximum.

4.3 Elucidating the Mechanism of Intramolecular TTA-UC

TTA-UC is governed by complex kinetics, but simulating the kinetic evolution of different species is possible. To take advantage of this possibility, simulations of the behavior of different

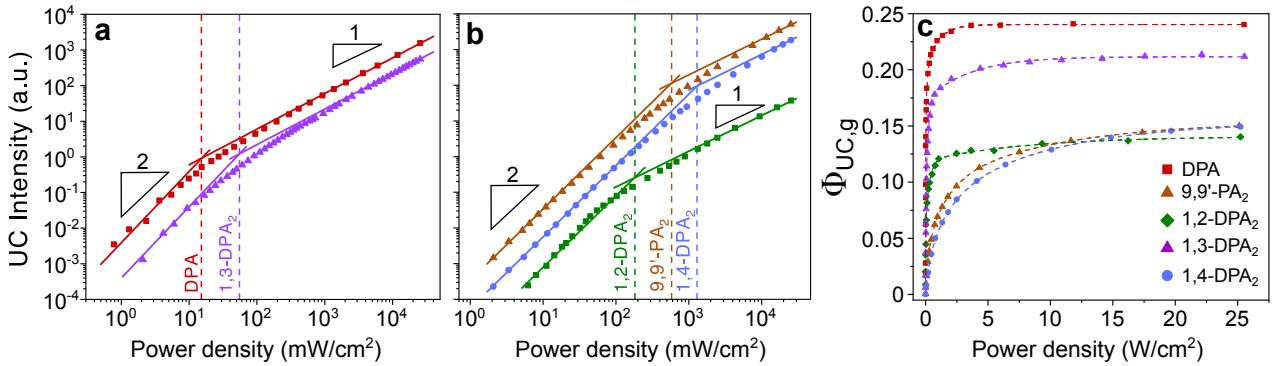

FIGURE 4.4: (a-b) Log-log plots of UC emission intensity versus excitation power density. The crossing point between the quadratic and linear regions, I_{th}, is indicated for each annihilator. (c) $\Phi_{UC,g}$ versus excitation power density. At high intensities, $\Phi_{UC,g}$ asymptotes towards its maximum value. Adapted with permission from ref. 184. Copyright 2021 American Chemical Society.

*i*TTA-UC mechanisms were performed and then compared with experiments. The simulations were performed using experimentally derived values of relevant parameters, and full details and results from the simulations are found in the Supporting Information of Paper I. Simulations and experiments focused on two different concentration regimes: one in which the ratio between ground state annihilator and sensitizer (*i.e.*, $[^1A]_0/[^1S]_0$) is high, which is the most common for TTA-UC systems in liquid media, and one in which $[^1A]_0/[^1S]_0$ is low (typically $[^1A]_0 \approx 10$ μM, $[^1S]_0 \approx 100$ μM).

Figure 4.5 presents comparisons between the simulated and experimentally measured UC emission kinetics for each system. At high $[^1A]_0/[^1S]_0$, there are little to no differences in the expected kinetics between the different models. The behavior of the two *i*TTA-UC models also coincides with the kinetics of a model in which any *i*TTA-UC contributions are forbidden (Figure 4.5c), indicating that contributions from *i*TTA-UC under normal conditions are negligible.

Much larger differences are seen when moving to low $[^1A]_0/[^1S]_0$. Here, the TETA model predicts that the DPA system should yield the fastest emission kinetics, with the rise time in particular being significantly shorter than for the dimers (Figure 4.5e). On the contrary, the DS model predicts that the rise time of the dimers is shorter than for DPA (Figure 4.5f). Given the nature of the DS model, the faster early time kinetics would be expected, as the *i*TTA-UC pathway depends on TET_2 from $^3S^*$, an event which is likely to take place at early times. Interestingly, experiments show that the dimers have a faster rise time than DPA, indicating that the DS mechanism is responsible for the observed kinetics at low $[^1A]_0/[^1S]_0$.

As is evident from Figure 4.5h, all dimers show evidence of *i*TTA-UC. It could, thus, be helpful to evaluate the performance of the dimers as a group in order to better understand how the additional *i*TTA-UC pathway affects overall performance. To do so, the mean steady-state UC intensity of the dimers at different $[^1A]_0/[^1S]_0$ was compared to that of DPA (Figure 4.6). At low $[^1A]_0/[^1S]_0$, the mean UC intensity of the dimers increase relative to DPA as predicted by the DS model, while at high $[^1A]_0/[^1S]_0$ the predictions of the TETA model better coincide with experiments. This is to be expected given that the influence from the mechanism proposed in the TETA model will be more pronounced when increasing $[^1A]_0$. The

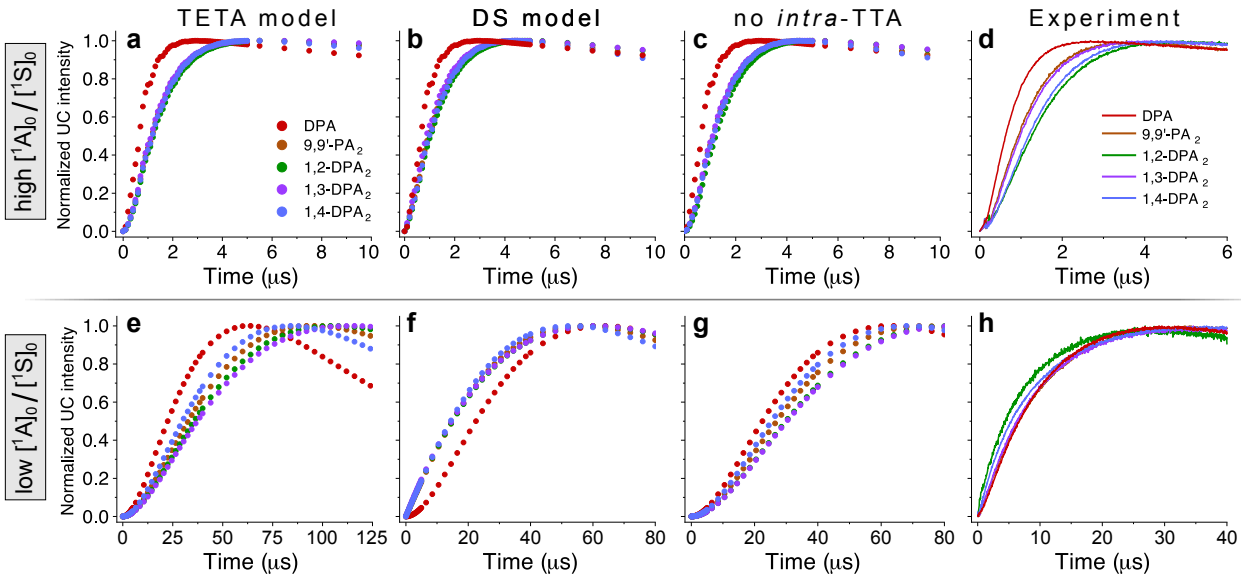

FIGURE 4.5: Simulation results for the (a, e) TETA model, (b, f) DS model, (c, g) model where *i*TTA-UC contributions are disallowed, and (d, h) experimental kinetic traces from delayed UC fluorescence emanating from (a-d) samples with $[^1S]_0 = 5$ μM and $[^1A]_0 = 1$ mM (*i.e.*, $[^1A]_0/[^1S]_0 = 200$), and (e-h) samples with $[^1S]_0 = 100$ μM and $[^1A]_0 = 5$ μM (*i.e.*, $[^1A]_0/[^1S]_0 = 0.05$). Emission monitored at 430 or 510 nm (for 1,2-DPA$_2$). Adapted with permission from ref. 184. Copyright 2021 American Chemical Society.

accuracy of the measurements at low $[^1A]_0/[^1S]_0$ is rather poor, as the measured UC spectra are low in intensity and strongly affected by inner filter effects. Nonetheless, the steady-state measurements further indicate that the DS mechanism is responsible for the TTA-UC behavior we see from the dimers at low $[^1A]_0/[^1S]_0$.

4.4 Conclusions Regarding Intramolecular TTA-UC

To summarize, the findings of Paper I suggest that *i*TTA-UC is an active pathway in DPA dimer molecules. This additional pathway is primarily governed by a second sensitization step in which a singly excited triplet annihilator becomes doubly excited following TET from a second sensitizer molecule (as proposed in the DS model). The additional *i*TTA-UC pathway leads to improved performance of these dimers at low $[^1A]_0/[^1S]_0$ ratios. In terms of overall TTA-UC performance, systems with the reference monomer DPA still outperforms the dimers at normal conditions, with 1,3-DPA$_2$ showing outstanding performance among the dimers. A much longer τ_T was found in 1,3-DPA$_2$ compared with the other dimers, which was attributed to decreased electronic coupling due to the two chromophore moieties being covalently linked in the meta-position.

These results are of importance for the development of TTA-UC systems intended for solid-state applications, such as for PV. In the solid state, diffusional motion is hindered, and energy transfer events will be increasingly dependent on exciton migration. This means that *inter*molecular TTA is obstructed in the solid state, and that *i*TTA-UC will have an important role. Additionally, the mechanism proposed in the TETA model would be improbable in the

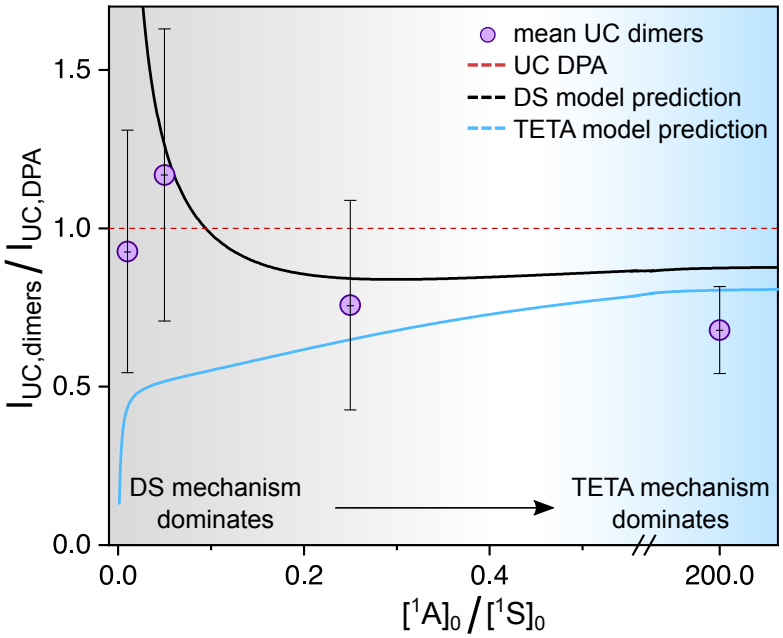

FIGURE 4.6: Comparison between the UC emission of DPA and dimers as a group. The abscissa signifies the ratio between ground state annihilator and sensitizer concentrations, and the ordinate the mean relative UC emission of the dimers compared to that of DPA. Purple circles are the experimental mean values of dimer UC emission divided by that of DPA and are compared with the corresponding intensity ratios predicted by the DS (black solid line) and TETA (blue solid line) models. The red dotted line represents the UC emission of DPA and is included as a reference point. Reprinted with permission from ref. 184. Copyright 2021 American Chemical Society.

solid state as it relies on diffusional encounter between annihilators. Several systems taking advantage of the DS mechanism have been reported both before[67,69] and after[76,88] Paper I was published, with a few promising examples of efficient *i*TTA-UC in solid-state systems. While more studies are still needed, these collective efforts are bringing new insights and moving the field closer to the ultimate goal of harnessing *i*TTA-UC for solar applications.

5

Visible-to-UV TTA-UC in Solution

In this chapter, the main findings from Paper II,[193] Paper III,[194] and Paper IV[195] are presented. These studies focus on different aspects of using TTA-UC to transform visible light to UV light. In Paper II, a set of potential annihilator molecules were paired with cadmium sulfide (CdS) nanocrystal (NC) sensitizers. The CdS NCs were decorated with a number of different organic ligands, from hereon called mediator molecules, which act as triplet reservoirs, elongating τ_T of the sensitizer and, thus, promoting subsequent TET to the annihilators in solution.[141,142] Previous efforts on using NC sensitizers for vis-to-UV TTA-UC yielded only moderate Φ_{UC},[104,105] and we sought to investigate the different energy transfer steps and how to optimize them in a systematic fashion.

5.1 Using CdS Nanocrystals as Triplet Sensitizers

Figure 5.1 presents the full set of compounds investigated in this study. Three different sizes of CdS NCs were synthesized using the hot injection method,[196] with shorter reaction times at higher injection temperatures yielding larger NCs. These are referred to according to their respective absorption maxima in nm, with CdS 393 and CdS 426 having the smallest (3.1 nm) and largest (4.3 nm) diameters, respectively (Figure 5.1a). All three sizes of CdS NCs exhibit photoluminescence quantum yields (Φ_{PL}) between 20-30%, which is a significant improvement from previous studies employing CdS NCs as sensitizers.[104] A high Φ_{PL} signifies suppressed non-radiative decay, allowing for more efficient subsequent TET events.

The CdS NCs exhibit multi-exponential photoluminescence kinetics, but the amplitude-weighted average lifetime, $<\tau>$, can still be used as a proxy to determine the TET efficiency from CdS NCs to surface mediators (Φ_{TET1}). The CdS/mediator assemblies were constructed by simply adding the mediator to a CdS solution under mixing, with no subsequent washing step to remove excess mediator left in solution. Omitting subsequent washing was key in obtaining well-functioning systems. As is evident from the excited state energies presented in Figure 5.1b and Table 5.1, Φ_{TET1} is sensitive to the energy alignment between CdS NCs and surface-bound mediators. Previous studies have mainly used 1-naphthoic acid (1-NCA) as the triplet mediator,[104–106] but our results show that also phenanthrene-3-carboxylic acid (3-PCA) and biphenyl-4-carboxylic acid (4-BCA) can accept the triplet from the NCs, albeit only from CdS 393 in the case of 4-BCA (Table 5.1).

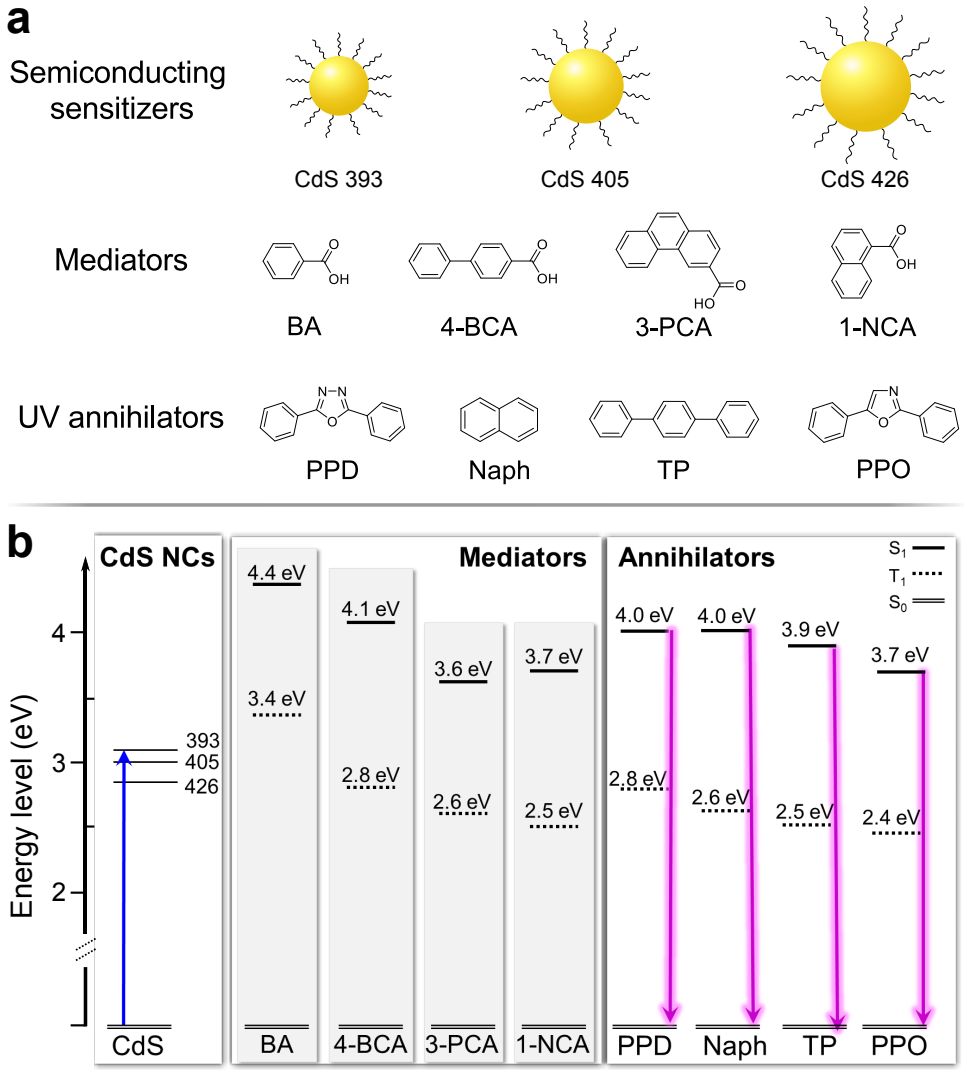

FIGURE 5.1: (a) Compounds used in this study: CdS NCs with different diameters, ranging from 3.1 nm (CdS 393) to 4.3 nm (CdS 426). Four mediators: benzoic acid (BA), biphenyl-4-carboxylic acid (4-BCA), phenanthrene-3-carboxylic acid (3-PCA), and 1-naphthoic acid (1-NCA). Four UV emitting annihilators: 2,5-diphenyl-1,3,4-oxadiazole (PPD), naphthalene (Naph), *p*-terphenyl (TP), and 2,5-diphenyloxazole (PPO). (b) Energy level diagram of the compounds under investigation. Adapted with permission from ref. 193. Copyright 2021 Wiley-VCH GmbH.

TABLE 5.1: Energy levels of mediator compounds and their quenching behavior when assembled with CdS NCs.

	S_1 (eV)	T_1 (eV)	$<\tau>^a$ (ns)			Φ_{TET1} (%)		
			CdS 393	**CdS 405**	**CdS 426**	**CdS 393**	**CdS 405**	**CdS 426**
BA	4.4	3.4	16.9	17.0	14.3	-[b]	-	-
4-BCA	4.1	2.8	5.11	17.0	14.3	70	-	-
3-PCA	3.6	2.6	1.34	1.21	3.23	92	93	78
1-NCA	3.7	2.5	1.67	1.65	5.67	90	90	58

[a]PL lifetime in the presence of 300 μM mediator. [b]No PL quenching observed.

Interestingly, the systems using 3-PCA as the mediator show slightly higher Φ_{TET1} than the respective systems using 1-NCA, despite 3-PCA having a higher T_1 energy than 1-NCA. Our hypothesis is that 3-PCA might have a slightly stronger binding affinity to the NC surface, or that the position of the carboxylic group in 3-PCA results in the phenanthrene core being slightly closer to the NC surface. Additionally, despite 4-BCA having a lower T_1 energy than all sizes of CdS NCs, TET_1 (Figure 5.2) was only realized when paired with CdS 393. This result indicates that a substantial thermodynamic driving force of at least 0.2 eV is needed to afford TET_1 in systems using CdS NCs as sensitizers, consistent with previous studies on TET between semiconductor NCs and surface-anchored ligands.[197–199]

5.1.1 Achieving Efficient Vis-to-UV TTA-UC

The CdS/mediator assemblies were subsequently used to sensitize a set of annihilator molecules with different S_1 and T_1 energies (Figure 5.1). Out of these, PPO[65,101,104–106,108] and *p*-terphenyl (TP)[107,110] have been used as annihilators previously, whereas 2,5-diphenyl-1,3,4-oxadiazole (PPD) and naphthalene (Naph) are investigated as annihilators for the first time. In contrast to the mediator, the annihilator is kept free in solution, allowing it to come in close contact with both the sensitizer and other annihilator molecules. A schematic of the full TTA-UC process using NC/mediator assemblies as the sensitizer is shown in Figure 5.2.

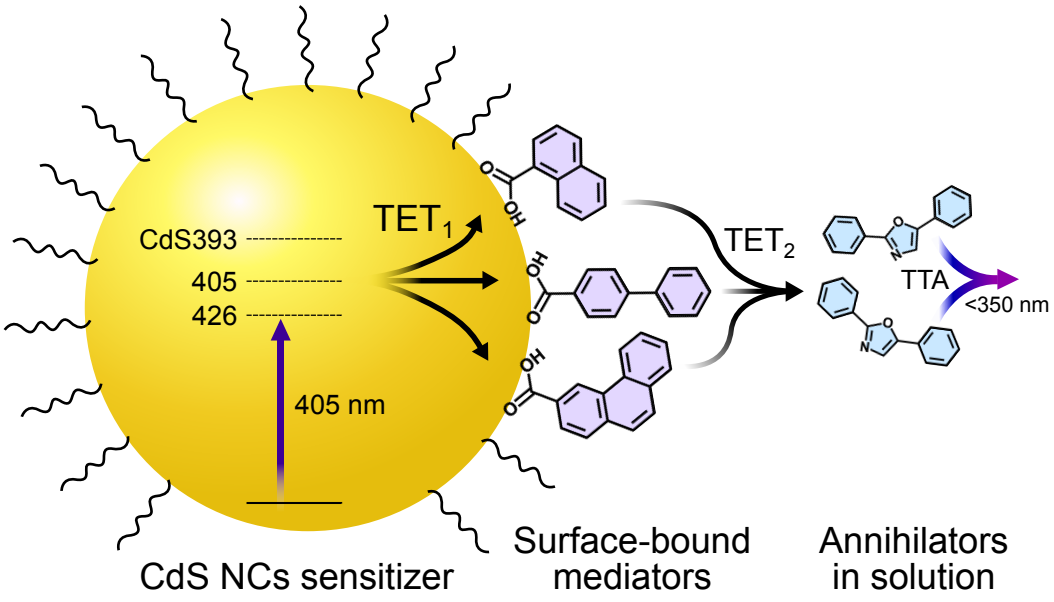

FIGURE 5.2: Schematic of the full NCs-based TTA-UC process. The CdS NC excited state is formed following 405 nm excitation. Two separate TET events are then needed before TTA in solution is achieved. The system energies may be varied by changing the size of the CdS NCs and by using different mediator/annihilator pairs. Wiggly lines represent oleic acid ligands, which stabilize the CdS NCs during and following synthesis.

The normalized steady-state absorption and emission spectra of the annihilators are presented in Figure 5.3. All annihilators have significant emission in the UV region and fulfil

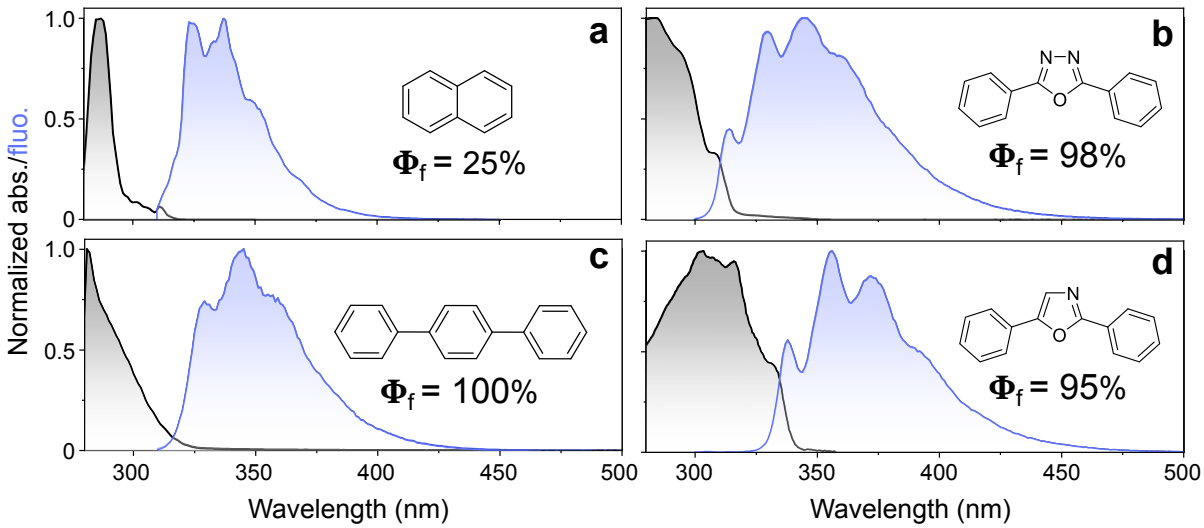

FIGURE 5.3: (A) Normalized steady-state absorption and fluorescence of (a) naphthalene (Naph), (b) 2,5-diphenyl-1,3,4-oxadiazole (PPD), (c) *p*-terphenyl (TP), and (d) 2,5-diphenyloxazole (PPO) in toluene.

the energy requirement for TTA. Aside from Naph, all annihilators also have high Φ_f, making them great annihilator candidates. However, their TTA-UC performance differ significantly, with PPO far outperforming the other annihilators. A high $\Phi_{UC,g}$ of 10.4% was measured for the CdS 405/3-PCA/PPO system, which is on par with the efficiency of a system using a new compound based on naphthalene, 1,4-bis((triisopropylsilyl)ethynyl)naphthalene (N-2TIPS), as the annihilator.[102] The full set of measured $\Phi_{UC,g}$ for all different combinations of sensitizer, mediator, and annihilator are given in Table 5.2.

Evident from Table 5.2 is that the TTA-UC efficiencies are greatly affected by the system energetics. Crucial to achieve high $\Phi_{UC,g}$ is a high Φ_{TET1}, and it seems that $\Phi_{UC,g}$ does not scale linearly with Φ_{TET1}, but rather it decreases even more strongly. This can be understood from the bimolecular nature of TTA. If the annihilator triplet concentration, $[^3A^*]$, decreases due to a lowering of Φ_{TET1}, the decrease in Φ_{TTA} will be even more pronounced as it is quadratically dependent on $[^3A^*]$. Further, to achieve TTA-UC altogether it is required that the T_1 energy of the annihilator is the same or lower than that of the mediator. Significantly, the systems using PPO as the annihilator perform much better than all other systems, which is interpreted in terms of a more efficient secondary TET event (TET_2, Figure 5.2) from mediator to annihilator.

While the performance of PPD as an annihilator is difficult to assess given that only one NC/mediator assembly works for sensitization of PPD, it is interesting to look at the trends in $\Phi_{UC,g}$ for the remaining annihilators. In general, using CdS 393 or CdS 405 yields the highest $\Phi_{UC,g}$, highlighting that a high thermodynamic driving force for TET_1 between NCs and mediators is needed. Naph performs poorly overall, which can be explained by its low Φ_f of only 25% and a relatively short τ_T.[200] A slight improvement in $\Phi_{UC,g}$ is seen when using 4-BCA as mediator, again highlighting that also TET_2 benefits from a sufficient thermodynamic driving force.

The T_1 energy of 2.53 eV for TP was obtained from the literature,[201] which would indicate that TET_2 from both 3-PCA ($E(T_1)$ = 2.56 eV) and 4-BCA ($E(T_1)$ = 2.78 eV) should be

somewhat efficient. In Paper III, we argue that the value for $E(T_1)$ of TP used herein might be underestimated, and instead refer to a literature value of 2.62 eV.[202] This value seems to better match also the findings in Paper II, with an inefficient TET_2 event explaining the low efficiencies found in systems using 1-NCA or 3-PCA as mediators. Nonetheless, it is promising that the performance of TP as an annihilator drastically improves when using the CdS 393/4-BCA assembly as sensitizer, almost matching the performance of the respective system with PPO. Using 4-BCA as mediator should result in equally efficient TET_2 to TP and PPO, thus indicating that not only PPO but also TP can undergo TTA quite efficiently. This is especially interesting given that TP emits much deeper in the UV region than PPO (Figure 5.3), which could be important for certain applications.[96]

TABLE 5.2: Measured TTA-UC quantum yields ($\Phi_{UC,g}$, %)[a].

Sensitizer	Φ_{TET1} (%)	Annihilator			
		PPD	**Naph**	**TP**	**PPO**
CdS 393/4-BCA	70	0.2	0.07	1.6	2.6
CdS 393/3-PCA	92	-[b]	0.04	0.4	8.8
CdS 393/1-NCA	90	-	-	0.2	8.4
CdS 405/3-PCA	93	-	0.03	0.2	10.4
CdS 405/1-NCA	90	-	-	0.1	9.1
CdS 426/3-PCA	78	-	0.01	0.08	6.0
CdS 426/1-NCA	58	-	-	-	3.6

[a]Determined relative to a theoretical 50% maximum in deaerated toluene with an experimental error of approx. ±10%. [b]No UC emission detected.

5.2 Further Improvements of TTA-UC Efficiencies

The rather complex systems used in Paper II, which depend on the successful assembly of NCs and mediators, as well as on realizing two separate TET events, made it difficult to make a fair assessment of the investigated annihilators. In Paper III,[194] we therefore sought to simplify the systems under investigation, with the goal being that sensitization of all annihilators should be efficient, and equally so. In Paper II, PPO and TP stood out as promising annihilator candidates for vis-to-UV TTA-UC, while PPD likely was not properly sensitized in any of the investigated CdS-based systems. These three annihilators were chosen for further investigation, together with N-2TIPS,[102,103] 2,5-diphenylfuran (PPF), and 2-phenylindene (2PI). PPF and 2PI were investigated as annihilators for the first time, to the best of our knowledge. This set of six annihilators hold several of the properties needed in an efficient annihilator, including a high Φ_f of at least 75% in the UV region, and a high thermodynamic driving force for TTA (Table 5.3). Their molecular structures and normalized steady-state absorption and emission spectra are presented in Figure 5.4a.

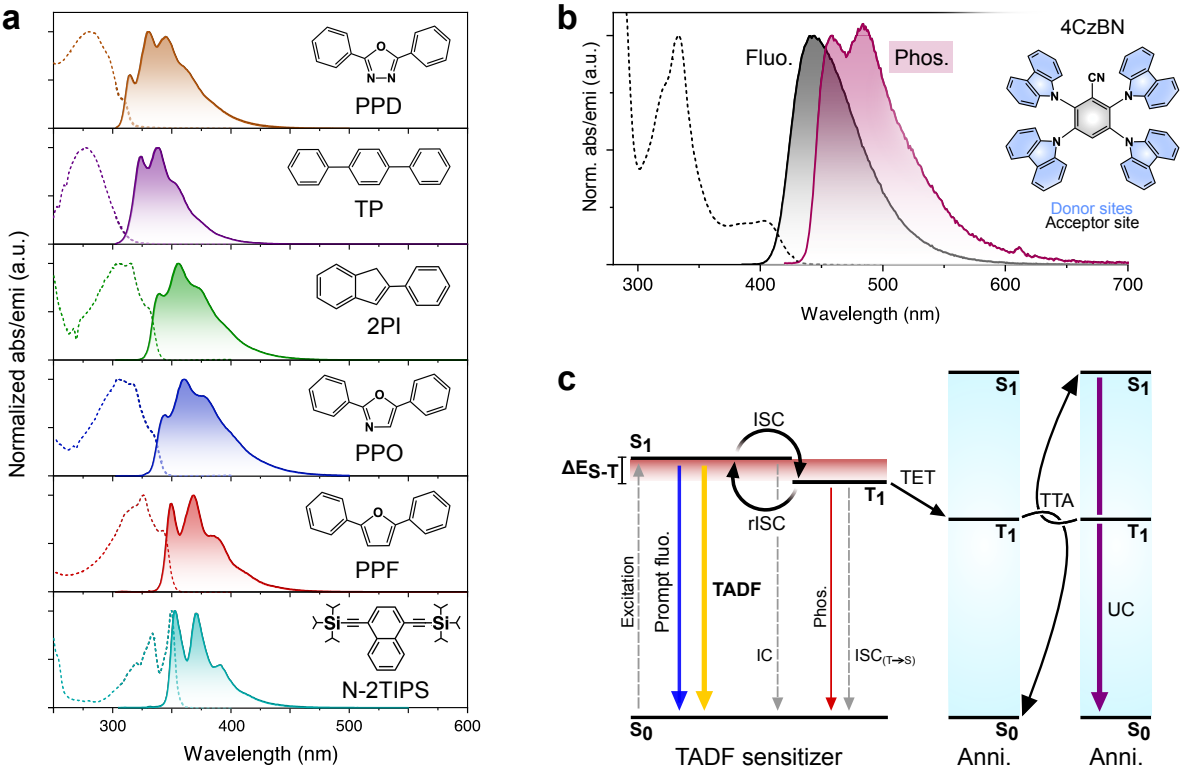

FIGURE 5.4: (a) Normalized steady-state absorption and fluorescence of investigated UV-emitting annihilators. (b) Steady-state absorption, fluorescence, and phosphorescence of the sensitizer 4CzBN, alongside its molecular structure. (c) Jablonski diagram of the TTA-UC process with a TADF-type sensitizer. Adapted with permission from ref. 194. Copyright 2022 American Chemical Society.

TABLE 5.3: Excited state energies and fluorescence quantum yield of investigated annihilators.

	S_1^a (eV)	T_1^b (eV)	Φ_f
PPD	3.99	2.82[d]	0.88
TP	3.98	2.62[e]	0.92
2PI	3.71	2.22[e]	0.85
PPO	3.67	2.40[e]	0.78
PPF	3.59	2.28	0.79
N-2TIPS	3.53	2.12[f]	0.77

[a]First singlet excited state energy, determined from the intersection of normalized steady-state absorption and fluorescence spectra. [b]First triplet excited state energy, determined from the highest energy peak position of phosphorescence, collected at 77 K in 2-methyltetrahydrofuran or collected from the literature when applicable. [c]Fluorescence quantum yield of optically dilute samples. $\lambda_{ex} = 300$ nm, determined relative to TP in deaerated cyclohexane ($\Phi_f = 0.93$).[203] [d]Reference 204. [e]Reference 202. [f]Reference 102.

5.2.1 Using a High-Energy TADF-Active Sensitizer

To certify that equally efficient TET proceeds to all annihilators, it was crucial to find a sensitizer with a sufficiently high T_1 energy. We also sought to use a sensitizer free of rare-earth metals such as iridium,[95,102,111,116] and therefore focused our attention on purely organic compounds with TADF characteristics. It was found that 2,3,5,6-tetra(9H-carbazol-9-yl)benzonitrile (4CzBN, Figure 5.4b) was able to efficiently sensitize all annihilators, owing to a high T_1 energy of 2.71 eV, a high Φ_{ISC} of 0.89, and a long T_1 lifetime (τ_T = 62 μs). 4CzBN was originally designed as a blue TADF emitter for organic light-emitting diodes,[205] but due to a relatively large ΔE_{S-T} of 0.28 eV, rISC in 4CzBN is comparatively slow, which allows TET to proceed efficiently under optimized conditions. 4CzBN has a prompt fluorescence component with a Φ_f of 0.11, which is the reason why Φ_{ISC} is capped at 0.89. The prompt fluorescence is an unavoidable loss channel in TTA-UC systems employing TADF sensitizers, and will be present in the spectra of steady-state UC emission (Figure 5.5).

High annihilator concentrations of 1 or 10 mM were used throughout to promote TET, which was especially important in the case of PPD, to which k_{TET} was significantly slower. This was expected given the endothermic nature of TET from 4CzBN to PPD. It is not straight-

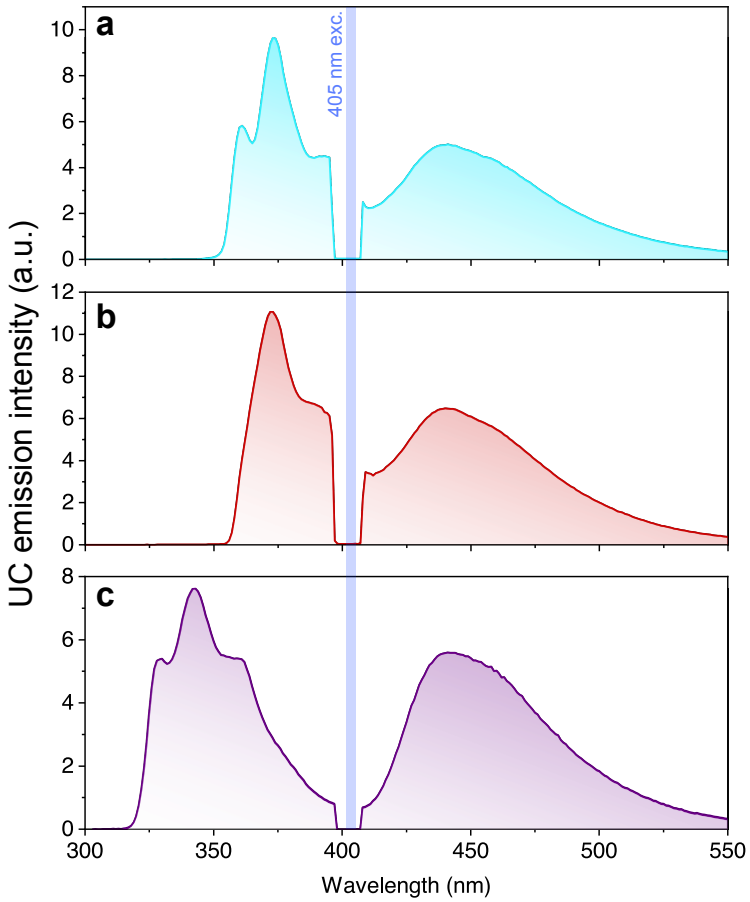

FIGURE 5.5: Steady-state UC emission spectra of samples with 25 μM 4CzBN and (a) 1 mM N-2TIPS, (b) 10 mM PPF, or (c) 10 mM TP. The broad long-wavelength feature is due to prompt fluorescence from 4CzBN. λ_{ex} = 405 nm, I_{ex} = 18 W cm^{-2}.

forward to evaluate Φ_{TET} in these systems, as the addition of annihilator molecules perturbs the excited state equilibrium of 4CzBN. The determination of k_{TET} from TADF-active sensitizers using Equation 2.12 have previously been carried out using changes in the overall steady-state emission intensity,[110] or using changes in the lifetime of the delayed component (τ_{DF}).[206] We used modelling to determine which approximate method most accurately mimics the analytical expression of Φ_{TET}, and found that for TADF sensitizers with moderate to high ΔE_{S-T} (>0.1 eV) using τ_{DF} as a proxy should yield accurate values of k_{TET} and Φ_{TET} (see Supporting Information of Paper III for more information).

Having realized the goal of equally efficient TET to all annihilators, the TTA performance of each annihilator was evaluated. Φ_{UC} was measured for all annihilators, from which $\Phi_{UC,g}$ could be deduced using a fitting procedure similar to that shown in Figure 2.8. To our delight, several of the TTA-UC systems exhibit conversion high efficiencies upon 405 nm excitation, with the N-2TIPS system in particular showing a record vis-to-UV $\Phi_{UC,g}$ of 16.8%. PPO, PPF, and TP show similar efficiencies well over 10%, whereas PPD and 2PI suffer from weaker performance (Table 5.4). The relatively poor performance of 2PI was in part explained by poor solubility in toluene, meaning that the effective 2PI concentration was much lower than anticipated. A few representative steady-state UC emission spectra are shown in Figure 5.5, with prompt fluorescence of 4CzBN being present at longer wavelengths in addition to the short-wavelength UC emission.

5.2.2 Full TTA-UC System Characterization

To understand the minutiae of the performance of each individual annihilator, we employed the new methodology that was detailed in Section 3.3. Some representative graphs of the performance of PPO are shown in Figure 5.6. From the set of time-resolved UC emission measurements that are shown in Figure 5.6a, τ_T, I_{th}, k_{TTA}, and Φ_{TTA} (*i.e.*, $\beta_{max}/2$) are extracted. Increasing I_{ex} leads to faster kinetics due to more efficient TTA, which in turn yields a higher β. The β value of each measurement, which was obtained by globally fitting the kinetic traces in Figure 5.6a to Equation 3.6 with a constant τ_T, were plotted to extract I_{th} by finding the I_{ex} that would yield $\beta = 0.5$ (Figure 5.6b). The extracted value of I_{th} was compared with that obtained using the traditional method, showing that similar results are obtained regardless of the methodology used, thus highlighting the applicability of the new methodology.

The full results are presented in Table 5.4, and it is again evident that a high $\Phi_{UC,g}$ results from annihilators with a long τ_T. In fact, the relationship between a long τ_T and beneficial behavior otherwise is indubitable, which is of course to be expected, but further reinforces the reliability of the new methodology utilized herein. It is also interesting to note that the extracted k_{TTA} values do not necessarily scale with TTA-UC performance. It instead seems that also relatively slow k_{TTA} ($<10^9$ M^{-1} s^{-1}) is sufficient to achieve high Φ_{TTA}, as long as τ_T is on, or at least near, the millisecond time scale.

The careful evaluation of all relevant TTA-UC parameters, with the evaluation of $\Phi_{UC,g}$ being especially important, allows further analysis of the spin-statistical factor, f. It was extracted using Equation 2.10 with f as an additional prefactor, and using the values of $\Phi_{UC,g}$ since f relates to the intrinsic ability to produce singlet excited states during TTA, not to the

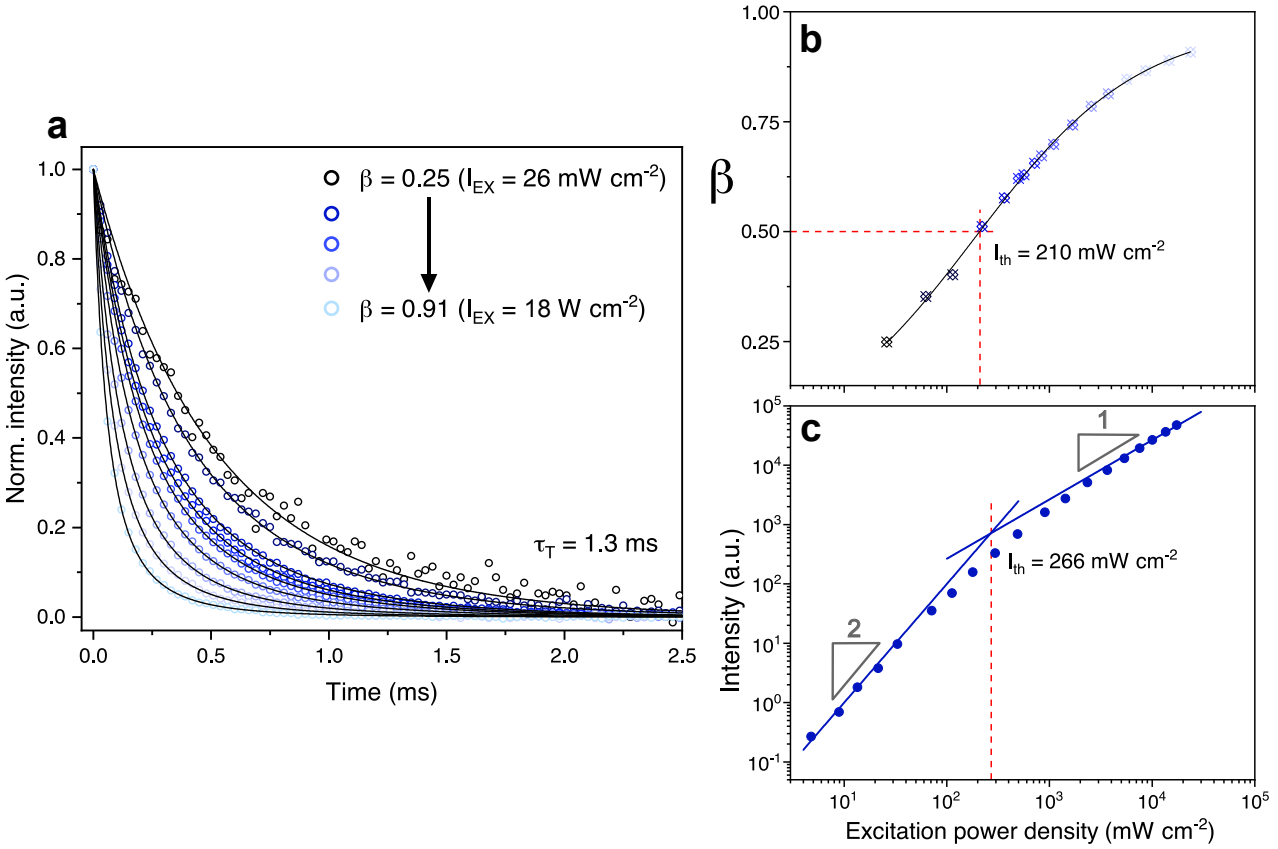

FIGURE 5.6: (a) Normalized excitation intensity-dependent kinetics of the UC emission of PPO. (b) Evaluation of I_{th} at $\beta = 0.5$ for PPO. Solid line is included as a guide for the eye. (c) Determination of I_{th} using the conventional method. Adapted with permission from ref. 194. Copyright 2022 American Chemical Society.

actual emission event. This analysis shows that most annihilators have f values around 0.4, which is to be expected (Table 5.4). Interestingly, N-2TIPS shows a slightly higher f of 0.54. The reason for this is unclear, but DFT calculations indicate that N-2TIPS have a T_2 energy above that of S_1, which was not the case for any other annihilator. This could potentially enable exothermic high-level rISC from T_2 to S_1, which has previously been used to explain elevated f values in, *e.g.*, rubrene.[177,207]

TABLE 5.4: Measured values of yields and rates important in TTA-UC.

	$\Phi_{UC,g}$ | Φ^a_{UC}	k_{TET} ($\times 10^9$ M^{-1} s^{-1})	τ_T (ms)	I_{th} (mW cm^{-2})	k_{TTA} ($\times 10^9$ M^{-1} s^{-1})	β^b_{max}	f
PPD	0.058 | 0.044	0.18	0.18	4900	2.87	0.67	0.22
TP	0.126 | 0.091	0.41	0.31	1700	3.30	0.77	0.40
2PI	0.044 | 0.039	2.1	0.075	>25,000	0.69	0.27	0.43
PPO	0.140 | 0.124	2.0	1.3	210	1.75	0.91	0.44
PPF	0.130 | 0.102	3.6	0.75	600	1.77	0.85	0.44
N-2TIPS	0.168 | 0.131	0.80	2.2	220	0.62	0.91	0.54

[a]Out of a 50% theoretical maximum. [b]Evaluated at 18 W cm^{-2}.

5.3 Substituent Effects on Triplet Excimer Formation and TTA

The results of Paper III show that a range of different UV-emitting annihilators can participate in TTA-UC with high efficiencies. However, even though the superior performance of N-2TIPS, with several reports of Φ_{UC} above 10%,[102,103,114,208] is potentially explained by high-level rISC contributions, other TTA-UC systems using naphthalene derivatives for annihilation have suffered from much lower efficiencies.[95,98,113] The poor performance of these systems is in part due to differences in the choice of sensitizer, but this explanation is not sufficient to account for all discrepancies. Particularly, a recent report on the inferior performance of 1-((triisopropylsilyl)ethynyl)naphthalene (N-1TIPS) caught our attention, as only minor differences in TTA-UC performance, emanating from differences in Φ_f, were to be expected.[114]

In Paper IV,[195] we therefore sought to investigate how structural modifications in naphthalene derivatives affect their suitability as annihilators in TTA-UC. Substituent effects in particular were investigated, with three different substituent motifs being used: trimethylsilyl (TMS), triisopropylsilyl (TIPS), and triphenylsilyl (TPhS, Figure 5.7a). Derivatives were synthesized according to the scheme in Figure 5.7b, resulting in monosubstituted (grouped together as N-1TXS) or disubstituted derivatives (N-2TXS). The choice of substituent has little to no influence on their optical properties; instead the addition of a second substituent is what invokes spectral changes (Figure 5.7c). A red-shift in absorption and fluorescence is seen for N-2TXS compared to N-1TXS, which limits the achievable anti-Stokes shift in subsequent TTA-UC. However, N-2TXS also show higher Φ_f of around 75%, whereas N-1TXS have a more modest Φ_f of around 50% (Table 5.5).

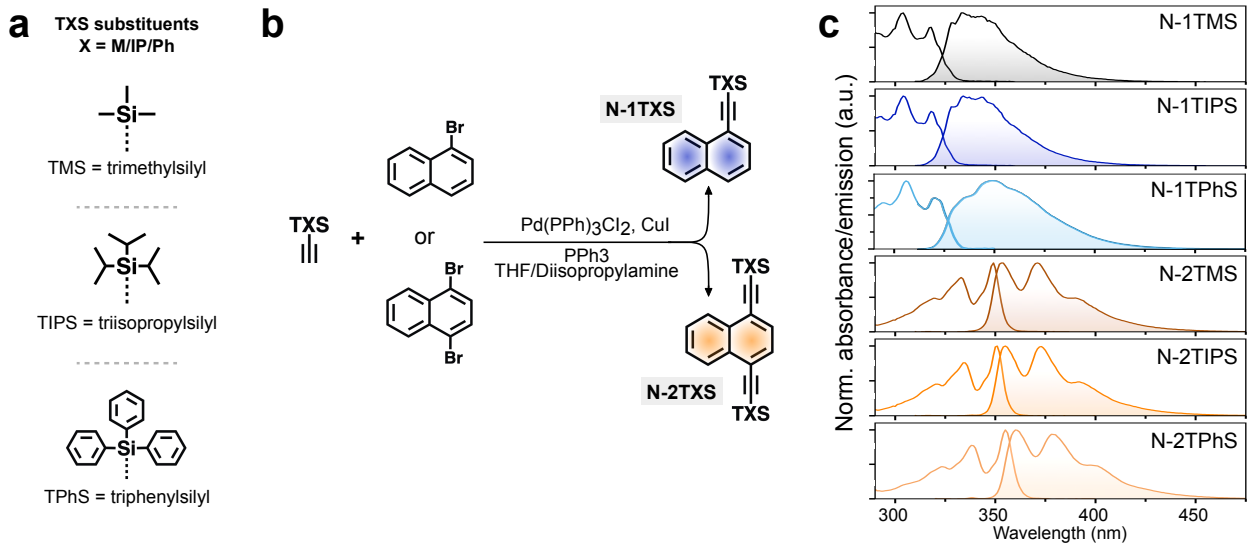

FIGURE 5.7: (a) Molecular structures of the substituents used for the synthesis of N-1TXS and N-2TXS. (b) Simplified synthetic routes of N-1TXS and N-2TXS. (c) Normalized steady-state absorption and emission (filled in) spectra of optically dilute N-1TXS and N-2TXS samples in deaerated toluene. Adapted with permission from ref. 195. Copyright 2023 American Chemical Society.

TABLE 5.5: Photophysical characteristics of N-1TXS and N-2TXS derivatives.

	S_1^a (eV)	T_1^b (eV)	$I_{em,max}$ (nm)	Φ_f^c
N-1TMS	3.83	2.39[b]	333	0.50
N-1TIPS	3.83	2.40[d]	334	0.52
N-1TPhS	3.79	2.38[b]	349	0.50
N-2TMS	3.53	2.12[b]	353	0.77
N-2TIPS	3.52	2.12[d]	355	0.78
N-2TPhS	3.47	2.12[b]	361	0.71

[a]First singlet excited state energy, determined from the intersection of normalized steady-state absorption and fluorescence spectra. [b]First triplet excited state energy, determined from the highest energy peak position of phosphorescence collected at 100 K in 2-methyltetrahydrofuran. [c]Fluorescence quantum yield of optically dilute samples, determined relative to 2-phenylindole in deaerated cyclohexane ($\Phi_f = 0.86$).[203] [d]Reference 102.

5.3.1 Self-Quenching by Ground State Annihilators in Naphthalene Derivatives

4CzBN was again used for triplet sensitization. Strongly exothermic TET proceeded efficiently to all annihilators, which facilitated fair comparison of the TTA performance of all annihilators. Interestingly, $\Phi_{UC,g}$ differs strongly between N-1TXS and N-2TXS, with the latter yielding much higher efficiencies (Table 5.6). While the difference between N-2TIPS ($\Phi_{UC,g} = 16.4\%$) and N-2TPhS (14.8%) is readily ascribed to their difference in Φ_f, the inferior performance of N-2TMS (7.8%) and N-1TXS ($\leq$5%) is harder to rationalize. τ_T values from samples with 1 mM annihilator followed the trend in $\Phi_{UC,g}$, with long τ_T (>3 ms) observed for N-2TIPS and N-2TPhS, but much shorter τ_T (<100 μs) for N-1TMS.

The large differences could not be rationalized from the molecular structures, but required other explanations. We thought about the possibility for self-quenching in our systems, and soon realized that neat naphthalene (and derivatives thereof) can form triplet excimers ($^3D^*$).[132,133,209,210] $^3D^*$ formation takes place between two annihilators in their S_0 and T_1 states, respectively, and would, thus, provide an additional deactivation pathway for the annihilator triplets, competing with that of TTA.

The presence of $^3D^*$ formation would affect the observed TTA-UC kinetics, and assuming that $^3D^*$ formation deactivates the annihilator triplets, the observed τ_T would be dependent on the annihilator ground state concentration ($[^1A]_0$) according to Equation 5.1.[211]

$$\tau_T^{-1} = k_T = k_{T0} + k_{exc}[^1A]_0 \tag{5.1}$$

Here, k_T is the observed rate of overall triplet deactivation, k_{T0} is the rate of first-order triplet deactivation, and k_{exc} is the pseudo first-order rate of (presumed) $^3D^*$ formation. The results from measurements of τ_T at four different concentrations could then be fitted to Equation 5.1 to extract k_{exc} for the different annihilators, which are presented in Figure 5.8.

Strikingly, in derivatives with the comparatively small TMS substituents, τ_T is significantly shortened when increasing $[^1A]_0$, signifying that S_0 annihilators indeed quench the T_1 annihilators. The triplets of N-1TMS are most strongly quenched, with an extracted k_{exc} of 1.6×10^7 M^{-1} s^{-1}, a value virtually identical to the rate previously reported for $^3D^*$ formation in neat

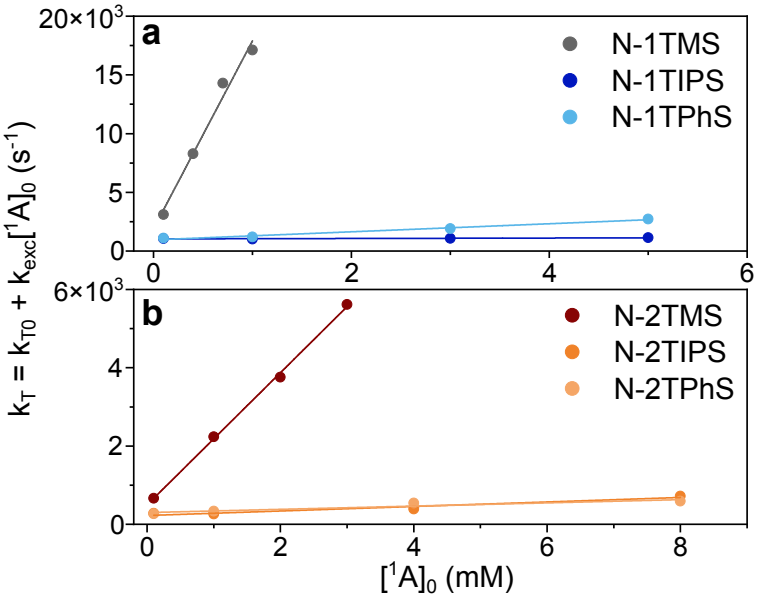

FIGURE 5.8: Linear fittings of Equation 5.1 to measured τ_T obtained at different $[^1A]_0$ for (a) N-1TXS, and (b) N-2TXS. Note that the x- and y-axes differ between the panels. Adapted with permission from ref. 195. Copyright 2023 American Chemical Society.

naphthalene.[132] N-1TPhS is also quenched to some extent (though not as strongly as the TMS derivatives), whereas the remaining annihilators show only minor changes in τ_T at different $[^1A]_0$ (Table 5.6).

The results from the quenching studies indicate that the rate of triplet deactivation can be controlled by the choice of substituents, with more bulky substituents impeding $^3D^*$ formation. Adding smaller TMS substituents seems to be insufficient, which is then reflected in the inferior TTA-UC performance of TMS derivatives. The number of substituents seems to have only a minor effect, even though N-1TXS in general form $^3D^*$ more efficiently than their N-2TXS counterparts. Additionally, k_{TTA} was extracted from time-resolved emission measurements, showing that N-1TXS have faster TTA than N-2TXS (Table 5.6). This trend is equal to that observed for k_{TET}, which is expected since both TET and TTA are diffusion-controlled processes.

TABLE 5.6: TTA-UC characteristics of N-1TXS and N-2TXS derivatives.

	k^a_{TET}	$\Phi^b_{UC,g}$	$[^1A]_0$ range (mM)	τ_T range (ms)	k_{exc} (M^{-1} s^{-1})	k^a_{TTA}
N-1TMS	2.0	0.013	0.1 → 1	0.32 → 0.058	1.6×10^7	4.6 ± 1.4
N-1TIPS	1.8	0.043	0.1 → 5	0.98 → 0.88	1.8×10^4	5.4 ± 1.6
N-1TPhS	1.6	0.050	0.1 → 5	0.91 → 0.37	3.4×10^5	5.5 ± 0.54
N-2TMS	1.1	0.078	0.1 → 3	1.5 → 0.18	1.7×10^6	1.7 ± 0.24
N-2TIPS	0.8	0.164	0.1 → 8	3.8 → 1.4	5.8×10^4	0.73 ± 0.10
N-2TPhS	1.0	0.148	0.1 → 8	3.7 → 1.7	4.0×10^4	0.84 ± 0.11

[a]($\times 10^9$ M^{-1} s^{-1}). [b]Out of a 50% theoretical maximum.

5.3.2 Experimental Evidence of Triplet Excimer Formation

$^3D^*$ have been suggested to form in some TTA-UC systems previously. In these cases, their presence were implied from investigations on the behavior of resulting singlet excimer fluorescence of the studied annihilators.[212,213] However, the presence of $^3D^*$ specifically was not

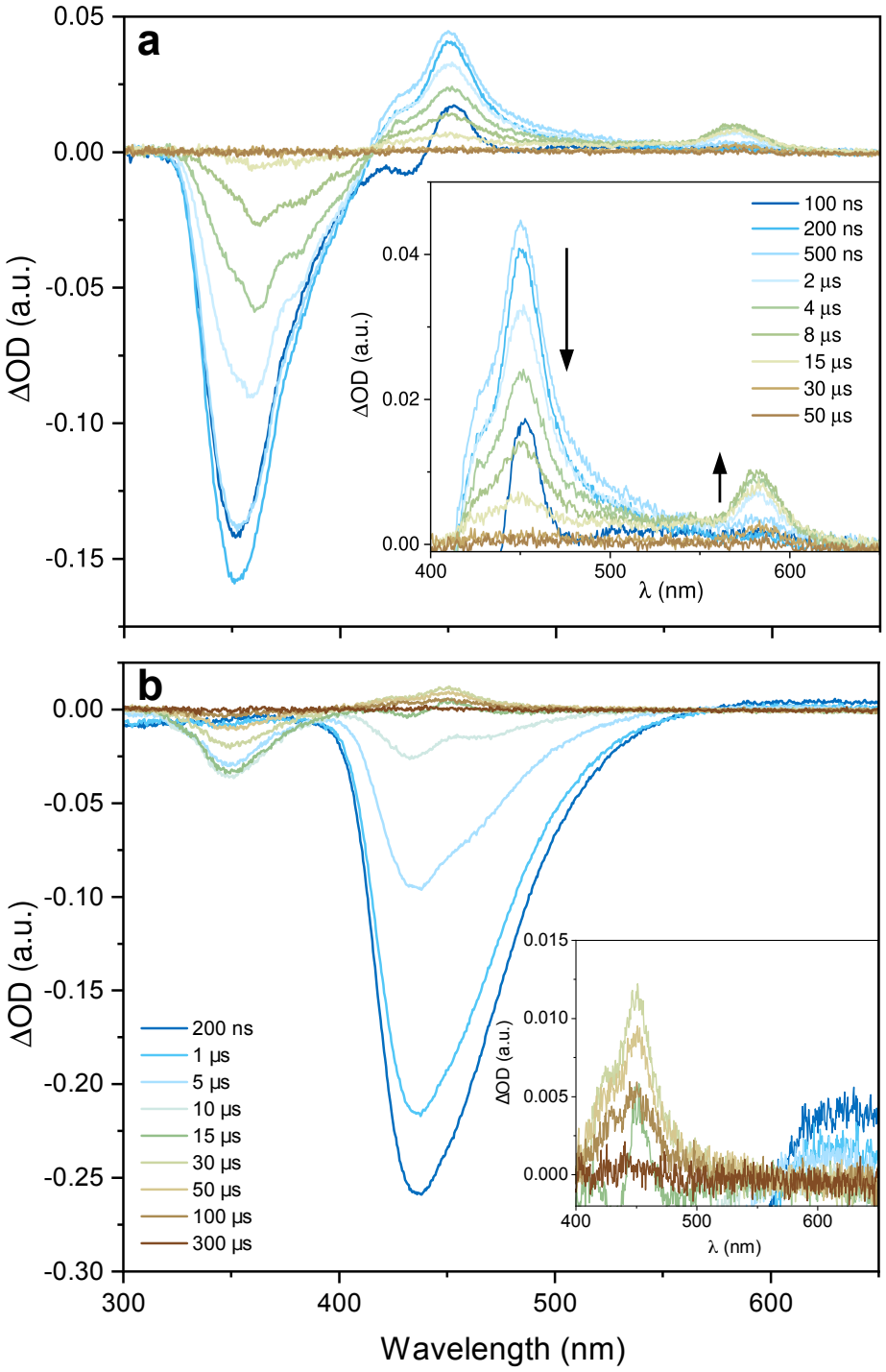

FIGURE 5.9: ns-TA spectra of samples consisting of 25 μM 4CzBN and (a) 8 mM N-1TMS, or (b) 100 μM N-1TMS, at indicated time delays. λ_{ex} = 410 nm, 1.4 mJ pulse^{-1}. Reprinted with permission from ref. 195. Copyright 2023 American Chemical Society.

experimentally verified. In our systems, no sign of either singlet or triplet excimer emission could be detected, and we instead turned to ns-TA to verify the presence of $^3D^*$. Naphthalene is known to have strong $T_1 \rightarrow T_n$ absorption at 400-450 nm,[214] whereas absorption at longer wavelengths (550-600 nm) has been assigned to $^3D^*$ absorption.[210,215–217]

ns-TA spectra of all investigated TTA-UC systems were collected. Figure 5.9 shows the spectra after indicated time delays at 410 nm excitation for a sample consisting of 25 μM 4CzBN and 8 mM N-1TMS (Figure 5.9a) or 100 μM N-1TMS (Figure 5.9b). $T_1 \rightarrow T_n$ absorption is evident in both samples around 450 nm as a result of TET from 4CzBN. This signal grows in concomitantly with a negative signal centered around 350 nm, which is due to UC emission from N-1TMS. Importantly, a second absorption feature, centered around 585 nm, can be seen in Figure 5.9a. This absorption grows in at later times, concomitantly with the decay of the $T_1 \rightarrow T_n$ absorption, suggesting that the 585 nm feature is formed from the T_1 state of N-1TMS. Its position matches well with previous designations of intramolecular $^3D^*$ absorption in dinaphthylmethanes[215,216] and naphthalenophanes,[217] suggesting that this is indeed absorption from the $^3D^*$ of N-1TMS. Further support for this designation is given based on the μs lifetime of this feature, as well as the absence of this feature in the low-concentration sample (Figure 5.9b). Although previously suggested,[212,213] these findings provide the first experimental evidence of the presence of $^3D^*$ in a TTA-UC system to date. The long-wavelength absorption feature was absent in all other samples, which is consistent with N-1TMS having the highest k_{exc}.

5.4 Conclusions Regarding Vis-to-UV TTA-UC

Annihilators for vis-to-UV TTA-UC have been studied systematically in Paper II, III, and IV, with important insights into the behavior of TTA-UC systems in general, and the performance of UV-emitting annihilators in particular, as a result. In Paper II, we used CdS NCs as sensitizers to investigate the performance of six different annihilators, showing that the precise alignment of system energetics is crucial to achieve efficient TTA-UC. High Φ_{UC} was obtained using PPO as the annihilator, especially when using 3-PCA as the surface-bound ligand. However, competitive performance was seen when using TP as an annihilator in the system employing the CdS NCs with the highest excited state energy.

In Paper III, the sensitizing protocol was simplified by exploiting a high triplet energy TADF-type sensitizer, circumventing the need for multiple TET steps. This allowed efficient sensitization of all investigated annihilators, allowing for facile comparison of their intrinsic properties. Several combinations provided unprecedented vis-to-UV TTA-UC efficiencies, with the 4CzBN/N-2TIPS pair in particular yielding a high $\Phi_{UC,g}$ of 16.8%. Additionally, a new methodology for extraction of some important TTA-UC parameters was utilized for the first time, which compared to previous methods requires simpler and fewer measurements, but with maintained, or even improved, accuracy.

Finally, in Paper IV the intrinsic TTA-UC properties of annihilators based on naphthalene were investigated. Substituent motifs of different size were used resulting in mono- or disubstituted derivatives. Big differences in TTA-UC performance were found, which were primarily ascribed to differences in τ_T of the annihilators. For derivatives with the smallest substituent, a strong dependence on the ground state annihilator concentration was found for τ_T. This

was interpreted in terms of triplet excimer formation competing with TTA-UC, which affects the observed emission kinetics. The first experimental verification of the presence of triplet excimers in a TTA-UC system was provided for N-1TMS, confirming that this additional pathway may be present in some TTA-UC systems. Importantly, the absence of triplet excimers in derivatives using bulkier substituents indicate that this detrimental process can be controlled by molecular design. These findings are likely to be of relevance also for annihilators based on, *e.g.*, benzene or anthracene, both of which may also form triplet excimers.[211,218–220]

6

Concluding Remarks and Outlook

This thesis serves to present foundational research on photochemical upconversion (TTA-UC). This process relies on the interplay between a light-absorbing triplet sensitizer, and an annihilator species which can form a high-energy, emissive singlet state through triplet-triplet annihilation (TTA). The work presented herein carefully investigates different aspects of TTA-UC performance in general, and the properties of the annihilator species in particular.

For some applications, finding solid-state solutions that do not rely on molecular diffusion is paramount. A possible avenue towards this end is to employ multichromophoric annihilators capable of holding multiple triplet excitons simultaneously, thus, allowing TTA to proceed in an intramolecular fashion. In this thesis, it is shown that intramolecular TTA may proceed in dimers based on diphenylanthracene, and that this pathway is especially important when the relative sensitizer-to-annihilator ratio is high. It is also shown that molecular geometry is of significance for dimeric annihilators, with coupling in the meta position leading to decreased electronic coupling and superior annihilator performance compared with other binding motifs.

Vis-to-UV TTA-UC is attractive to drive photochemical transformations such as photocatalytic water splitting, but the conversion efficiencies in this spectral region have typically been lower than for transformations within the visible region. This has been due to a scarcity in functioning sensitizer/annihilator pairs, and a lack of understanding regarding the inherent properties that controls TTA-UC. Herein, it has been shown that cadmium sulfide nanocrystals (NCs) decorated with triplet mediators can efficiently sensitize annihilators in solution. Large variations in the performance of the NC-based systems were seen, primarily owing to suboptimal energy alignment between the triplet excited states in the NCs, mediators, and annihilators. The best-performing systems, however, were on par with state of the art in terms of conversion efficiencies.

Further, it is demonstrated that switching to a high triplet energy sensitizer exhibiting thermally activated delayed fluorescence allows facile and efficient sensitization of an array of annihilator compounds. This results in highly efficient systems for a number of compounds, with the system employing N-2TIPS as the annihilator yielding a record vis-to-UV TTA-UC quantum yield of 16.8%. The sensitization scheme allows for a more in-depth annihilator characterization, with indications that the superior performance of N-2TIPS emanates from a slightly elevated spin-statistical factor. It is confirmed that a long triplet excited state lifetime (τ_T) of the annihilator is pivotal to its performance, and a new methodology is developed to more accurately determine this, and other, important TTA-UC parameters.

Efficient TET is typically ensured by employing high annihilator concentrations, but other processes competing with that of TTA could then also be facilitated. It is shown that annihi-

lators based on naphthalene are sensitive to changes in ground state concentration, and that this is due to triplet excimer ($^3D^*$) formation. In particular, the rate of $^3D^*$ formation can be modulated with the choice of substituents, with more bulky substituents (such as those found in N-2TIPS) effectively turning off $^3D^*$ formation. In derivatives with smaller substituents $^3D^*$ formation is prevalent, causing deteriorated TTA-UC performance and a shortened τ_T. These results highlight a detrimental pathway that has likely went unnoticed for some time, suggesting why many derivatives that seemingly should be well-behaving annihilators suffer from poor TTA-UC performance.

The prospect of using TTA-UC for solar energy applications remains bright, but several challenges remain in order to make TTA-UC technologically mature. Higher TTA-UC efficiencies across all ranges of the solar spectrum are needed. While efficient sensitization is achieved with relative ease (at least in solution), the shortcomings lie within the properties of the annihilator. Efforts in fully understanding the spin-statistical factor, f, and finding annihilators which maximize this value, will be of particular importance. The full understanding of spin-statistics is still lacking, but important insights have recently come to light, suggesting that f can be modulated upwards by changing the exchange coupling and intermolecular geometry.[177] It is still unclear precisely how the energetic alignment of triplet excited states affects f,[221] but hopefully a clearer picture will emerge shortly. It would also be beneficial if ways to lower the first triplet excited state while keeping the emissive singlet energetically unperturbed are found. This is especially vital for UV-emitting annihilators, for which energy losses during the TTA step are significant. The achievable anti-Stokes shift could then be greatly enhanced, further enabling excitation with green light.[99]

Utilization of TTA-UC for solar applications is still quite uncommon, and, to the best of my knowledge, no commercial applications harnessing TTA-UC are yet available. Combining TTA-UC with photovoltaics (PV) is perhaps the most appealing usage, but it has been impossible to find sensitizer/annihilator pairs that function well for the conversion of infrared light, impeding the development of systems that are applicable to silicon PV.[23] However, the emergence of new high-performance PV infrastructures, such as those based on perovskites,[222,223] may better align with the properties of efficient TTA-UC systems, as these materials typically exhibit larger band gaps.[174] Big challenges in retaining the high performance of many TTA-UC systems in the solid state remain, but it would come as no surprise if PV applications taking advantage of spectral conversion techniques are presented in the foreseeable future.

The same development could be expected for the utilization of vis-to-UV TTA-UC for photocatalytic water-splitting (and other photochemical transformations). It is becoming increasingly more feasible to combine vis-to-UV TTA-UC systems with sunlight excitation due to the recent development of systems with much higher conversion efficiencies (including the work presented in this thesis). While prominent challenges include the need for water-soluble TTA-UC infrastructures, compartmentalization, and a stronger mechanistic understanding of the underlying processes governing the photochemical transformations, it is likely that these will be overcome shortly, as interest in this research field has increased immensely only in the last few years. With the additional insights provided herein, the ultimate goal of using TTA-UC for improved solar energy conversion is closer than ever before.

7

Acknowledgements

During my five years at Chalmers I have crossed ways with a whole bunch of wonderful people, including colleagues, students, collaborators, and visitors. I would like to take this opportunity to thank all of you who have helped me along the way to completing my Ph.D. studies.

First of all, I would like to extend my heartfelt gratitude to my supervisor, Bo Albinsson. I first met you in the role as teacher in thermodynamics in the big undergrad course in chemistry, and for reasons that are not that clear to me more than 10 years later, you made a lasting impression on me. I guess it had to do with your way of being: jovial, enthusing, and no-nonsense. I reached out to you in the fall of 2017, asking for an opportunity to do my Master's Thesis work in your lab. You quickly came up with a project for me, with poor Fredrik (who at the time had just started his own Ph.D. studies) being strong-armed into supervising me. I'm so very glad that I contacted you, since this eventually led to me being employed in your lab.

These five years have been fantastic, and much of that is due to your guidance. From the very beginning, you made clear that the main purpose of my studies is not to publish as many papers as possible or to work as many hours as possible. No, I was here to learn. You have given me the freedom to explore things that I found interesting, and you have encouraged me to sit down and think things through instead of rushing ahead. Your trust in my abilities have been instrumental to my accomplishments. Your encouragement and interest in my leisure activities and personal life has also been much appreciated, as these are big parts of my life that I value highly.

Last, but certainly not least: I will sorely miss your jazzy piano playing and your anecdotes from the Gothenburg jazz music scene. I hope that we will get to make music together again some day!

To my co-supervisor Kasper Moth-Poulsen. Thank you for including me in your group as if I was one of your main students. Even though I haven't always been able to prioritize the meetings with your group, I have greatly enjoyed the additional perspectives that these interactions have brought me. It has been inspiring to discuss my projects with you, and you have encouraged me to dare to think outside of the box. Thanks also to my examiner Joakim Andréasson, for always providing a great atmosphere and for interesting discussions about science in general and kinetics in particular.

To Maria Abrahamsson. Thank you for putting together Journal Club and for so aptly assign-

ing me with inspiring teaching assignments. My teaching experience at Chalmers has been so rewarding and you have a big part in that. Thank you also for teaching me a lot about lasers and electron transfer, among other things.

A big thank you to current and previous members of the Spectroscopy Crew: Wera, Rasmus, Jessica, Deise, Hassan, Hanna, Andrew, Liam, Pauline, Alma, Lili, Elin, Betül, Long, Gerard, and Cassandra. Thank you for interesting presentations and discussions during our group meetings, and for always providing an enjoyable atmosphere at work. You have all been so helpful in the lab but are also great and compassionate people. I have been very lucky to have such a great group as my closest colleagues. You will all be sorely missed. A special thanks to Wera, Rasmus, Hassan, Liam, and Andrew for proof-reading my thesis.

A special thanks to Dr. Fredrik Edhborg. You took me under your wings as a Master's student and guided me through my Master's Thesis work despite being new to this area yourself. Since then you have been something of a big brother at the workplace. You were always open to discussions and to helping out when stuff didn't work as expected in the different labs. Your eye for details and strive for perfection have also been valued assets during my research. And if I ever worried that I would judge a paper in Journal Club too harshly, I could always count on you bringing some raspberry cake and being even harsher!

To Dr. Shima Ghasemi. Thank you for putting up with my ever increasing demands for new molecules, and for always accepting my suggestions with a big smile on your face!

To Dr. Victor Gray. Thank you for assisting me in the beginning of my time at floor 5, especially with the nanocrystal synthesis.

To Karl Börjesson. Thank you for letting me borrow some of your spectroscopy equipment.

To all collaborators. Thank you for widening my scientific horizon and for providing new opportunities for me in my research career.

To current and previous office colleagues: I have really enjoyed your company throughout these years - you are all great and friendly people that I will miss a lot! A special thanks to Dr. Hilda Sandström who has walked by my side throughout most of my time at Chalmers, being both a great scientist, colleague, and friend.

To all the people at floors five, eight and nine that I have interacted with. You have all been part of creating the great atmosphere that permeates our division, and I can only hope that my next workplace will be equally great!

To all students that I have encountered throughout my Ph.D. studies. The teaching experience here at Chalmers is something that I highly value, and you have all been part in making this a rewarding experience.

I'm very lucky to have many great friends outside of work. Thank you for being there for me in both times of fortune and of hardship, and I'm happy that I get to share many unforgettable memories in life with you.

Lastly, I would like to thank my family. My mother Christina, my father Per, and my brothers Erik and Johan. You all mean so much to me. Even though I know it's hard to fully comprehend the work I've performed, you have fully supported me throughout and showed interest in it, asking me questions and proudly told people about it. More importantly, you have always supported me in times when things got tough. Never have I ever had to question your love for me, which is all I could ever ask for. You are the best - I love you!

Eva, Ulf, Axel, Amanda, Sarah, and Emma. How lucky I am to have you in my life. I could not wish for greater in-laws: funny, compassionate, and lovely to spend time with.

Finally, to Lisa. Of all the things I have accomplished in life, being your husband and being the father of our daughter Ida is by far the things I'm most proud of. You are truly the love of my life, and I'm a better man for getting to spend it with you. You are not only compassionate, funny, and smart - you are also my greatest critic. Whenever I was in doubt over a figure, a formulation, or a presentation slide, you were there to provide invaluable feedback. My success as a scientist and as a human being is only possible because I have you by my side. I love you infinitely, and I can't wait for what the next chapter in life holds in store for us.

Axel Olesund, Gothenburg, November 2023

Bibliography

[1] F. Razi and I. Dincer. Renewable Energy Development and Hydrogen Economy in MENA Region: A Review. *Renew. Sustain. Energy Rev.* **2022**, *168*, 112763.

[2] M. Thirugnanasambandam, S. Iniyan, and R. Goic. A Review of Solar Thermal Technologies. *Renew. Sustain. Energy Rev.* **2010**, *14*(*1*), 312–322.

[3] International Energy Agency. Key World Energy Statistics 2022. https://iea.blob.core.windows.net/assets/830fe099-5530-48f2-a7c1-11f35d510983/WorldEnergyOutlook2022.pdf, 2022. Accessed 2023-07-05.

[4] P. Rappaport. The Photovoltaic Effect and its Utilization. *Solar Energy* **1959**, *3*(*4*), 8–18.

[5] W. Shockley and H. J. Queisser. Detailed Balance Limit of Efficiency of p-n Junction Solar Cells. *J. Appl. Phys.* **1961**, *32*(*3*), 510.

[6] B. Ehrler, E. M. Hutter, and J. J. Berry. The Complicated Morality of Named Inventions. *ACS Energy Lett.* **2021**, *6*(*2*), 565–567.

[7] M. Gul, Y. Kotak, and T. Muneer. Review on Recent Trend of Solar Photovoltaic Technology. *Energy Explor. Exploit.* **2016**, *34*(*4*), 485–526.

[8] The National Renewable Energy Laboratory. Best Research-Cell Efficiencies. https://www.nrel.gov/pv/assets/pdfs/best-research-cell-efficiencies.pdf, 2023. Accessed 2023-07-05.

[9] M. B. Smith and J. Michl. Recent Advances in Singlet Fission. *Annu. Rev. Phys. Chem.* **2013**, *64*(*1*), 361–386.

[10] M. Hanna and A. Nozik. Solar Conversion Efficiency of Photovoltaic and Photoelectrolysis Cells with Carrier Multiplication Absorbers. *J. Appl. Phys.* **2006**, *100*(*7*), 074510.

[11] M. J. Tayebjee, A. A. Gray-Weale, and T. W. Schmidt. Thermodynamic Limit of Exciton Fission Solar Cell Efficiency. *J. Phys. Chem. Lett.* **2012**, *3*(*19*), 2749–2754.

[12] B. Daiber, K. van den Hoven, M. H. Futscher, and B. Ehrler. Realistic Efficiency Limits for Singlet-Fission Silicon Solar Cells. *ACS Energy Lett.* **2021**, *6*(*8*), 2800–2808.

[13] P. Franken, A. E. Hill, C. Peters, and G. Weinreich. Generation of Optical Harmonics. *Phys. Rev. Lett.* **1961**, *7*(*4*), 118.

[14] M. Pawlicki, H. A. Collins, R. G. Denning, and H. L. Anderson. Two-Photon Absorption and the Design of Two-Photon Dyes. *Angew. Chem., Int. Ed.* **2009**, *48*(*18*), 3244–3266.

[15] A. Nadort, J. Zhao, and E. M. Goldys. Lanthanide Upconversion Luminescence at the Nanoscale: Fundamentals and Optical Properties. *Nanoscale* **2016**, *8*(*27*), 13099–13130.

[16] D. Kang, E. Jeon, S. Kim, and J. Lee. Lanthanide-Doped Upconversion Nanomaterials: Recent Advances and Applications. *BioChip J.* **2020**, *14*, 124–135.

[17] B. Mehrdel, A. Nikbakht, A. A. Aziz, M. S. Jameel, M. A. Dheyab, and P. M. Khaniabadi. Upconversion Lanthanide Nanomaterials: Basics Introduction, Synthesis Approaches, Mechanism and Application in Photodetector and Photovoltaic Devices. *Nanotechnology* **2021**, *33*(*8*), 082001.

[18] T. N. Singh-Rachford and F. N. Castellano. Photon Upconversion Based on Sensitized Triplet-Triplet Annihilation. *Coord. Chem. Rev.* **2010**, *254*(*21-22*), 2560–2573.

[19] J. Feng, J. Alves, D. M. de Clercq, and T. W. Schmidt. Photochemical Upconversion. *Annu. Rev. Phys. Chem.* **2023**, *74*(*1*), 145–168.

[20] S. P. Hill, T. Dilbeck, E. Baduell, and K. Hanson. Integrated Photon Upconversion Solar Cell via Molecular Self-Assembled Bilayers. *ACS Energy Lett.* **2016**, *1*(*1*), 3–8.

[21] T. Dilbeck and K. Hanson. Molecular Photon Upconversion Solar Cells Using Multilayer Assemblies: Progress and Prospects. *J. Phys. Chem. Lett.* **2018**, *9*(*19*), 5810–5821.

[22] Y. Zhou, C. Ruchlin, A. J. Robb, and K. Hanson. Singlet Sensitization-Enhanced Upconversion Solar Cells via Self-Assembled Trilayers. *ACS Energy Lett.* **2019**, *4*(*6*), 1458–1463.

[23] E. M. Gholizadeh, S. K. Prasad, Z. L. Teh, T. Ishwara, S. Norman, A. J. Petty, J. H. Cole, S. Cheong, R. D. Tilley, J. E. Anthony, S. Huang, and T. W. Schmidt. Photochemical Upconversion of Near-Infrared Light from Below the Silicon Bandgap. *Nat. Phot.* **2020**, *14*(*9*), 585–590.

[24] M. Wu, T.-A. Lin, J. O. Tiepelt, V. Bulović, and M. A. Baldo. Nanocrystal-Sensitized Infrared-to-Visible Upconversion in a Microcavity under Subsolar Flux. *Nano Lett.* **2021**, *21*(*2*), 1011–1016.

[25] T. Trupke, M. A. Green, and P. Würfel. Improving Solar Cell Efficiencies by Up-Conversion of Sub-Band-Gap Light. *J. Appl. Phys.* **2002**, *92*(*7*), 4117.

[26] T. Trupke, A. Shalav, B. S. Richards, P. Würfel, and M. A. Green. Efficiency Enhancement of Solar Cells by Luminescent Up-Conversion of Sunlight. *Sol. Energy Mater. Sol. Cells* **2006**, *90*(*18-19*), 3327–3338.

[27] The National Renewable Energy Laboratory. 2000 ASTM Standard Extraterrestrial Spectrum Reference E-490-00. https://www.nrel.gov/grid/solar-resource/spectra-astm-e490.html, 2023. Accessed 2023-08-25.

[28] B. Albinsson and A. Olesund. Untapping Solar Energy Resources. *Nat. Phot.* **2020**, *14*(*9*), 528–530.

[29] D. Beery, T. W. Schmidt, and K. Hanson. Harnessing Sunlight via Molecular Photon Upconversion. *ACS Appl. Mater. Interfaces* **2021**, *13*(*28*), 32601–32605.

[30] S. Eberhard, G. Finazzi, and F.-A. Wollman. The Dynamics of Photosynthesis. *Annu. Rev. Genet.* **2008**, *42*, 463–515.

[31] D. Gust, T. A. Moore, and A. L. Moore. Solar Fuels via Artificial Photosynthesis. *Acc. Chem. Res.* **2009**, *42*(*12*), 1890–1898.

[32] N. Roy, N. Suzuki, C. Terashima, and A. Fujishima. Recent Improvements in the Production of Solar Fuels: from CO_2 Reduction to Water Splitting and Artificial Photosynthesis. *BCSJ* **2019**, *92*(*1*), 178–192.

[33] Q. Wang and K. Domen. Particulate Photocatalysts for Light-Driven Water Splitting: Mechanisms, Challenges, and Design Strategies. *Chem. Rev.* **2019**, *120*(*2*), 919–985.

[34] K. Mazloomi and C. Gomes. Hydrogen as an Energy Carrier: Prospects and Challenges. *Renew. Sust. Energ. Rev.* **2012**, *16*(*5*), 3024–3033.

[35] A. J. Bard and M. A. Fox. Hydrogen and Oxygen. *Acc. Chem. Res* **1995**, *28*, 141–145.

[36] R. Abe. Recent Progress on Photocatalytic and Photoelectrochemical Water Splitting under Visible Light Irradiation. *J. Photochem. Photobiol. C: Photochem.* **2010**, *11*(*4*), 179–209.

[37] A. Fujishima and K. Honda. Electrochemical Photolysis of Water at a Semiconductor Electrode. *Nature* **1972**, *238*(*5358*), 37–38.

[38] C.-H. Liao, C.-W. Huang, and J. C. Wu. Hydrogen Production from Semiconductor-Based Photocatalysis via Water Splitting. *Catalysts* **2012**, *2*(*4*), 490–516.

[39] H. Ahmad, S. K. Kamarudin, L. J. Minggu, and M. Kassim. Hydrogen from Photo-Catalytic Water Splitting Process: A Review. *Renew. Sust. Energ. Rev.* **2015**, *43*, 599–610.

[40] T. Takata, J. Jiang, Y. Sakata, M. Nakabayashi, N. Shibata, V. Nandal, K. Seki, T. Hisatomi, and K. Domen. Photocatalytic Water Splitting with a Quantum Efficiency of Almost Unity. *Nature* **2020**, *581*(*7809*), 411–414.

[41] P. Zhou, I. A. Navid, Y. Ma, Y. Xiao, P. Wang, Z. Ye, B. Zhou, K. Sun, and Z. Mi. Solar-to-Hydrogen Efficiency of More than 9% in Photocatalytic Water Splitting. *Nature* **2023**, *613*(*7942*), 66–70.

[42] R. S. Khnayzer, J. Blumhoff, J. A. Harrington, A. Haefele, F. Deng, and F. N. Castellano. Upconversion-Powered Photoelectrochemistry. *Chem. Commun.* **2012**, *48*(*2*), 209–211.

[43] C. Ye, J. Wang, X. Wang, P. Ding, Z. Liang, and X. Tao. A New Medium for Triplet–Triplet Annihilated Upconversion and Photocatalytic Application. *Phys. Chem. Chem. Phys.* **2016**, *18*(*5*), 3430–3437.

[44] A. Monguzzi, A. Oertel, D. Braga, A. Riedinger, D. K. Kim, P. N. Knusel, A. Bianchi, M. Mauri, R. Simonutti, D. J. Norris, et al. Photocatalytic Water-Splitting Enhancement by Sub-Bandgap Photon Harvesting. *ACS Appl. Mater. Interfaces* **2017**, *9*(*46*), 40180–40186.

[45] S. Chandrasekaran, Y.-L. T. Ngo, L. Sui, E. J. Kim, D. K. Dang, J. S. Chung, and S. H. Hur. Highly Enhanced Visible Light Water Splitting of CdS by Green to Blue Upconversion. *Dalton Trans.* **2017**, *46*(*40*), 13912–13919.

[46] M. Barawi, F. Fresno, R. Pérez-Ruiz, and V. A. De La Peña O'Shea. Photoelectrochemical Hydrogen Evolution Driven by Visible-to-Ultraviolet Photon Upconversion. *ACS Appl. Energy Mater.* **2019**, *2*(*1*), 207–211.

[47] J. Fang, Y. Chen, W. Wang, L. Fang, C. Lu, C. Zhu, J. Kou, Y. Ni, and Z. Xu. Highly Efficient Photocatalytic Hydrogen Generation of g-C_3N_4-CdS Sheets Based on Plasmon-Enhanced Triplet–Triplet Annihilation Upconversion. *Appl. Catal. B* **2019**, *258*, 117762.

[48] Y. Liu, T. Yu, Y. Zeng, J. Chen, G. Yang, and Y. Li. Coupling Red-to-Blue Upconversion Organic Microcrystals with $Cd_{0.5}Zn_{0.5}S$ for Efficient and Durable Photocatalytic Hydrogen Production. *Chem. Asian J.* **2022**, *17*(*13*), e202200343.

[49] C. A. Parker and C. G. Hatchard. Delayed Fluorescence from Solutions of Anthracene and Phenanthrene. *Proc. Chem. Soc.* **1962**, *269*(*1339*), 574–584.

[50] G. Bergamini, P. Ceroni, M. Maestri, V. Balzani, S.-K. Lee, and F. Vögtle. Forward (Singlet–Singlet) and Backward (Triplet–Triplet) Energy Transfer in a Dendrimer with Peripheral Naphthalene Units and a Benzophenone Core. *Photochem. Photobiol. Sci.* **2004**, *3*(*9*), 898–905.

[51] R. R. Islangulov, D. V. Kozlov, and F. N. Castellano. Low Power Upconversion using MLCT Sensitizers. *Chem. Commun.* **2005**, *30*, 3776–3778.

[52] W. Zhao and F. N. Castellano. Upconverted Emission from Pyrene and Di-tert-butylpyrene Using $Ir(ppy)_3$ as Triplet Sensitizer. *J. Phys. Chem. A* **2006**, *110*(*10*), 11440–11445.

[53] X. Cao, B. Hu, and P. Zhang. High Upconversion Efficiency from Hetero Triplet–Triplet Annihilation in Multiacceptor Systems. *J. Phys. Chem. Lett.* **2013**, *4*(*14*), 2334–2338.

[54] S. Hoseinkhani, R. Tubino, F. Meinardi, and A. Monguzzi. Achieving the Photon Up-Conversion Thermodynamic Yield Upper Limit by Sensitized Triplet–Triplet Annihilation. *Phys. Chem. Chem. Phys.* **2015**, *17*(*6*), 4020–4024.

[55] A. Monguzzi, R. Tubino, and F. Meinardi. Diffusion Enhanced Upconversion in Organic Systems. *Int. J. Photoenergy* **2008**, *5*.

[56] S. Baluschev, T. Miteva, V. Yakutkin, G. Nelles, A. Yasuda, and G. Wegner. Up-Conversion Fluorescence: Noncoherent Excitation by Sunlight. *Phys. Rev. Lett.* **2006**, *97*(*14*).

[57] A. Haefele, J. Blumhoff, R. S. Khnayzer, and F. N. Castellano. Getting to the (Square) Root of the Problem: How to Make Noncoherent Pumped Upconversion Linear. *J. Phys. Chem. Lett.* **2012**, *3*(*3*), 299–303.

[58] V. Gray, D. Dzebo, A. Lundin, J. Alborzpour, M. Abrahamsson, B. Albinsson, and K. Moth-Poulsen. Photophysical Characterization of the 9,10-Disubstituted Anthracene Chromophore and its Applications in Triplet-Triplet Annihilation Photon Upconversion. *J. Mater. Chem. C* **2015**, *3*(*42*), 11111–11121.

[59] Y. V. Aulin, M. van Sebille, M. Moes, and F. C. Grozema. Photochemical Upconversion in Metal-Based Octaethyl Porphyrin–Diphenylanthracene Systems. *RSC Adv.* **2015**, *5*(*130*), 107896–107903.

[60] V. Gray, A. Dreos, P. Erhart, B. Albinsson, K. Moth-Poulsen, and M. Abrahamsson. Loss Channels in Triplet-Triplet Annihilation Photon Upconversion: Importance of Annihilator Singlet and Triplet Surface Shapes. *Phys. Chem. Chem. Phys.* **2017**, *19*(*17*), 10931–10939.

[61] C. Gao, S. K. K. Prasad, B. Zhang, M. Dvorak, M. J. Y. Tayebjee, D. R. McCamey, T. W. Schmidt, T. A. Smith, and W. W. H. Wong. Intramolecular versus Intermolecular Triplet Fusion in Multichromophoric Photochemical Upconversion. *J. Phys. Chem. C* **2019**, *123*(*33*), 20181–20187.

[62] W. Larsson, M. Morimoto, M. Irie, J. Andréasson, and B. Albinsson. Diarylethene Isomerization by Using Triplet–Triplet Annihilation Photon Upconversion. *Chem. Eur. J.* **2023**, *29*(*13*), e202203651.

[63] V. Gray, K. Moth-Poulsen, B. Albinsson, and M. Abrahamsson. Towards Efficient Solid-State Triplet-Triplet Annihilation Based Photon Upconversion: Supramolecular, Macromolecular and Self-Assembled Systems. *Coord. Chem. Rev.* **2018**, *362*, 54–71.

[64] R. R. Islangulov, J. Lott, C. Weder, and F. N. Castellano. Noncoherent Low-Power Upconversion in Solid Polymer Films. *J. Am. Chem. Soc.* **2007**, *129*(*42*), 12652–12653.

[65] P. B. Merkel and J. P. Dinnocenzo. Low-Power Green-to-Blue and Blue-to-UV Upconversion in Rigid Polymer Films. *J. Lumin.* **2009**, *129*(*3*), 303–306.

[66] S. H. Lee, M. A. Ayer, R. Vadrucci, C. Weder, and Y. C. Simon. Light Upconversion by Triplet-Triplet Annihilation in Diphenylanthracene-Based Copolymers. *Polym. Chem.* **2014**, *5*(*24*), 6898–6904.

[67] A. J. Tilley, B. E. Robotham, R. P. Steer, and K. P. Ghiggino. Sensitized Non-Coherent Photon Upconversion by Intramolecular Triplet-Triplet Annihilation in a Diphenylanthracene Pendant Polymer. *Chem. Phys. Lett.* **2015**, *618*, 198–202.

[68] P. C. Boutin, K. P. Ghiggino, T. L. Kelly, and R. P. Steer. Photon Upconversion by Triplet-Triplet Annihilation in $Ru(bpy)_3$- and DPA-Functionalized Polymers. *J. Phys. Chem. Lett.* **2013**, *4*(*23*), 4113–4118.

[69] D. Dzebo, K. Börjesson, V. Gray, K. Moth-Poulsen, and B. Albinsson. Intramolecular Triplet-Triplet Annihilation Upconversion in 9,10-Diphenylanthracene Oligomers and Dendrimers. *J. Phys. Chem. C* **2016**, *120*(*41*), 23397–23406.

[70] X. Yu, X. Cao, X. Chen, N. Ayres, and P. Zhang. Triplet–Triplet Annihilation Upconversion from Rationally Designed Polymeric Emitters with Tunable Inter-Chromophore Distances. *Chem. Comm.* **2015**, *51*(*3*), 588–591.

[71] R. Vadrucci, A. Monguzzi, F. Saenz, B. D. Wilts, Y. C. Simon, and C. Weder. Nanodroplet-Containing Polymers for Efficient Low-Power Light Upconversion. *Adv. Mater.* **2017**, *29*(*41*), 1702992.

[72] K. Sripathy, R. W. MacQueen, J. R. Peterson, Y. Y. Cheng, M. Dvořák, D. R. McCamey, N. D. Treat, N. Stingelin, and T. W. Schmidt. Highly Efficient Photochemical Upconversion in a Quasi-Solid Organogel. *J. Mater. Chem. C* **2015**, *3*(*3*), 616–622.

[73] P. Duan, N. Yanai, H. Nagatomi, and N. Kimizuka. Photon Upconversion in Supramolecular Gel Matrixes: Spontaneous Accumulation of Light-Harvesting Donor-Acceptor Arrays in Nanofibers and Acquired Air Stability. *J. Am. Chem. Soc.* **2015**, *137*(*5*), 1887–1894.

[74] R. Vadrucci, C. Weder, and Y. C. Simon. Organogels for Low-Power Light Upconversion. *Mater. Horiz.* **2015**, *2*(*1*), 120–124.

[75] D. F. Barbosa de Mattos, A. Dreos, M. D. Johnstone, A. Runemark, C. Sauvée, V. Gray, K. Moth-Poulsen, H. Sundén, and M. Abrahamsson. Covalent Incorporation of Diphenylanthracene in Oxotriphenylhexanoate Organogels as a Quasi-Solid Photon Upconversion Matrix. *J. Chem. Phys.* **2020**, *153*(*21*), 214705.

[76] F. Edhborg, H. Bildirir, P. Bharmoria, K. Moth-Poulsen, and B. Albinsson. Intramolecular Triplet–Triplet Annihilation Photon Upconversion in Diffusionally Restricted Anthracene Polymer. *J. Phys. Chem. B* **2021**, *125*, 6255–6263.

[77] M. Wu, J. Jean, V. Bulović, and M. A. Baldo. Interference-Enhanced Infrared-to-Visible Upconversion in Solid-State Thin Films Sensitized by Colloidal Nanocrystals. *Appl. Phys. Lett.* **2017**, *110*(*21*), 211101.

[78] D. G. Bossanyi, Y. Sasaki, S. Wang, D. Chekulaev, N. Kimizuka, N. Yanai, and J. Clark. In Optimized Rubrene-Based Nanoparticle Blends for Photon Upconversion, Singlet En-

ergy Collection Outcompetes Triplet-Pair Separation, not Singlet Fission. *J. Mater. Chem. C* **2022**, *10*(*12*), 4684–4696.

[79] R. Enomoto and Y. Murakami. Solvent-Free Temperature Gradient Melt Formation of Efficient Visible-to-UV Photon Upconversion Organic Films with Subsolar Threshold and over 100 h Photostability in Air. *J. Mater. Chem. C* **2023**, *11*(*5*), 1678–1683.

[80] T. Ishwara, J. Feng, D. M. de Clercq, R. Geng, J. Alves, D. R. McCamey, M. P. Nielsen, and T. W. Schmidt. Nanoporous Solid-State Sensitization of Triplet Fusion Upconversion. *ACS Energy Lett.* **2023**, *8*, 4078–4084.

[81] K. Börjesson, D. Dzebo, B. Albinsson, and K. Moth-Poulsen. Photon Upconversion Facilitated Molecular Solar Energy Storage. *J. Mater. Chem. A* **2013**, *1*(*30*), 8521–8524.

[82] Y. Y. Cheng, A. Nattestad, T. F. Schulze, R. W. MacQueen, B. Fückel, K. Lips, G. G. Wallace, T. Khoury, M. J. Crossley, and T. W. Schmidt. Increased Upconversion Performance for Thin Film Solar Cells: a Trimolecular Composition. *Chem. Sci.* **2016**, *7*(*1*), 559–568.

[83] C. Simpson, T. M. Clarke, R. W. MacQueen, Y. Y. Cheng, A. J. Trevitt, A. J. Mozer, P. Wagner, T. W. Schmidt, and A. Nattestad. An Intermediate Band Dye-Sensitised Solar Cell using Triplet–Triplet Annihilation. *Phys. Chem. Chem. Phys.* **2015**, *17*(*38*), 24826–24830.

[84] Y. L. Lin, M. Koch, A. N. Brigeman, D. M. Freeman, L. Zhao, H. Bronstein, N. C. Giebink, G. D. Scholes, and B. P. Rand. Enhanced Sub-Bandgap Efficiency of a Solid-State Organic Intermediate Band Solar Cell using Triplet–Triplet Annihilation. *Energy Environ. Sci.* **2017**, *10*(*6*), 1465–1475.

[85] D. Beery, J. P. Wheeler, A. Arcidiacono, and K. Hanson. CdSe Quantum Dot Sensitized Molecular Photon Upconversion Solar Cells. *ACS Appl. Energy Mater.* **2020**, *3*(*1*), 29–37.

[86] D. Beery, A. Arcidiacono, J. P. Wheeler, J. Chen, and K. Hanson. Harnessing Near-Infrared Light via S_0 to T_1 Sensitizer Excitation in a Molecular Photon Upconversion Solar Cell. *J. Mater. Chem. C* **2022**, *10*(*12*), 4947–4954.

[87] C. Gao, B. Zhang, C. R. Hall, L. Li, Y. Chen, Y. Zeng, T. A. Smith, and W. W. Wong. Triplet Fusion Upconversion using Sterically Protected 9,10-Diphenylanthracene as the Emitter. *Phys. Chem. Chem. Phys.* **2020**, *22*(*11*), 6300–6307.

[88] S. Mattiello, S. Mecca, A. Ronchi, A. Calascibetta, G. Mattioli, F. Pallini, F. Meinardi, L. Beverina, and A. Monguzzi. Diffusion-Free Intramolecular Triplet–Triplet Annihilation in Engineered Conjugated Chromophores for Sensitized Photon Upconversion. *ACS Energy Lett.* **2022**, *7*(*8*), 2435–2442.

[89] C. Kerzig and O. S. Wenger. Sensitized Triplet–Triplet Annihilation Upconversion in Water and its Application to Photochemical Transformations. *Chem. Sci.* **2018**, *9*(*32*), 6670–6678.

[90] A. Tokunaga, L. M. Uriarte, K. Mutoh, E. Fron, J. Hofkens, M. Sliwa, and J. Abe. Photochromic Reaction by Red Light via Triplet Fusion Upconversion. *J. Am. Chem. Soc.* **2019**, *141*(*44*), 17744–17753.

[91] B. D. Ravetz, A. B. Pun, E. M. Churchill, D. N. Congreve, T. Rovis, and L. M. Campos. Photoredox Catalysis using Infrared Light via Triplet Fusion Upconversion. *Nature* **2019**, *565*(*7739*), 343–346.

[92] C. G. Lopez-Calixto, M. Liras, R. Pérez-Ruiz, et al. Synchronized Biphotonic Process Triggering CC Coupling Catalytic Reactions. *Appl. Catal. B* **2018**, *237*, 18–23.

[93] F. Glaser and O. S. Wenger. Sensitizer-Controlled Photochemical Reactivity via Upconversion of Red Light. *Chem. Sci.* **2023**, *14*(*1*), 149–161.

[94] M. Majek, U. Faltermeier, B. Dick, R. Pérez-Ruiz, and A. Jacobi von Wangelin. Application of Visible-to-UV Photon Upconversion to Photoredox Catalysis: The Activation of Aryl Bromides. *Chem. Eur. J.* **2015**, *21*(*44*), 15496–15501.

[95] B. Pfund, D. M. Steffen, M. R. Schreier, M. S. Bertrams, C. Ye, K. Börjesson, O. S. Wenger, and C. Kerzig. UV Light Generation and Challenging Photoreactions Enabled by Upconversion in Water. *J. Am. Chem. Soc.* **2020**, *142*(*23*), 10468–10476.

[96] T. J. Zähringer, J. A. Moghtader, M.-S. Bertrams, B. Roy, M. Uji, N. Yanai, and C. Kerzig. Blue-to-UVB Upconversion, Solvent Sensitization and Challenging Bond Activation Enabled by a Benzene-Based Annihilator. *Angew. Chem., Int. Ed.* **2023**, *62*(*8*), e202215340.

[97] Q. Zhou, B. M. Wirtz, T. H. Schloemer, M. C. Burroughs, M. Hu, P. Narayanan, J. Lyu, A. O. Gallegos, C. Layton, D. J. Mai, et al. Spatially Controlled UV Light Generation at Depth Using Upconversion Micelles. *Adv. Mater.* **2022**, page 2301563.

[98] H. Li, C. Wang, F. Glaser, N. Sinha, and O. S. Wenger. Metal–Organic Bichromophore Lowers the Upconversion Excitation Power Threshold and Promotes UV Photoreactions. *J. Am. Chem. Soc.* **2023**, *145*(*20*), 11402–11414.

[99] Y. Wei, K. Pan, X. Cao, Y. Li, X. Zhou, and C. Yang. Multiple Resonance Thermally Activated Delayed Fluorescence Sensitizers Enable Green-to-Ultraviolet Photon Upconversion: Application in Photochemical Transformations. *CCS Chemistry* **2022**, *4*(*12*), 3852–3863.

[100] L. D. Næsborg, R. Jeyaseelan, M. Utikal, and C. Daniliuc. Photocyclization by a Triplet-Triplet Annihilation Upconversion Pair in Water – Avoiding UV-Light and Oxygen Removal. *Chem. Sci.* **2023**, *14*(*40*), 11040–11044.

[101] T. N. Singh-Rachford and F. N. Castellano. Low Power Visible-to-UV Upconversion. *J. Phys. Chem. A* **2009**, *113*(*20*), 5912–5917.

[102] N. Harada, Y. Sasaki, M. Hosoyamada, N. Kimizuka, and N. Yanai. Discovery of Key TIPS-Naphthalene for Efficient Visible-to-UV Photon Upconversion under Sunlight and Room Light. *Angew. Chem., Int. Ed.* **2021**, *60*(*1*), 142–147.

[103] M. Uji, N. Harada, N. Kimizuka, M. Saigo, K. Miyata, K. Onda, and N. Yanai. Heavy Metal-Free Visible-to-UV Photon Upconversion with over 20% Efficiency Sensitized by a Ketocoumarin Derivative. *J. Mater. Chem. C* **2022**, *10*(*12*), 4558–4562.

[104] V. Gray, P. Xia, Z. Huang, E. Moses, A. Fast, D. A. Fishman, V. I. Vullev, M. Abrahamsson, K. Moth-Poulsen, and M. L. Tang. CdS/ZnS Core–Shell Nanocrystal Photosensitizers for Visible to UV Upconversion. *Chem. Sci.* **2017**, *8*(*8*), 5488–5496.

[105] S. He, X. Luo, X. Liu, Y. Li, and K. Wu. Visible-to-Ultraviolet Upconversion Efficiency above 10% Sensitized by Quantum-Confined Perovskite Nanocrystals. *J. Phys. Chem. Lett.* **2019**, *10*(*17*), 5036–5040.

[106] K. Okumura, N. Yanai, and N. Kimizuka. Visible-to-UV Photon Upconversion Sensitized by Lead Halide Perovskite Nanocrystals. *Chem. Lett.* **2019**, *48*(*11*), 1347–1350.

[107] H. L. Lee, M. S. Lee, H. Park, W. S. Han, and J. H. Kim. Visible-to-UV Triplet-Triplet Annihilation Upconversion from a Thermally Activated Delayed Fluorescence/Pyrene Pair in an Air-Saturated Solution. *Korean J. Chem. Eng.* **2019**, *36*(*11*), 1791–1798.

[108] S. Hisamitsu, J. Miyano, K. Okumura, J. K. Hui, N. Yanai, and N. Kimizuka. Visible-to-UV Photon Upconversion in Nanostructured Chromophoric Ionic Liquids. *ChemistryOpen* **2020**, *9*(*1*), 14–17.

[109] S. He, Y. Han, J. Guo, and K. Wu. Entropy-Powered Endothermic Energy Transfer from $CsPbBr_3$ Nanocrystals for Photon Upconversion. *J. Phys. Chem. Lett.* **2022**, *13*(*7*), 1713–1718.

[110] N. Yanai, M. Kozue, S. Amemori, R. Kabe, C. Adachi, and N. Kimizuka. Increased Vis-to-UV Upconversion Performance by Energy Level Matching Between a TADF Donor and High Triplet Energy Acceptors. *J. Mater. Chem. C* **2016**, *4*(*27*), 6447–6451.

[111] P. Duan, N. Yanai, and N. Kimizuka. A Bis-Cyclometalated Iridium Complex as a Benchmark Sensitizer for Efficient Visible-to-UV Photon Upconversion. *Chem. Commun.* **2014**, *50*(*86*), 13111–13113.

[112] Y. Murakami, A. Motooka, R. Enomoto, K. Niimi, A. Kaiho, and N. Kiyoyanagi. Visible-to-Ultraviolet (<340 nm) Photon Upconversion by Triplet-Triplet Annihilation in Solvents. *Phys. Chem. Chem. Phys.* **2020**, *22*(*46*), 27134–27143.

[113] J. A. Kübler, B. Pfund, and O. S. Wenger. Zinc (II) Complexes with Triplet Charge-Transfer Excited States Enabling Energy-Transfer Catalysis, Photoinduced Electron Transfer, and Upconversion. *JACS Au* **2022**, *2*(*10*), 2367–2380.

[114] X. Cao, K. Pan, J. Miao, X. Lv, Z. Huang, F. Ni, X. Yin, Y. Wei, and C. Yang. Manipulating Exciton Dynamics toward Simultaneous High-Efficiency Narrowband Electroluminescence and Photon Upconversion by a Selenium-Incorporated Multiresonance Delayed Fluorescence Emitter. *J. Am. Chem. Soc.* **2022**, *144*(*50*), 22976–22984.

[115] T. J. Zähringer, M.-S. Bertrams, and C. Kerzig. Purely Organic Vis-to-UV Upconversion with an Excited Annihilator Singlet Beyond 4 eV. *J. Mater. Chem. C* **2022**, *10*(*12*), 4568–4573.

[116] L. Schmid, F. Glaser, R. Schaer, and O. S. Wenger. High Triplet Energy Iridium(III) Isocyanoborato Complex for Photochemical Upconversion, Photoredox and Energy Transfer Catalysis. *J. Am. Chem. Soc.* **2022**, *144*(*2*), 963–976.

[117] X. Lin, Z. Chen, Y. Han, C. Nie, P. Xia, S. He, J. Li, and K. Wu. ZnSe/ZnS Core/Shell Quantum Dots as Triplet Sensitizers toward Visible-to-Ultraviolet B Photon Upconversion. *ACS Energy Lett.* **2022**, *7*(*3*), 914–919.

[118] W. Sun, A. Ronchi, T. Zhao, J. Han, A. Monguzzi, and P. Duan. Highly Efficient Photon Upconversion based on Triplet–Triplet Annihilation from Bichromophoric Annihilators. *J. Mater. Chem. C* **2021**, *9*(*40*), 14201–14208.

[119] E. Schrödinger. An Undulatory Theory of the Mechanics of Atoms and Molecules. *Phys. Rev.* **1926**, *28*(*6*), 1049.

[120] W. Pauli. Über den Zusammenhang des Abschlusses der Elektronengruppen im Atom mit der Komplexstruktur der Spektren. *Zeitschrift für Physik* **1925**, *31*(*1*), 765–783.

[121] F. Hund. Atomtheoretische Deutung des Magnetismus der seltenen. Erden. *Zeitschrift für Physik* **1925**, *33*(*1*), 855–859.

[122] C. Grewer and H.-D. Brauer. Mechanism of the Triplet-State Quenching by Molecular Oxygen in Solution. *J. Phys. Chem.* **1994**, *98*(*16*), 4230–4235.
[123] J. R. Lakowicz. *Principles of Fluorescence Spectroscopy.* Springer, 2006.
[124] M. Kasha. Characterization of Electronic Transitions in Complex Molecules. *Discuss. Faraday Soc.* **1950**, *9*, 14–19.
[125] S. Murata, C. Iwanaga, T. Toda, and H. Kokubun. Fluorescence and Radiationless Transitions from the Second Excited States of Azulene Derivatives. *Berichte der Bunsengesellschaft für physikalische Chemie* **1972**, *76*(*11*), 1176–1183.
[126] C. M. Marian. Spin-Orbit Coupling and Intersystem Crossing in Molecules. *Wiley Interdiscip. Rev. Comput. Mol. Sci.* **2012**, *2*(*2*), 187–203.
[127] F. B. Dias, T. J. Penfold, and A. P. Monkman. Photophysics of Thermally Activated Delayed Fluorescence Molecules. *Methods Appl. Fluoresc.* **2017**, *5*(*1*).
[128] R. E. Blankenship. *Molecular mechanisms of photosynthesis.* John Wiley & Sons, 2021.
[129] T. Förster and K. Kasper. Ein Konzentrationsumschlag der Fluoreszenz. *Zeitschrift für Physikalische Chemie* **1954**, *1*(*5_6*), 275–277.
[130] T. Förster and K. Kasper. Ein Konzentrationsumschlag der Fluoreszenz des Pyrens. *Zeitschrift für Elektrochemie, Berichte der Bunsengesellschaft für physikalische Chemie* **1955**, *59*(*10*), 976–980.
[131] J. Birks. Excimers. *Rep. Prog. Phys.* **1975**, *38*(*8*), 903.
[132] T. Takemura, H. Baba, and Y. Shindo. Excimer Phosphorescence of Naphthalene in Fluid Solution. *Chem. Lett.* **1974**, *3*(*9*), 1091–1096.
[133] E. A. Chandross and C. J. Dempster. Excimer Fluorescence and Dimer Phosphorescence from a Naphthalene Sandwich Pair. *J. Am. Chem. Soc.* **1970**, *92*(*3*), 704–706.
[134] N. J. Turro, M. Aikawa, and A. Yekta. A Comparison of Intermolecular and Intramolecular Excimer Formation in Detergent Solutions. Temperature Effects and Microviscosity Measurements. *J. Am. Chem. Soc.* **1979**, *101*(*3*), 772–774.
[135] K. A. Zachariasse, G. Duveneck, and R. Busse. Intramolecular Excimer Formation with 1,3-Di(1-Pyrenyl)Propane. Decay Parameters and Influence of Viscosity. *J. Am. Chem. Soc.* **1984**, *106*(*4*), 1045–1051.
[136] T. Förster. Zwischenmolekulare Energiewanderung und Fluoreszenz. *Annalen der Physik* **1948**, *437*(*1-2*), 55–75.
[137] D. L. Dexter. A Theory of Sensitized Luminescence in Solids. *J. Chem. Phys.* **1953**, *21*(*5*), 836–850.
[138] B. Albinsson, M. P. Eng, K. Pettersson, and M. U. Winters. Electron and Energy Transfer in Donor–Acceptor Systems with Conjugated Molecular Bridges. *Phys. Chem. Chem. Phys.* **2007**, *9*(*44*), 5847 – 5864.
[139] J. B. Birks. *Photophysics of Aromatic Molecules.* Wiley Interscience, 1970.
[140] V. Gray, D. Dzebo, M. Abrahamsson, B. Albinsson, and K. Moth-Poulsen. Triplet–Triplet Annihilation Photon-Upconversion: Towards Solar Energy Applications. *Phys. Chem. Chem. Phys.* **2014**, *16*(*22*), 10345–10352.
[141] C. Mongin, S. Garakyaraghi, N. Razgoniaeva, M. Zamkov, and F. N. Castellano. Direct Observation of Triplet Energy Transfer from Semiconductor Nanocrystals. *Science* **2016**, *351*(*6271*), 369–372.

[142] S. Garakyaraghi, C. Mongin, D. B. Granger, J. E. Anthony, and F. N. Castellano. Delayed Molecular Triplet Generation from Energized Lead Sulfide Quantum Dots. *J. Phys. Chem. Lett.* **2017**, *8*(*7*), 1458–1463.

[143] L. Nienhaus, M. Wu, N. Geva, J. J. Shepherd, M. W. B. Wilson, V. Bulović, T. Van Voorhis, M. A. Baldo, and M. G. Bawendi. Speed Limit for Triplet-Exciton Transfer in Solid-State PbS Nanocrystal-Sensitized Photon Upconversion. *ACS Nano* **2017**, *11*(*8*), 7848–7857.

[144] A. Ronchi, C. Capitani, G. Gariano, V. Pinchetti, M. L. Zaffalon, F. Meinardi, S. Brovelli, and A. Monguzzi. High Photon Upconversion Efficiency with Hybrid Triplet Sensitizers by Ultrafast Hole-Routing in Electronic-Doped Nanocrystals. *Adv. Mater.* **2020**, *32*, 2002953.

[145] Z. A. VanOrman, C. R. Conti, G. F. Strouse, and L. Nienhaus. Red-to-Blue Photon Upconversion Enabled by One-Dimensional CdTe Nanorods. *Chem. Mater.* **2021**, *33*(*1*), 452–458.

[146] C. J. Imperiale, P. B. Green, M. Hasham, and M. W. Wilson. Ultra-Small PbS Nanocrystals as Sensitizers for Red-to-Blue Triplet-Fusion Upconversion. *Chem. Sci.* **2021**, *12*(*42*), 14111–14120.

[147] Y. Zhang, T. S. Lee, J. M. Favale, D. C. Leary, J. L. Petersen, G. D. Scholes, F. N. Castellano, and C. Milsmann. Delayed Fluorescence from a Zirconium(IV) Photosensitizer with Ligand-to-Metal Charge-Transfer Excited States. *Nat. Chem.* **2020**, *12*(*4*), 345–352.

[148] C. Wang, F. Reichenauer, W. R. Kitzmann, C. Kerzig, K. Heinze, and U. Resch-Genger. Efficient Triplet-Triplet Annihilation Upconversion Sensitized by a Chromium(III) Complex via an Underexplored Energy Transfer Mechanism. *Angew. Chem., Int. Ed.* **2022**, *61*(*27*), e202202238.

[149] M. R. Schreier, X. Guo, B. Pfund, Y. Okamoto, T. R. Ward, C. Kerzig, and O. S. Wenger. Water-Soluble Tris(cyclometalated) Iridium(III) Complexes for Aqueous Electron and Energy Transfer Photochemistry. *Acc. Chem. Res.* **2022**, *55*(*9*), 1290–1300.

[150] M. Gouterman. Spectra of Porphyrins. *J. Mol. Spectrosc.* **1961**, *6*, 138–163.

[151] J. Zhao, W. Wu, J. Sun, and S. Guo. Triplet Photosensitizers: from Molecular Design to Applications. *Chem. Soc. Rev.* **2013**, *42*(*12*), 5323–5351.

[152] A. K. Bansal, W. Holzer, A. Penzkofer, and T. Tsuboi. Absorption and Emission Spectroscopic Characterization of Platinum-Octaethyl-Porphyrin (PtOEP). *Chem. Phys.* **2006**, *330*(*1-2*), 118–129.

[153] C. de Mello Donegá. Synthesis and Properties of Colloidal Heteronanocrystals. *Chem. Soc. Rev.* **2011**, *40*(*3*), 1512–1546.

[154] The Royal Swedish Academy of Sciences. Popular Information: The Nobel Prize in Chemistry 2023. https://www.nobelprize.org/prizes/chemistry/2023/popular-information, 2023. Accessed 2023-10-04.

[155] G. D. Scholes. Controlling the Optical Properties of Inorganic Nanoparticles. *Adv. Funct. Mater.* **2008**, *18*(*8*), 1157–1172.

[156] Z. Huang, X. Li, M. Mahboub, K. M. Hanson, V. M. Nichols, H. Le, M. L. Tang, and C. J. Bardeen. Hybrid Molecule-Nanocrystal Photon Upconversion Across the Visible and Near-Infrared. *Nano Lett.* **2015**, *15*(*8*), 5552–5557.

[157] G. B. Piland, Z. Huang, M. Lee Tang, and C. J. Bardeen. Dynamics of Energy Transfer from CdSe Nanocrystals to Triplet States of Anthracene Ligand Molecules. *J. Phys. Chem. C* **2016**, *120*(*11*), 5883–5889.

[158] R. Lai, Y. Sang, Y. Zhao, and K. Wu. Triplet Sensitization and Photon Upconversion using InP-based Quantum Dots. *J. Am. Chem. Soc.* **2020**, *142*(*47*), 19825–19829.

[159] Y. Han, S. He, X. Luo, Y. Li, Z. Chen, W. Kang, X. Wang, and K. Wu. Triplet Sensitization by "Self-Trapped" Excitons of Nontoxic $CuInS_2$ Nanocrystals for Efficient Photon Upconversion. *J. Am. Chem. Soc.* **2019**, *141*, 13033–13037.

[160] W. Liang, C. Nie, J. Du, Y. Han, G. Zhao, F. Yang, G. Liang, and K. Wu. Near-Infrared Photon Upconversion and Solar Synthesis Using Lead-Free Nanocrystals. *Nat. Phot.* **2023**, *17*(*4*), 346–353.

[161] J. T. Dubois and M. Cox. Singlet—Singlet Energy Transfer in Fluid Solutions. *J. Chem. Phys.* **1963**, *38*(*10*), 2536–2541.

[162] W. L. Dilling. The Effect of Solvent on the Electronic Transitions of Benzophenone and its o- and p-Hydroxy Derivatives. *J. Org. Chem.* **1966**, *31*(*4*), 1045–1050.

[163] H. Uoyama, K. Goushi, K. Shizu, H. Nomura, and C. Adachi. Highly Efficient Organic Light-Emitting Diodes From Delayed Fluorescence. *Nature* **2012**, *492*(*7428*), 234–238.

[164] K. Goushi, K. Yoshida, K. Sato, and C. Adachi. Organic Light-Emitting Diodes Employing Efficient Reverse Intersystem Crossing for Triplet-to-Singlet State Conversion. *Nat. Phot.* **2012**, *6*(*4*), 253–258.

[165] Q. Zhang, J. Li, K. Shizu, S. Huang, S. Hirata, H. Miyazaki, and C. Adachi. Design of Efficient Thermally Activated Delayed Fluorescence Materials for Pure Blue Organic Light Emitting Diodes. *J. Am. Chem. Soc.* **2012**, *134*(*36*), 14706–14709.

[166] Y. Im and J. Y. Lee. Recent Progress of Green Thermally Activated Delayed Fluorescent Emitters. *J. Inf. Disp.* **2017**, *18*(*3*), 101–117.

[167] T. C. Wu, D. N. Congreve, and M. A. Baldo. Solid State Photon Upconversion Utilizing Thermally Activated Delayed Fluorescence Molecules as Triplet Sensitizer. *Appl. Phys. Lett.* **2015**, *107*(*3*), 031103.

[168] K. Sandros. Transfer of Triplet State Energy in Fluid Solutions. *Acta Chem. Scand.* **1964**, *18*, 2355–2374.

[169] F. Edhborg, A. Olesund, and B. Albinsson. Best Practice in Determining Key Photophysical Parameters in Triplet–Triplet Annihilation Photon Upconversion. *Photochem. Photobiol. Sci.* **2022**, *21*(*7*), 1143–1158.

[170] Y. Y. Cheng, B. Fuckel, T. Khoury, R. G. Clady, N. Ekins-Daukes, M. J. Crossley, and T. W. Schmidt. Entropically Driven Photochemical Upconversion. *J. Phys. Chem. A* **2011**, *115*(*6*), 1047–1053.

[171] J. Isokuortti, S. R. Allu, A. Efimov, E. Vuorimaa-Laukkanen, N. V. Tkachenko, S. A. Vinogradov, T. Laaksonen, and N. A. Durandin. Endothermic and Exothermic Energy Transfer Made Equally Efficient for Triplet–Triplet Annihilation Upconversion. *J. Phys. Chem. Lett.* **2019**, *11*(*1*), 318–324.

[172] E. Radiunas, M. Dapkevičius, S. Raišys, S. Juršėnas, A. Jozeliūnaitė, T. Javorskis, U. Šinkevičiūtė, E. Orentas, and K. Kazlauskas. Impact of t-Butyl Substitution in a

Rubrene Emitter for Solid State NIR-to-Visible Photon Upconversion. *Phys. Chem. Chem. Phys.* **2020**, *22*(*14*), 7392–7403.

[173] A. Monguzzi, J. Mezyk, F. Scotognella, R. Tubino, and F. Meinardi. Upconversion-Induced Fluorescence in Multicomponent Systems: Steady-State Excitation Power Threshold. *Phys. Rev. B* **2008**, *78*(*19*), 195112.

[174] J. K. Gallaher, K. M. Wright, L. Frazer, R. W. MacQueen, M. J. Crossley, F. N. Castellano, and T. W. Schmidt. High Efficiency Deep Red to Yellow Photochemical Upconversion Under Solar Irradiance. *Energy Environ. Sci.* **2021**, *14*(*10*), 5541–5551.

[175] L. Nienhaus, J.-P. Correa-Baena, S. Wieghold, M. Einzinger, T.-A. Lin, K. E. Shulenberger, N. D. Klein, M. Wu, V. Bulovic, T. Buonassisi, et al. Triplet-Sensitization by Lead Halide Perovskite Thin Films for Near-Infrared-to-Visible Upconversion. *ACS Energy Lett.* **2019**, *4*(*4*), 888–895.

[176] Y. Zhou, F. N. Castellano, T. W. Schmidt, and K. Hanson. On the Quantum Yield of Photon Upconversion via Triplet–Triplet Annihilation. *ACS Energy Lett.* **2020**, *5*(*7*), 2322–2326.

[177] D. G. Bossanyi, Y. Sasaki, S. Wang, D. Chekulaev, N. Kimizuka, N. Yanai, and J. Clark. Spin Statistics for Triplet–Triplet Annihilation Upconversion: Exchange Coupling, Intermolecular Orientation, and Reverse Intersystem Crossing. *JACS Au* **2021**, *1*(*12*), 2188–2201.

[178] R. Ieuji, K. Goushi, and C. Adachi. Triplet–Triplet Upconversion Enhanced by Spin–Orbit Coupling in Organic Light-Emitting Diodes. *Nat. Commun.* **2019**, *10*(*1*), 1–10.

[179] T. Miyashita, P. Jaimes, A. Mardini, M. Fumanal, and M. L. Tang. High-Level Reverse Intersystem Crossing and Molecular Rigidity Improve Spin Statistics for Triplet–Triplet Annihilation Upconversion. *J. Phys. Chem. Lett.* **2023**, *14*, 6119–6126.

[180] S. N. Sanders, T. H. Schloemer, M. K. Gangishetty, D. Anderson, M. Seitz, A. O. Gallegos, R. C. Stokes, and D. N. Congreve. Triplet Fusion Upconversion Nanocapsules for Volumetric 3D Printing. *Nature* **2022**, *604*(*7906*), 474–478.

[181] Y. Murakami and K. Kamada. Kinetics of Photon Upconversion by Triplet–Triplet Annihilation: a Comprehensive Tutorial. *Phys. Chem. Chem. Phys.* **2021**, *23*(*34*), 18268–18282.

[182] A. Beer. Bestimmung der Absorption des rothen Lichts in farbigen Flüssigkeiten. *Annalen der Physik und Chemie* **1852**, *162*(*5*), 78–88.

[183] P. Ceroni. *The Exploration of Supramolecular Systems and Nanostructures by Photochemical Techniques*. Springer Science & Business Media, 2011.

[184] A. Olesund, V. Gray, J. Mårtensson, and B. Albinsson. Diphenylanthracene Dimers for Triplet–Triplet Annihilation Photon Upconversion: Mechanistic Insights for Intramolecular Pathways and the Importance of Molecular Geometry. *J. Am. Chem. Soc.* **2021**, *143*(*15*), 5745–5754.

[185] S. M. Bachilo and R. B. Weisman. Determination of Triplet Quantum Yields from Triplet-Triplet Annihilation Fluorescence. *J. Phys. Chem. A* **2000**, *104*(*33*), 7713–7714.

[186] Y. Matsui, M. Kanoh, E. Ohta, T. Ogaki, and H. Ikeda. Triplet–Triplet Annihilation-Photon Upconversion Employing an Adamantane-linked Diphenylanthracene Dyad Strategy. *J. Photochem. Photobiol. A* **2020**, *387*, 112107.

[187] C. J. Imperiale, P. B. Green, E. G. Miller, N. H. Damrauer, and M. W. B. Wilson. Triplet-Fusion Upconversion Using a Rigid Tetracene Homodimer. *J. Phys. Chem. Lett.* **2019**, *10*(*23*), 7463–7469.

[188] A. B. Pun, S. N. Sanders, M. Y. Sfeir, L. M. Campos, and D. N. Congreve. Annihilator Dimers Enhance Triplet Fusion Upconversion. *Chem. Sci.* **2019**, *10*(*14*), 3969–3975.

[189] C. Fan, L. Wei, T. Niu, M. Rao, G. Cheng, J. J. Chruma, W. Wu, and C. Yang. Efficient Triplet-Triplet Annihilation Upconversion with an Anti-Stokes Shift of 1.08 eV Achieved by Chemically Tuning Sensitizers. *J. Am. Chem. Soc.* **2019**, *141*(*38*), 15070–15077.

[190] G. C. Solomon, D. Q. Andrews, T. Hansen, R. H. Goldsmith, M. R. Wasielewski, R. P. Van Duyne, and M. A. Ratner. Understanding Quantum Interference in Coherent Molecular Conduction. *J. Chem. Phys.* **2008**, *129*(*5*), 054701.

[191] C. R. Arroyo, R. Frisenda, K. Moth-Poulsen, J. S. Seldenthuis, T. Bjørnholm, and H. S. van der Zant. Quantum Interference Effects at Room Temperature in OPV-Based Single-Molecule Junctions. *Nanoscale Res. Lett.* **2013**, *8*(*1*), 234.

[192] M. Gantenbein, L. Wang, A. A. Al-Jobory, A. K. Ismael, C. J. Lambert, W. Hong, and M. R. Bryce. Quantum Interference and Heteroaromaticity of Para- and Meta-Linked Bridged Biphenyl Units in Single Molecular Conductance Measurements. *Sci. Rep.* **2017**, *7*(*1*), 1–9.

[193] L. Hou, A. Olesund, S. Thurakkal, X. Zhang, and B. Albinsson. Efficient Visible-to-UV Photon Upconversion Systems Based on CdS Nanocrystals Modified with Triplet Energy Mediators. *Adv. Funct. Mater.* **2021**, *31*(*47*), 2106198.

[194] A. Olesund, J. Johnsson, F. Edhborg, S. Ghasemi, K. Moth-Poulsen, and B. Albinsson. Approaching the Spin-Statistical Limit in Visible-to-Ultraviolet Photon Upconversion. *J. Am. Chem. Soc.* **2022**, *144*(*8*), 3706–3716.

[195] A. Olesund, S. Ghasemi, K. Moth-Poulsen, and B. Albinsson. Bulky Substituents Promote Triplet–Triplet Annihilation Over Triplet Excimer Formation in Naphthalene Derivatives. *J. Am. Chem. Soc.* **2023**, *145*(*40*), 22168–22175.

[196] Z. Li, Y. Ji, R. Xie, S. Y. Grisham, and X. Peng. Correlation of CdS Nanocrystal Formation with Elemental Sulfur Activation and its Implication in Synthetic Development. *J. Am. Chem. Soc.* **2011**, *133*(*43*), 17248–17256.

[197] N. J. Thompson, M. W. Wilson, D. N. Congreve, P. R. Brown, J. M. Scherer, T. S. Bischof, M. Wu, N. Geva, M. Welborn, T. Van Voorhis, V. Bulovi, M. G. Bawendi, and M. A. Baldo. Energy Harvesting of Non-Emissive Triplet Excitons in Tetracene by Emissive PbS Nanocrystals. *Nat. Mater.* **2014**, *13*(*11*), 1039–1043.

[198] M. Tabachnyk, B. Ehrler, S. Gélinas, M. L. Böhm, B. J. Walker, K. P. Musselman, N. C. Greenham, R. H. Friend, and A. Rao. Resonant Energy Transfer of Triplet Excitons from Pentacene to PbSe Nanocrystals. *Nat. Mater.* **2014**, *13*(*11*), 1033–1038.

[199] C. Mongin, P. Moroz, M. Zamkov, and F. N. Castellano. Thermally Activated Delayed Photoluminescence from Pyrenyl-Functionalized CdSe Quantum Dots. *Nat. Chem.* **2017**, *10*(*2*), 225–230.

[200] S. L. Murov, I. Carmichael, and G. L. Hug. *Handbook of Photochemistry*. Marcel Dekker, New York, 1993.

[201] A. P. Marchetti and D. R. Kearns. Investigation of Singlet-Triplet Transitions by the Phosphorescence Excitation Method. IV. The Singlet-Triplet Absorption Spectra of Aromatic Hydrocarbons. *J. Am. Chem. Soc.* **1967**, *89*(*4*), 768–777.

[202] P. B. Merkel and J. P. Dinnocenzo. Thermodynamic Energies of Donor and Acceptor Triplet States. *J. Photochem. Photobiol. A* **2008**, *193*(*2-3*), 110–121.

[203] I. Berlman. *Handbook of Fluorescence Spectra of Aromatic Molecules*. Academic Press: New York, 1971.

[204] C. Rulliere and P. C. Roberge. Photophysics of Aryl Substituted 1,3,4-Oxadiazoles: The Triplet State of 2.5-Diphenyl-1,3,4-Oxadiazole. *Chem. Phys. Lett.* **1983**, *97*(*2*), 247–252.

[205] D. Zhang, M. Cai, Y. Zhang, D. Zhang, and L. Duan. Sterically Shielded Blue Thermally Activated Delayed Fluorescence Emitters with Improved Efficiency and Stability. *Mater. Horiz.* **2016**, *3*(*2*), 145–151.

[206] W. Chen, F. Song, S. Tang, G. Hong, Y. Wu, and X. Peng. Red-to-Blue Photon Up-Conversion with High Efficiency Based on a TADF Fluorescein Derivative. *Chem. Commun.* **2019**, *55*(*30*), 4375–4378.

[207] Y. Y. Cheng, B. Fückel, T. Khoury, R. G. C. R. Clady, M. J. Y. Tayebjee, N. J. Ekins-Daukes, M. J. Crossley, and T. W. Schmidt. Kinetic Analysis of Photochemical Upconversion by Triplet-Triplet Annihilation: Beyond Any Spin Statistical Limit. *J. Phys. Chem. Lett* **2010**, *1*, 1795–1799.

[208] N. Harada, M. Uji, B. Singh, N. Kimizuka, and N. Yanai. Porous Film Impregnation Method for Record-Efficiency Visible-to-UV Photon Upconversion and Subsolar Light Harvesting. *J. Mater. Chem. C* **2023**, *11*, 8002–8006.

[209] S. Okajima, P. Subudhi, and E. Lim. Triplet Excimer Formation and Phosphorescence in Fluid Solutions of Diarylalkanes: Excimer Phosphorescence of Dinaphthylalkanes and Monomer Phosphorescence of Diphenylpropane. *J. Chem. Phys.* **1977**, *67*(*10*), 4611–4615.

[210] X. Wang, W. G. Kofron, S. Kong, C. S. Rajesh, D. A. Modarelli, and E. C. Lim. Transient Absorption Probe of Intermolecular Triplet Excimer of Naphthalene in Fluid Solutions: Identification of the Species Based on Comparison to the Intramolecular Triplet Excimers of Covalently-Linked Dimers. *J. Phys. Chem. A* **2000**, *104*(*7*), 1461–1465.

[211] J. Saltiel, G. R. Marchand, R. Dabestani, and J. M. Pecha. The Quenching of Anthracene Triplet by Ground-State Anthracene. *Chem. Phys. Lett.* **1983**, *100*(*3*), 219–222.

[212] C. Ye, V. Gray, J. Mårtensson, and K. Börjesson. Annihilation Versus Excimer Formation by the Triplet Pair in Triplet–Triplet Annihilation Photon Upconversion. *J. Am. Chem. Soc.* **2019**, *141*(*24*), 9578–9584.

[213] C. Ye, V. Gray, K. Kushwaha, S. Kumar Singh, P. Erhart, and K. Börjesson. Optimizing Photon Upconversion by Decoupling Excimer Formation and Triplet Triplet Annihilation. *Phys. Chem. Chem. Phys.* **2020**, *22*(*3*), 1715–1720.

[214] G. Porter and F. Wilkinson. Energy Transfer from the Triplet State. *Proc. R. Soc. A: Math. Phys. Eng. Sci.* **1961**, *264*(*1316*), 1–18.

[215] S. H. Modiano, J. Dresner, and E. C. Lim. Intramolecular Photoassociation and Photoinduced Charge Transfer in Bridged Diaryl Compounds. 1. Photoassociation in the Lowest Triplet State of 2,2'-Dinaphthylmethane and 2,2'-Dinaphthyl Ether. *J. Phys. Chem.* **1991**, *95*(*23*), 9144–9151.

[216] S. H. Modiano, J. Dresner, J. Cai, and E. C. Lim. Intramolecular Photoassociation and Photoinduced Charge Transfer in Bridged Diaryl Compounds. 4. Temporal Studies of Intramolecular Triplet Excimer Formation in Dinaphthylmethanes and Dinaphthyl Ethers. *J. Phys. Chem.* **1993**, *97*(*14*), 3480–3485.

[217] M. Yamaji, K. Shima, J. Nishimura, and H. Shizuka. Laser Flash Photolysis Studies on Dynamic Behaviour of Triplet Naphthalenophanes Sensitized by Triplet Benzophenone. *J. Chem. Soc., Faraday Trans. 1* **1997**, *93*(*6*).

[218] V. Vijay, M. Madhu, R. Ramakrishnan, A. Benny, and M. Hariharan. Through-Space Aromatic Character in Excimers. *Chem. Commun.* **2020**, *56*(*2*), 225–228.

[219] G. A. George and G. C. Morris. Triplet Excimer Emission from Halogenated Benzenes. *Mol. Cryst. Liq.* **1971**, *15*(*1*), 65–73.

[220] T. F. Hunter and M. G. Stock. Triplet-State Lifetime of Vapour-Phase Benzene. *Chem. Phys. Lett.* **1973**, *22*(*2*), 368–370.

[221] L. Naimovičius, E. Radiunas, B. Chatinovska, A. Jozeliūnaitė, E. Orentas, and K. Kazlauskas. Functionalized Diketopyrrolopyrrole Compounds for NIR-to-Visible Photon Upconversion. *J. Mater. Chem. C* **2023**, *11*(*2*), 698–704.

[222] H. J. Snaith. Present Status and Future Prospects of Perovskite Photovoltaics. *Nat. Mater.* **2018**, *17*(*5*), 372–376.

[223] F. Xu, M. Zhang, Z. Li, X. Yang, and R. Zhu. Challenges and Perspectives toward Future Wide-Bandgap Mixed-Halide Perovskite Photovoltaics. *Adv. Energy Mat.* **2023**, *13*(*13*), 2203911.